REMOVAL OF AROMATIC AMINES AND HEAVY METALS FROM WASTEWATER USING NANOADSORBENT

Ph.D. THESIS

by

SEHASPREET KAUR TOOR

DEPARTMENT OF CHEMICAL ENGINEERING
THAPAR INSTITUTE OF ENGINEERING AND TECHNOLOGY
(Deemed to be University)
PATIALA -147004

May, 2019

REMOVAL OF AROMATIC AMINES AND HEAVY METALS FROM WASTEWATER USING NANOADSORBENT

A THESIS

Submitted in partial fulfilment of the requirements for the award of the degree

of

DOCTOR OF PHILOSOPHY

by

SEHASPREET KAUR TOOR

DEPARTMENT OF CHEMICAL ENGINEERING
THAPAR INSTITUTE OF ENGINEERING AND TECHNOLOGY
(Deemed to be University)
PATIALA -147004

May, 2019

CANDIDATE'S DECLARATION

I hereby certify that the work which is being presented in the thesis entitled **"REMOVAL OF AROMATIC AMINES AND HEAVY METALS FROM WASTEWATER USING NANOADSORBENT"** in partial fulfillment of the requirements for the award of the degree of Doctor of Philosophy and submitted in the Department of Chemical Engineering of Thapar Institute of Engineering and Technology, Patiala is an authentic record of my own work carried out during a period from July 2014 to May 2019 under the supervision of Dr. J. P. Kushwaha, Associate Professor, Department of Chemical Engineering, Thapar Institute of Engineering and Technology, Patiala, Punjab, India and Dr. V. K. Sangal, Associate Professor, Department of Chemical Engineering, Malaviya National Institute of Technology, Jaipur, Rajasthan, India.

The matter presented in the thesis has not been submitted by me for the award of any other degree of this or any other Institute.

Sehaspreet

(SEHASPREET KAUR TOOR)

This is to certify that the above statement made by the candidate is correct to the best of our knowledge.

Dr. J. P. Kushwaha
Supervisor

Dr. V.K. Sangal
Supervisor

ABSTRACT

Existence of water has led to evolution of life on our magnificent planet earth. But regrettably, quality of our water resources is declining continuously due to population explosion, industrialization, civilization, domestic activities and environmental changes. 5–10 billion tons of industrial effluents is generated annually worldwide, out of which maximum amount is dumped untreated into rivers, lakes and oceans leading to water pollution. More than seven hundred organic (azo-dyes, benzene, phenols, DDT, aromatic amines etc.) and inorganic pollutants (heavy metals like arsenic, cadmium, chromium, cyanide, fluoride, lead, mercury, selenium etc.) have been reported in water. Some of these pollutants like aromatic amines and heavy metals are alarming because of their highly toxic, mutagenic and carcinogenic nature and urgently need to be removed from wastewater.

Chemical compounds with one or more aromatic rings along with amino substituents (-NH_2, -NH- or nitrogen group(s)) are classified as aromatic amines. They are well known components in wide variety of wastewater including those from textile and dye processing industries, synthetic polymer industries, tanneries, oil refining processes and several other chemical process industries. Carcinogenic and mutagenic nature of aromatic amines are known since 1895 due to which twenty-two types of aromatic amines including 4-chloro-*o*-toluidine (4-COT) and 4-Amino-bi-phenyl (4-ABP) above 30 mg/L in effluents have been restricted by European Union Standards (1907/2006), therefore need to be treated before discharge.

On the other hand, heavy metals are the high atomic weight and high density (≈5 times higher than water) elements present naturally in our ecosystem. Zinc is present in the earth's crust in abundance. However, its increasing concentration in wastewater as Zinc ion [(Zn (II)] owe to various commercial manufacturing units results to certain adverse diseases including skin irritations, vomiting, stomach cramps and anaemia. Chromium, contrarily is present in our surroundings in two forms: trivalent [Cr (III)] and hexavalent [Cr (VI)]. Cr (VI) is about five hundred times more noxious than [Cr (III)] due to its ability to oxidize additional species. Innumerable industries are responsible for introduction of excess Cr with wastewater causing eyes infection, allergy, asthma, dermatitis, cancer and skin irritation including burns. Therefore, various agencies like World health organization (WHO) and

Environmental protection agency (EPA) have set a bearable limit for these heavy metals in industrial effluents.

Numerous physico-chemical techniques (precipitation, coagulation, flocculation, adsorption, ion-exchange); electrochemical methods and biological techniques are available in literature for removal of both aromatic amines and heavy metals from wastewater. However, these techniques have been demonstrated to be unfavourable because of high cost involvement, high energy consumption and production of large volume of toxic by-product as sludge. Adsorption is reported to be very efficacious for wastewater treatment with simple operational conditions. Many authors used activated carbon for organics removal from wastewater including aromatic amines like diphenylamine (DPAM), napthylamine (NAM), and aniline. Similarly, various researches had efficiently used activated carbon prepared from agricultural waste for heavy metals (Zn (II), Cr (VI) and Pb (II)) removal. However, its use is confined due to their limited adsorption capacity and high quantity requirement. Therefore, to overcome these demerits, latterly investigators have focused on the development of adsorbents possessing larger surface area and pore size such as zeolites and mesoporous silica nanoparticles.

Discovery of ordered mesoporous materials has led a new path towards the research on synthesis and application of these materials. Mobil Composition of Matter No. 41 (MCM-41) is a synthetic-ordered mesoporous silica characterised by high surface area, high pore volume with uniform pore size distribution exhibiting excellent thermal, hydrothermal and hydrolytic stability. A number of researchers have reported removal of azo dyes from textile wastewater using MCM-41 as adsorbent. Adsorptive removal of aromatic amines such as p-chloroaniline, benzidine, aniline, 4-methylaniline and naphthalamine on polymeric nano-adsorbents has been reported by various authors but only single study for the adsorption of aromatic amine aniline onto MCM-41 has been reported so far. No study was available for the adsorptive removal of aromatic amines 4-chloro-*o*-toluidine (4-COT) and 4-amino-bi-phenyl (4-ABP) using MCM-41. If we consider heavy metal ions adsorption onto MCM-41, numerous work has been reported. However, no research has been reported on zinc removal using MCM-41. Also literature lacks study on simultaneous removal of two or more metal ions. No work has been reported concerning the multicomponent system for heavy metals removal using MCM-41 including Zn (II) and Cr (VI). Considering these gaps in literature, present study has been undertaken in which MCM-41 was synthesized and

characterize for enhanced adsorption of aromatic amines (4- chloro-*o*-toluidine, 4-aminobiphenyl) and heavy metals (Cr^{6+}, Zn^{2+}). Effect of various adsorption parameters such as contact time, pH, adsorbent dose, adsorbate concentration and temperature on removal of both aromatic amines and heavy metals has been studied followed by kinetic and thermodynamic studies.

MCM-41 nanoparticles were synthesized via hydrothermal method. Synthesized material was then characterized by various characterization techniques including XRD, BET, FTIR, FE-SEM and TEM. BET surface area of synthesized MCM-41 was found to be 502.77 $m^2 g^{-1}$. BJH model exhibited 0.85 $cm^3 g^{-1}$ pore volume with 3.21 nm pore size of MCM-41. Nitrogen adsorption/desorption isotherm plot obtained from BET analysis, was found to be of type IV with H1 hysteresis loop which confirms the mesoporous nature of synthesized MCM-41. XRD spectra of MCM-41 exhibited a single peak at 0.98, which is associated with the hexagonal mesophase structure. Since the material is not crystalline at the atomic level, no reflections are observed at higher angles. FE-SEM images clearly revealed the spherical uniform structure of MCM-41 within the size of 70-100 nm. TEM micrographs showed that the MCM-41 is hexagonal, and possesses evenly distributed pore system with a uniform mesoporous channels array.

Batch adsorption experiments were performed for aromatic amines and heavy metals removal. Optimum conditions for 4-COT and 4-ABP treatment were obtained as: pH_i =2, m=0.2 g/L and t=2h. Pseudo-first-order and pseudo-second-order kinetic models were applied to study the adsorption kinetics. Further, adsorption rate controlling mechanism was investigated using intra-particle diffusion model. Interactions of 4-COT and 4-ABP molecule with the surface of MCM-41 were investigated and adsorption process controlling mechanism was explored. Langmuir, Freundlich, Temkin and D-R isotherm (Dubinin-Radushkevich) models were used to represent the adsorption equilibrium data.

Effect of temperature for adsorption of 4-COT and 4-ABP onto MCM-41was studied at C_0 values ranging from 10-300 mg/L, pH_i= 2, m_{opt}=0.2 g/L and t= 2h by varying temperature (T) in the range of 283-318 K. It was observed that the adsorption of both 4-COT and 4-ABP onto MCM-41 increases with rise in temperature due enhanced movement of the amine molecules to the MCM-41 surface. Thermodynamic parameters were obtained from the linear plot of ln K_D versus 1/T. Value of K_D was found to decreases with raised T.

The positive ΔH° value illustrates the occurrence of energy barrier in amines adsorption on MCM-41, which reveals the endothermic nature of adsorption. Positive value of ΔS° indicates high degree of freedom of the adsorbed adsorbate. Negative ΔG° values represent the amines adsorption onto MCM-41 is feasible and spontaneous.

Similarly, adsorptive interaction of toxic Zn (II) heavy metal in aqueous solution with synthesized mesoporous silica based MCM-41 was investigated. Further, the effects of presence of Cr (VI) heavy metal on the adsorption of Zn (II) and vice versa were investigated by simultaneous competitive binary adsorption from Cr (VI) and Zn (II) aqueous binary solution. Optimum conditions for Zn (II) treatment were obtained as: pH_i =7, m=0.1 g/L and t=2h. Competitive adsorption of both Cr (VI) and Zn (II) from their binary solution was studied at 288−308K temperatures. Obtained equilibrium data were then fitted to different competitive multicomponent isotherm models like Langmuir (extended), Freundlich isotherm (extended), Sheindrof-Rebuhn-Sheintuch (SRS) isotherm and Redlich-Peterson isotherm (modified) models, and various isotherms and interaction parameters were calculated.

The adsorption capacity (q_e) upsurges with the increase in C_0 and T values, showing adsorption process as adsorbate limiting. It was observed that at any temperature, for persistent Cr (VI) concentration, the equilibrium adsorption uptake of Zn (II) upsurges with increase in initial Zn (II) concentration, whereas, the equilibrium adsorption uptake of Zn (II) declines uninterruptedly with increasing the Cr (VI) concentration. Similar trend was seen for Cr (VI) adsorption with increasing concentration of Zn (II). Zn (II) and Cr (IV) adsorption from their binary aqueous mixture was found antagonistic type. The modified R-P isotherm model suits best to the experimental data obtained from binary adsorption for Zn (II) and Cr (VI) onto MCM-41 at 308 K with lowest MPSD value of 74.47, followed by extended-Freundlich isotherm model and SRS model.

ACKNOWLEDGEMENTS

I devotedly thank the Almighty for providing me the potency to persist on the path to success.

A statement of thanks is not evident to inculcate my deep sense of gratitude and obligation to all who helped me in one way or another in completion of thesis. I would like to take this opportunity to thank many people who helped and encouraged me throughout this research.

I express my deep and sincere gratitude as well as profound regards to **Dr. Jai Prakash Kushwaha and Dr. Vikas K. Sangal** for providing me an opportunity to work under their guidance. Their immense knowledge, expertise and valuable suggestions, patience and motivation provided a great platform for learning and performing research. Their enthusiasm and optimism made this experience both rewarding and enjoyable. Their feedback and editorial comments were also valuable for writing of this thesis

Besides my advisors, I would like to thank the rest of my doctoral committee members: **Dr. Bonamali Pal, Dr. Rajeev Mehta** and **Dr. S. K. Ahuja** for their insightful comments and encouragement.

With the deep sense of gratitude I express my sincere thanks to Head, Department of Chemical engineering, **Prof. H. Bhunia,** who has at all times been very supportive and accommodating.

I would like to thank **Prof. R. K. Gupta** (former Head), **all the faculty members and Staff** of the Department of Chemical Engineering for their cooperation during the duration of this work.

I would like to thank **entire staff** of the **SAI Labs, TIET, Patiala** and **MRC-MNIT, Jaipur** for analysis of my prepared samples.

I sincerely thank to **University Grant Commission, India and Thapar Institute of Engineering and Technology, Patiala** for providing financial support and conducive environment to undertake the research work.

I express my deep sense of gratitude to my family and in-laws. I am thankful to my parents for their great support throughout my life. Words cannot express how grateful I am to my mother, father, grand-mother, grand-father and brother for all of the sacrifices that

they have made on my behalf. Their prayer for me was what sustained me this far. I would cherish every moment where my parents were so keen and curious to know about the details and progress of my work, which boosted my confidence. I would like to appreciate my husband **Er. Robinpreet Singh Sidhu** for always been my emotional strength.

I would like to thank all my colleague and friends **(Ravneet Kaur, Manisha Sharma, Kumar Gaurav, Kamaljit Singh, Bandhana Sharma, Parminder Kaur, Metali Sarkar, Meenakshi, Steffi Talwar and Suman Duhan)** for their constant optimistic support and motivation.

(SEHASPREET KAUR TOOR)

CONTENTS

LIST OF TABLES

LIST OF FIGURES

NOMENCLATURE

ABBREVIATIONS

4-COT	4-chloro-*o*- toluidine
4-ABP	4-aminobiphenyl
MCM-41	Mobil Composition of Matter No. 41
MSN's	Mesoporous silica nanoparticles
BET	Brunauer-Emmett-Teller
FTIR	Fourier transform infrared spectroscopy
XRD	X-ray diffraction
SEM	Scanning Electron Microscopy
EDX	Energy-dispersive X-ray spectroscopy
TEM	Transmission Electron Microscopy
MPSD	Marquardt's percent standard deviation
ppm	Parts per million
rpm	Revolutions per minute

NOTATIONS

pH_i	Initial pH
pH_f	Final pH
m	Adsorbent dose (g/L)
m_{opt}	Optimum adsorbent dose (g/L)
t	Time (min)
T	Temperature (K)

C_0	Initial concentration of adsorbate (mg/L)
C_f	Final concentration of adsorbate (mg/L)
C_t	Concentration of adsorbate at any time t (mg/L)
C_e	Equilibrium concentration of adsorbate (mg/L)
q_t	Adsorption capacity at time t (mg/g)
q_e	Equllibrium adsorption capacity (mg/g)
$q_{e\,exp}$	Equllibrium adsorption capacity (experimental)
k_f	pseudo-first-order rate constant (min^{-1})
k_s	pseudo-second-order rate constant (g/mg/min)
h	Initial adsorption rate (mg/g/min)
K_L	Langmuir constant (L/mg)
K_F	Freundlich constant
1/n	Heterogeneity factor
B, A_T	Temkin constant (L/g)
K_{DR}	Dubinin-Radushkevich isotherm constant (mol^2/ kJ^2)
$\acute{\varepsilon}$	Polanyi potential
Q_{DR}	Theoretical isotherm saturation adsorption capacity (mg/g)
E	Energy of adsorption (kJ/mol)
k_{id}	Intra-particle diffusion rate constant (mg/g $min^{½}$)
I	Intercept (mg/g)
K_{EL}	Extended- Langmuir constant
a_{12}, a_{21}	Competition coefficient
Ad_i	Individual component adsorption
Ad_{tot} %	Total adsorption yield

K_D	Equilibrium constant
R	Universal gas constant (8.314 J/mol K)

GREEK LETTERS

ΔH^0	Heat of adsorption (kJ/mol K)
ΔS°	Entropy change (kJ/mol)
ΔG°	Gibbs free energy change (kJ/mol)

Chapter – 1

INTRODUCTION

1.0. GENERAL

Earth has been bestowed upon by the existence of water which led to evolution of life. Over two thirds of earth's surface is covered with water in forms of oceans, rivers, lakes and inland waters. Unfortunately, these resources are deteriorating rapidly both quantity and quality wise. This situation is attributed to population explosion, industrialization, domestic misuse, geological changes etc. 5–10 billion tons of industrial effluents is generated annually worldwide, out of which maximum amount is dumped directly into rivers, lakes and oceans untreated causing water pollution (https://www.explainthatstuff.com/waterpollution). Presently, water pollution has become a serious issue as it not only threat the aquatic plants and animals, but enters the food chain and effect human health to serious extent. This problem is expected to get even worse over coming years. It is predicted that within decade the present water quantity will decrease to one-third, affecting the life of more than one billion people.

If we consider India, it will be a 'water stressed country' by 2020 with great decrease in water availability to 1600 cum/ person/year. Growing urbanization leads to the discharge of gallons of wastewater in environment. 80% of the total domestic supplied water is liberated as wastewater according to the Central Pollution Control Board (CPCB). Major cities generate around 38,250 MLD (Millions of liters per day) of wastewater in India, which is expected to raise 3.5 times by 2050 (http://vilindia.com/waste-water). The treatment plants in the country are capable of handling only 30% of total generation from which around 55% are operating. If we focus on our industries, 60% of total generated (13468 MLD) industrial effluent is discharged after treatment using activated carbon, air flotation, sand filtration, tank stabilization, sludge drying beds etc. which not only complex and expensive but require regular maintenance. More than seven hundred organic (azo- dyes, Benzene, phenols, DDT, aromatic amines etc.) and inorganic pollutants (heavy metals like Arsenic, Cadmium, Chromium, Cyanide, Fluoride, Lead, Mercury, Selenium etc.) have been reported in wastewater (Ali et al., 2006). Some of these pollutants like aromatic amines and heavy metals are highly toxic due to their hazardous mutagenic and carcinogenic nature and urgently need to be removed from wastewater.

1.1. Aromatic Amines and Heavy Metals

Aromatic amines are defined as compounds containing amino substituents (-NH_2, -NH- or nitrogen group(s)) in aromatic rings. From its simplest form such as aniline to its complex form of conjugated or heterocyclic arrangements having several substituents, found to be toxic in nature. Due to large scale use in number of industries, these amines are reported to enter environment in prominent quantity during the last decade causing carcinogenic and mutagenic effects.

Naturally occurring elements of high atomic weight and density (at least 5 times of water) (Tchounwou et al., 2012) are known as heavy metals including arsenic, copper, cadmium, chromium, lead, mercury, nickel, zinc etc. They are known for their toxicity, non-biodegradability and persistent nature even at low concentration. They are highly required for industrial development which in return is dumped in the form of wastewater. Due to their solubility in water, they can enter into food chain by various aquatic animals and vegetables and may accumulate in human body causing adverse effects.

1.1.1. Sources of aromatic amines and heavy metals in wastewater

a) Aromatic amines: Aromatic amines are liberated in excess in wastewater by number of industries i.e. dyes and textile industries, leather and tannery industry, adhesives and rubbers, pharmaceuticals, synthetic polymers industries, pesticides, agro-industries and oil refining (Bafana et al., 2007; Bafana et al., 2008; Klibanov et al., 1981). Dye and textile industries do not liberate aromatic amines directly in wastewater. They actually discharge Azo dyes (synthetically made organic colorants containing single or double nitrogen-nitrogen bond (R-N=N-R) group), which can be cleaved to form two or more aromatic amines after reduction (for example in the presence of sodium dithionite ($Na_2S_2O_4$)) (Garrigo et al., 2002). Incomplete dye degradation during aerobic-anaerobic biological treatment technique also came up with generation of colorless toxic aromatic amines intermediates (Jayapal et al., 2018). Benzidine based Congo red dye for example can be reduced in vivo to produce carcinogenic aromatic amines (N, N-dimethyl-p-phenylenediamine and N-methyl-p-phenylenediamine) (Garrigo et al., 2002).

Aromatic amine 4-Chloro-*o*-toluidine (4-COT) / 4-chloro-2-methylaniline is a hydrochloride salt and used as an intermediate to produce C.I. 12800, pigment red 7, and pigment yellow 49 azo dyes.

b) Heavy metals: Innumerable industries such as chemical, electroplating, dye and textile, mining, tanneries and leather, paper and pulp, glass and pharmaceutical are responsible for liberation of prominent amount of heavy metals in wastewater (Sharma et al., 2009).

Zinc is abundantly present in the Earth's crust naturally, ranked 23rd among the present elements. Human activities such as mining, coal/ fossil fuel combustion and industrial effluents from steel processing, galvanization, electroplating, paint, batteries, smelting, pesticides and fertilizer, etc. are collectively responsible for increasing concentration of Zinc and Chromium in wastewater (Fellenz et al., 2017; Dinker and Kulkarni, 2015).

1.1.2. Environmental and health impacts of aromatic amines and heavy metals

a) Aromatic amines: Ever since 1895, the toxic and carcinogenic nature of aromatic amines are known. They enter human body by ingestion, inhalation and skin contact. Few aromatic amines are carcinogenic or mutagenic even at minute concentrations. Aromatic amines exposure specifically to benzidine, 2-naphthylamine, and 4-aminobiphenyl causes the risk of bladder cancer. 1, 4-diamino benezene, was reported causing skin irritation, permanent blindness, vomiting gastritis and hypertension (Manzetti et al., 2012). Aromatic amines effects lungs which include upper respiratory tract irritation, congestion, respiratory distress, face, neck, pharynx and tongue oedema. They have been classified as "polar narcotics" in terms of aquatic toxicity. Anilines has been proved to be more toxic than any other pollutant. Algae and a number of fish species like daphnia magna is highly effected by aniline (phenylamine, aminobenzene) (Garrigo et al., 2002).

Popp et al. (1992) studied the mutagenic and carcinogenic effects of aromatic amine 4- Chloro-o-toluidine in humans and found adequate evidence proving that it can be responsible for urinary bladder cancer in humans along with mutagenic effects. Hemangioma **(a** blood vessel tumor in the spleen) of mice were also reported due to excessive exposure of 4-chloro-o-toluidine (NTP, 2011). International Agency for Research on Cancer (IARC) had classified 4-Aminobiphenyl as carcinogenic to humans (Gnanamami et al., 2004). It has also been reported as endocrine disruptor (Kumar et al., 2008).

b) Heavy metals: Almost all heavy metals including arsenic, cadmium, chromium, lead, mercury, nickel, selenium etc. are notorious water pollutants even at low concentration due to non- biodegradable nature (Ali et al., 2006).

In the environment, chromium is found in the form of trivalent [Cr (III)] and hexavalent [Cr (VI)] ions. Cr (VI) has ability to oxidize other species. Due to this it is toxic by five hundred times more than its Cr (III) form. Cr (VI) (i.e. CrO_4^{2-} and $Cr_2O_7^{2-)}$ is very toxic whose accidental intake damages kidney and liver, upsets stomach, causes irritation of eyes, allergy and asthma. It can also burn skin sometimes. Further, it is retained in our body for long time, which causes cancer in lung and kidney and can even lead to death.

Zinc is an essential element for human growth. But if its concentration increases beyond the limit, serious consequences like vomiting, skin irritations, stomach cramps, anemia, depression, lethargy could occur. It leads to poor growth and mental fever (Hojati et al., 2014; Azimi et al., 2017).

1.1.3. Discharge limit of aromatic amines and heavy metals of various countries

Aromatic amines: Harmful and toxic nature of aromatic amines enforced different countries to set rules and regulations on the use of these stuffs. European Union (EU) Directive (Directive 2002/61/EC) and Chinese National Standards (GB/T17592-2006) sets regulations for the use of azo-dye in different industries effluents with maximum allowed levels of aromatic amines are 30 ppm and 20 mg/kg, respectively. According to EU directive, 22 aromatic amines (Table 1.1) producing azo-dyes have been prohibited to use. Apart from these, two other amines are also prohibited by Chinese National standards clearly listed in Table 1.1. Four aromatic amines i.e. 4-Chloro-*o* –toluidine, 4-Aminobiphenyl, Benzidine and 2-Naphthylamine has been put under the category of class 1 carcinogenic.

However, the Indian norms are stipulated as <50 ppm. In India, from 30th January 1993, manufacturing, consumption, storage and sale of benzidine based dyestuffs were banned by law. Discharge limits of heavy metals of various countries is clearly documented in Table 1.2 with least permissible limit of 100 µg/L (0.1 ppm) for Chromium and maximum of 5000 µg/L (5 ppm) for Zinc. These low disposal values in ppm itself depicts the harmful and toxic nature of heavy metals which urgently need to be treated.

Table 1.1. List of European Union (EU) Directive and restricted aromatic amines.

CAS Number	Chemical Name	CAS Number	Chemical Name
95-69-2	4-Chloro-*o* -toluidine	119-90-4	3,3'-Dimethoxybenzidine
92-67-1	4-Aminobiphenyl	119-93-7	3,3'-Dimethylbenzidine
92-87-5	Benzidine	838-88-0	3,3'-Dimethyl-4,4'-diamino-diphenylmethane
91-59-8	2-Naphthylamine	101-14-4	4,4'-Methylene-bis-(2-chloro aniline)
90-04-0	*o* -Anisidine	101-80-4	4,4'-Oxydianiline
99-55-8	2-Amino-4-nitrotoluene	139-65-1	4,4'-Thiodianiline
106-47-8	*p* -Chloroaniline	95-80-7	2,4-Toluenediamine
97-56-3	*o* -Aminoazotoluene	95-53-4	*o*-Toluidine
120-71-8	*p* –Cresidine	137-17-7	2,4,5-Trimethylaniline
615-05-4	2,4-Diaminoanisole	60-09-3	4-Amino azobenzene*
101-77-9	4,4'-Diamino-diphenyl methane	95-68-1	2,4-Xylidine**
91-94-1	3,3'-Dichlorobenzidine	87-62-7	2,6-Xylidine**

Source: Directive 2002/61/EC

*Applicable in the European Union Regulation Only

** Applicable in the Chinese Regulation only

Table 1.2. Discharge limits of heavy metals of various countries.

Parameter	CCME	China	BIS and CPCB	FEPA
Chromium mg/L	0.001	-	0.1	<0.1
Copper mg/L	<1	1	3	<1
Iron mg/L	0.3	-	3	20
Manganese mg/L	0.005	2	2	0.005
Zinc mg/L	0.03	5	5	<10

Source: Ghaly et al., 2014

CCME - Canadian Council of Ministers of the Environment; BIS - Bureau of Indian Standards; CPCB – Central Pollution Control Board; FEPA - Federal Environmental Protection Agency (United States)

1.2. Available Methods for Treatment of Aromatic Amines and Heavy Metals from Wastewater

Various physical or physico-chemical methods such as precipitation, coagulation/ flocculation, adsorption, ion exchange, and membrane filtration including reverse osmosis; biological and electrochemical techniques have been reported and efficiently used for the removal of both aromatic amines and heavy metals (Sharma et al., 2009).

1.2.1. Biological Treatment

Biological treatment is a secondary treatment process using wide variety of micro-organisms and bacteria whereby removal takes place either by contaminants adsorption on the activated sludge or by biological degradation. On the basis of the presence of oxygen in the system, it classifies into 2 types: aerobic and anerobic treatment.

Biological treatment reported so far for aromatic amines removal proceeds in two stages. The first stage comprises of reductive cleavage of azo dyes, forming colorless aromatic amines in anaerobic conditions. The second stage implicates aromatic amines degradation aerobically but suffers from major drawback of long retention times (Işik et al., 2003; Koupaie et al., 2011; Baeta et al., 2015). Enzymes such as phenol oxidases (Husain et al., 2000); Horseradish peroxidase (Klibanov et al., 1981); Tyrosinase (Wada et al., 1995) catalysed the oxidation of water soluble aromatic amines into water insoluble products.

Biofiltration system degrade the pollutants by aerobic/anaerobic biological degradation using facultative, bacteria, fungi, algae and protozoa microorganisms attached to a porous medium. Srivastava et al. (2008) reviewed different heavy metals removal microbial cloning technique, conditions and efficiency by genetically modified microorganisms. Chan et al. (2013) utilized three microalgae; *Chlorella vulgaris*, *Spirulina maxima* and a naturally growing algae sample found in the wastewater for treatment of heavy metals (Zn and Cu) and maximum removal up to 81.7% of the copper and zinc up to 94.1% after 10 days were reported.

1.2.2. Electrochemical Treatment

Electro-chemical Techniques i.e. consist of electro-coagulation, electro-flotation and electro-oxidation and electro-Fenton methods are used which break down the contaminants into simpler fragments using electrodes. Electrodialysis /ion oxidation had shown good electro-degradation of some of the aromatic amines (Pacheco et al., 2011). Zheng et al. (2019) successfully investigated the complete degradation of *p*-chloro-aniline using electrochemical reactor consists of Ti/SnO_2-Sb anode after 90 minutes of electrolysis.

Zhao et al. (2018 (b)) reports various research trends for the treatment of chromium pollution from wastewater using electrochemical-based remediation strategies. Authors clearly describes various electrochemical methods including electro-deionization, electro-dialysis, electrochemical reduction, and electrocoagulation and their efficiency at various conditions for Cr remediation.

1.2.3. Physical or physico-chemical techniques

Physical or physico-chemical techniques includes number of conventional methods such as precipitation, coagulation/ flocculation, adsorption, ion exchange, and membrane filtration including reverse osmosis and chemical oxidation etc. Literature includes extensive study on these methods i.e. froth flotation (Nyssen et al., 1990), reverse osmosis (Gómez et al., 2009), chemical oxidation (Laha et al., 1990; Casero et al., 1997; Alam et al., 2000) for effective removal of aromatic amines from wastewater. Kurnianwan et al. (2006) and Fu et al. (2011) reviewed the various research articles on different physico-chemical methods for treatment of heavy metals. It is evident from the literature that the method of adsorption is the most frequently and vastly applied process and efficiently used worldwide for the treatment of contaminated wastewater.

1.2.3.1. Adsorption: Adsorption is simple, effective and economically attractive surface phenomenon in which pollutant (adsorbate) in form of gas or liquid gets adsorbed onto the surface of the adsorbent. Adsorbents are generally solid substances exists in different forms i.e. spherical pellets, rods, monoliths, etc. with radius of about 0.25-5mm and high surface area. It doesn't discharge any harmful byproducts and offers large treatment efficiency. Activated carbon has been the most popular adsorbent and been reported for adsorption of many aromatic amines (Oda et al., 1983) and heavy metals (Selvi et al., 2001; Rao et al., 2008).

But each of the techniques mentioned in section 1.2 has its technical and economical limitations briefly described in Table 1.3. However, among these numerous techniques practised so-far for wastewater treatment, adsorption has proved to be the most flexible, reliable, effective and economical method.

Adsorption using activated carbon is efficient but is a cost intensive process as it is required in huge quantities and requires larger contact times (Table. 1.3.).These shortcomings has fascinated scientists to develop inexpensive adsorbents using different agricultural and industrial by-products such as fly ash, coal ash, rice husk, coconut husk (Bhatnagar et al., 2006), biochar (Wang et al., 2019), clay materials (Bentonite, montmorillonite) etc. have been used effectively.

Biomass of *Azadirachta indica* bark has been used by King et al. (2008) to remove Zn metal ions with adsorption capacity of 33.49 mg/g. Mishra and Tripathi et al. (2008) tested *Eichhornia crassipes* (water hyacinth) for removal of Cr and Zn from metal solution. Megatelli et al. (2009) studied the adsorption of distinct metal ions cadmium, copper and zinc using aquatic plant *Lemnagibba* under controlled conditions and found that Zn and Cu removal was rapid initially, followed by slower process. Recently, Bagherjeri et al. (2019) reported the use of Bentonite for aromatic amines adsorption. Use of waste by-products as adsorbents contributes well towards waste management and prove to be efficient economic method for wastewater treatment efficiently replacing activated carbon (Fu et al., 2011).

Table 1.3. Limitations and advantages of various methods for aromatic amines and heavy metals removal.

Treatment methodology	Advantages	Limitations
Precipitation, Coagulation, flocculation	Low capital requirement. Less detention time. Efficient filtration process.	Formation of sludge. Fixed operating conditions.
Aerobic process / Anaerobic process	Decolourization of almost all types of dyes. Produces bio gas that can be recycled.	Expensive treatment. Longer acclimatization phase. Cannot be applied to toxic effluents.
Enzymatic treatment	Effective only for specific compounds. Requires shorter contact time.	Isolation of enzyme and its cleansing is difficult. Interferences can decrease the efficiency.
Chemical oxidation process	Eliminates all type of impurity without any discrimination.	Cost intensive process.
Electro-chemical	No additional chemicals are required. Cleaner and Compact.	Cost intensive process; due to high energy requirement.
Reverse Osmosis	Disposes very less amount which minimalizes the disposal cost.	Membranes need to be replaced after certain time period.
Adsorption using activated carbon	Simple and economically attractive. Do not discharge any harmful by products. Easy lab scale to field scale setup.	Huge quantity of adsorbent is needed. Time consuming treatment.

Since last two decades, nanotechnology and its applications has been developed in almost all branches of engineering, science and technology. Wastewater treatment by different nanoparticles has been extensively explored by different research groups (Amin et al., 2014; Kurniawan et al., 2012). Various nano-size adsorbents had been successfully synthesized with distinct properties of large surface area and pore size and used for effective removal of various water pollutants depicting enhanced adsorption capacity at cheap price (Kyzas et al., 2015; Sharma et al., 2009; Wang et al., 2012). Recently more emphasis has been paid to replace conventional adsorbents with nanoparticles and nanoadsorbents including mesoporous materials as viable alternatives to these available adsorbents.

1.2.3.2. Nanoadsorbents and mesoporous materials: Due to small size and high surface areas, large number of active sites are available at surface making unique physical and chemical properties such as high reactivity which makes them promising efficient absorbing material than other materials. Main features includes ease of separation, efficiency, cost effectiveness and ability for functionalization to enhance their affinity towards a particular contaminant. Nanoadsorbents can be broadly classified as metallic and metal- oxide nanoparticles, magnetic nanoparticles, carbonaceous nanoparticles and silica nanoparticles etc.

Mesoporous material contains pores within diameters 2 to 50 nm; microporous material as a material having pores less than 2 nm in diameter and pores larger than 50 nm in diameter comes under the category of macroporous materials as per IUPAC nomenclature. Porous materials having large porosities (more than 0.4), and small pore diameters within the range of (1-100 nm) are called nanoporous materials (Lu & Zhau 2004). From past few years, the use of mesoporous silica-based nanoparticles/ nanoadsorbents has created extensive interest for researchers for wastewater treatment due to their unique properties including large surface area, ordered pore structure and controllable pore size.

1.2.3.3. Mesoporous silica nanoparticles (MSNs): Nanoparticles containing silica as parent compound and having pore size within 2-50 nm range are known as mesoporous silica nanoparticles (MSNs).

MCM-41, stands for the Mobil Composition of Matter No. 41, associated with M41S family, is a synthetic ordered mesoporous silica of hexagonal geometry, developed by Mobile scientists in 1992 (Zhao et al., 2012). It overcome the demerits of zeolites of small pore size and are characterized with high surface area and mesoporous pore size distribution. Their thermal, hydrothermal and hydrolytic stability along with pore size can be improved by varying silica content, surfactant used and synthesis conditions (Table 2.1) as per requirement. This encourages its possible applications for adsorption and catalytic processes. (Mirzajani et al., 2016; Santos et al., 2013).

Chapter – 2

LITERATURE REVIEW

2.0. GENERAL

This chapter comprehends the review of literature available so far for removal of aromatic amines and heavy metals from wastewater using various adsorbents with main emphasis on mesoporous silica nanoparticles MCM-41. Based on literature review research gaps have been identified and objectives were set.

2.1. TREATMENT OF AROMATIC AMINES AND HEAVY METALS USING ACTIVATED CARBON

Activated carbon, occasionally called active charcoal is a carbon material with characteristics of high surface area and pores in the structure which lets adsorption of small molecules with high adsorption capacity due to which it has vast applications in the field of gas or liquid purification. Owing to good adsorption capacity and easy operation towards dissolved components in wastewater, it has been the first preference for treatment of industrial and municipal wastewater using the process of adsorption since 1940s.

2.1.1. Adsorption of Aromatic Amines using Activated Carbon

Oda et al. (1983) demonstrated the surface acidity effect on the adsorption of various aromatic amines i.e. aniline, N methylaniline and N, N-dimethylaniline along with 4 types of phenols and sovents benzene and ethyl-alcohol by 12 different types of activated carbons of different surface area (680-1160 m^2/g), pore structure, pore volume (0.25-0.13 ml/g) and acidity. It was found that the when adsorbent was heated, no change in the pore structure was observed. However, adsorption decreases with heating of carbon. With Increase in acidity, adsorption selectivity and capacity increases. The adsorption behavior of Diphenylamine (DPAM), Napthylamine (NAM), and aniline on pyrolusite and activated carbon has been studied by Rao et al. (2001). Pyrolusite shows remarkable sorption capacity for diphenylamine and napthylamine as compared to aniline. The maximum adsorption of NAM occurred in the concentration range 4–20 g mL^{-1} on pyrolusite (95%) and 4–50 g mL^{-1} on activated carbon (100%).

Three different aromatic compounds i.e. phenol, aniline and nitrobenzene was adsorbed onto surface modification of commercially available activated carbon (Villacañas et al., 2006). Activated carbon was modified with HNO_3 (chemically treated) and H_2 (thermally treated) with not much change in the texture of the adsorbent. Maximum removal for aniline was achieved by HNO_3 modified activated carbon at pH=2, which may be attributed to electrostatic interactions. However, at all other pH maximum removal was obtained by basic H_2 modified activated carbon owe to dispersive interactions. Further, it was found that surface area is a key factor in adsorption and adsorption capacity is directly proportional to surface area. Li et al. (2009) also modified commercially available activated carbon with different acids HNO_3, HCl and HF and adsorbed aniline, pyridine, phenol and benzene with maximum adsorption capacity of 2.612 mmol/g for aniline. It was concluded that adsorption capacity decreases to great extent with increase in surface acidity with surface area exhibiting least effect.

2.1.2. Adsorption of Heavy Metals using Activated Carbon

Selvi et al. (2001) prepared activated carbon from coconut tree sawdust and used it as efficient adsorbent to remove Cr (VI) from aqueous solution. Time of adsorption, solution pH, adsorbate concentration and adsorbent dose was varied to study their effects on adsorption. Maximum adsorption capacity of 3.46 mg/g at pH-3 using Langmuir isotherm was obtained. Acidic pH favours adsorption as Cr (VI) exists in the anionic form $HCrO_4^{2-}$, which shows large attraction towards protonated adsorbent. Rao et al. (2008) utilized an agricultural waste (*ceiba pentandra hulls)* to prepare activated carbon and studied its ability as adsorbent for heavy metal (Zinc and lead) removal. It was observed that maximum removal of lead (99.5%) and zinc (99.1%) was obtained at optimum conditions of pH-6, Adsorbent dose=10 g/L, adsorbate concentration= 50 mg/L with equilibrium time of 50 minutes. Maximum adsorption capacity of 25.5 and 24.1 mg/g for lead and zinc respectively was calculated using Freundlich isotherm.

Adebisi et al. (2017) prepared activated carbon using palm oil mill effluent and utilized it for Pb (II) and Zn (II) removal from wastewater. Influence of adsorbent dose and initial metal ions concentration was done over ample range and observed that increase in both metal ion concentration and dose, adsorption capacity increases with maximum adsorption capacity of 94.34 mg/g and 68.49 mg/g for Pb (II) and Zn (II) respectively at 353.15 K. Thermodynamic data reveals the feasible and endothermic nature of adsorption. Whereas, Li et al. (2018)

prepared activated carbon from coal mixed sewage sludge and modified it with thiol for application of heavy metal removal. They achieved 1094 m^2/g adsorption surface area with maximum adsorption capacity of 238.1mg/g for Pb (II) metal ion.

Recently, Gu et al. (2019) prepared magnetic activated carbon by coating Fe_3O_4 nanoparticles on activated carbon and employed it for Cu (II) removal. Fe_3O_4 magnetic nanoparticles synthesized by co-precipitation method when loaded onto carbon material not only increases its adsorption capacity but also enhances separation and regeneration efficacy. With Langmuir adsorption capacity of 20.7 mg/g, adsorption proves to follow chemical ion exchange instead of physical adsorption.

2.2. TREATMENT OF AROMATIC AMINES AND HEAVY METALS USING VARIOUS NANOPARTICLES

Adsorption using nanoparticles have proved to be promising method for treatment of wastewater. However, it is governed by surface properties of the adsorbent like surface area and ion exchange sites. Number of scientific groups and investigators had explored vast variety of nano-materials for selective water pollutants removal.

2.2.1. Adsorption of Aromatic Amines using Various Nanoparticles

Polymer based nanoparticles have been reported by various research groups for aromatic amines removal from wastewater with high efficacy. Bifunctional polymeric resin (LS-2) was synthesized by Jianguo and co-workers (2005) by fixing of sulfonic groups on the resin surface. It was reported as efficient nano-adsorbent for aniline and 4-methyl-aniline adsorption.

Coated magnetic nanoparticles were synthesized and applied for removal of three carcinogenic aromatic amines i.e. p-chloroaniline, benzidine and α-Napthalamine by Aksoy et al. (2012) with high percentage removal of 44-97% in the pH-range 3 to 8.5 with maximum removal reported at pH=3. Electrostatic interactions and hydrogen bonding evidenced to be main reasons beyond adsorption. Adsorption study of same three amines along with azo dyes were reported by Yilmaz et al. (2010) using two cyclodextrin (glucose based molecules) with main emphasis on sorption mechanism involved.

Water solube polymer Polyacrlamide (PAM) has been used extensively for treatment of wastewater. An et al. (2009) successfully functionalized acrylamide (AM) by grafting method. Grafting was done on the silica gel surface step by step using 3 methacryloxypropyl trimethoxy-silane (MPS). This prepared novel adsorbent PAM/SiO_2 has high adsorption capacity of 26.84 mg/g for aniline adsorption. Additional, it possesses excellent reusability.

Erdemir et al. (2009) investigated removal of three carcinogenic aromatic amines i.e. Benzidine, p-chloroaniline and napthylamine using polymer calix[*n*] arenes. Nearly at each pH, octacarboxylic acid which is derivative of p-tert- butylcalix [8] arene showed better affinity. Maximum removal upto 84% for $n = 5$ and 99% for $n = 6$ at pH 4.0 was obtained. The main advantage of these type of adsorbents is easy regeneration by simple washing in acidic media with 2M HCl which doesn't effect sorption capacities. Carboxylic acid derivative of calix[*n*]arenes (5) and (6) shows higher adsorption capacities than calix[*n*]arenes (1) and (2). Similar studies have been done by Akceylan et al. (2009) for the removal of same three aromatic amines i.e. Benzidine, p-chloroaniline, napthylamine using calix[4]arene-based polymer with removal efficiency of about 95-97%.

Kakavandi et al. (2013) investigated Fe_3O_4 nanoparticles modified activated carbon as an adsorbent for aniline removal and obtained maximum adsorption capacity of 90.91 mg/g at pH = 6, contact time=5h and 20°C. These magnetic nanoparticles exhibits large surface area and shows rapid and easy separation from aqueous media. Cu^{2+} impregnated chitosan/alumina nanocomposite synthesized by Zavareh et al. (2015) proves to be highly selective material towards aniline in presence of Cu (II) anions.

Rani et al. (2017) synthesized metal hexacyanoferrates nanocubes by green process for removal of some carcinogenic amines with maximum removal for p-anisidine followed by p-toluidine, aniline and *p*-chloroaniline and concluded that adsorption of these amines depends directly on the surface area of adsorbent and basicity of amines.

2.2.2. Adsorption of Heavy Metals using Various Nanoparticles

Hundreds of nanoparticles have proved to be efficient selective adsorbent towards all heavy metals. They include metallic oxide nanoparticles (Al_2O_3, ZnO, and TiO_2 NPs), metallic nanoparticles (Au, Ag NPs), magnetic nanoparticles (Fe_2O_3 NPs); carbon and silicon nanotubes; silicon nanomaterials (SiO_2); nanofibers; nanoclays; polymer-based nano

adsorbents and xerogels and aerogels have been reported for various heavy metal ions removal including As(III), As(VI), Cu(II), Cr(VI), Zn(II), Co(II), Hg(II) etc. The potential of nanomaterials as nanoadsorbents for heavy metal removal and their many advances have been critically scanned and discussed in various review articles (Ali 2012; Khajeh et al., 2013; Kyzas et al., 2015; Sharma et al., 2009) and summarized below:

a) Metal/ metal-oxide/ magnetic nanoparticles: Variety of metal oxides are synthesized in nano-scale like manganese and magnesium oxides, titanium oxides, aluminum oxides, Zinc oxides, copper oxide, iron oxides, cerium oxides etc. for wastewater remedies with main emphasis on shape, size and stability as removal efficacy depends highly on surface area, shape, pore size and affinity towards metal ions of these synthesized materials. To control size and shape different synthesis approaches have been followed. They include chemical co-precipitation method, hydrothermal method, micro-emulsions, sol-gel method, liquid phase reduction, thermal decomposition or reduction, gas or liquid reduction etc. Co-precipitation, hydrothermal method and sol-gel method are the mostly applied methods in literature (Hua et al., 2012).

Magnetic nanoparticles include various iron oxide nanoparticles with good magnetic properties. Fe_3O_4 or Fe_2O_3 nanoparticles can be synthesized by Co-precipitation method which provide high removal percentage of about 87% for Cr (VI) and 94.1 % for Ni (II) (Hua et al., 2012). To further improve the removal percentage these iron oxide nanoparticles were coated with different metals such as $MnFe_2O_4$, $MgFe_2O_4$, $ZnFe_2O_4$, $CuFe_2O_4$, Ni Fe_2O_4 with $MnFe_2O_4$ shows maximum removal of 99.5% for Cr (VI) metal ions at pH=2 from wastewater (Ali, 2012). Not much work has been reported for Zn(II) but nanocrystalline akaganeite give adsorption capacity of 35 mg/g for Zn(II) and 80 mg/g for Cr (VI) removal whereas maghemite shows low adsorption capacity of 19.2 mg/g for Cr (VI) (Hua et al., 2012). Along with high efficiency and less contact time, metal and metal oxide nanoparticles reported to be reused number of times due to easy regeneration with NaOH or HCl solutions.

b) Polymer based nanoadsorbents: For utilization of polymer as an efficient adsorbent it should possess perfect strength, adjustable surface groups, regeneration capability, harmless and degradable in environment. Synthesis methods can be classified as self- assembly process, sol gel process, dispersion or assembling of nano-building blocks and interpenetrating method.

Number of polymers had been reported to functionalized distinct nanomaterials for heavy metal ions removal like PPy-PANI nanofibers, poly(ethyleneimine)-silica gel, PPy-montmorillonite clay composite, PMAA grafted chitosan –betonite composites, Polyamido-amine modified GO and so on (Zhao et al., 2018 (a)).

Magnetic nanoparticles has been also modified by various researchers to improve their efficacy towards heavy metals. They include Fe/ PANI and PVA-Fe nanocomposites, Carboxymethyl- β cyclodextrin-Fe_3O_4, PPy/ Fe_3O_4 nanocomposites etc. Fe/PANI proves to be more efficient among them all with maximum adsorption capacity of 434.78 mg/g for Cr (VI) removal followed by PPy/ Fe_3O_4 nanocomposites with 169.49 mg/g (Zhao et al. 2018 (a)).

c) Carbon based nanoadsorbents: They include nanoparticles with carbon as main ingredient. They range from fullerenes, carbon nanotubes, graphene, graphene oxides and quantum dots based on carbon. In wastewater treatment, graphene and carbon nanotubes had drawn much attention in recent years.

Highly stable carbon nanotubes are of two types: Single wall carbon nanotube (SWCNT) and multiwall carbon nanotube (MWCNT). These tubes are oxidized with $KMnO_3$, H_2O_2 or HNO_3 to get more hydrophilic surface and to increases its ion exchange capacity (Ali, 2012). However, no oxidation is required for graphene. Xu et al. (2018) compiled the data of reported oxidized /modified/ functionalized CNT's in field of wastewater treatment and conclude that preparation methods and conditions plays the vital role in size, structure, composition and affinity towards different pollutants. Few studies address the effect of synthesis conditions like temperature, pH, time and chemicals used.

Graphene oxide was modified with variety of materials like iron oxides i.e. Fe_3O_4/GO, $MnFe_3O_4$/GO, NH_2-Fe_3O_4/GO etc. with $MnFe_3O_4$/GO exhibiting highest adsorption capacity of 207 mg/g (Xu et al., 2018). Similarly, CNT'S were functionalized by numerous research groups with organic, inorganic and magnetic materials like OH-MWCNT, COOH-MWCNT, Fe $^{2+/}$ Fe_3O_4 MWCNT, TiO_2-MWCNT to enhance its adsorption capacity from15.9 mg/g for MWCNT to181.8 mg/g for CS-MWCNT-COOH (Xu et al., 2018).

d) Mesoporous silica based nanoadsorbents: This class came into existence in 1992 by mobil oil company who formed mesoporous silica known as M41S phase with three main representatives MCM-41 **(**hexagonal arrangement of mesoporous), MCM-48 (cubic

arrangement of mesopores) and MCM-50 (laminar structure) extended by other materials SBA-15, SBA-16, SBA-3, FDU-12 (based on different synthesis methods and precursors taken) etc. MCM-41 has been chosen by maximum researchers due to ease in synthesis procedure and attraction towards diverse pollutants, organic (azo-dyes, aromatic amines, alcohols etc.) as well as inorganic including different metal ions tabulated in table 2.2 and 2.3.

Adsorption using nanoparticles have proved to be promising method for treatment of wastewater. However, it is governed by surface properties of the adsorbent like surface area of the adsorbent and ion exchange sites. Recently, mesoporous silica nanoparticles (MSNPs) has found out to be an effective adsorbent with large surface area, pore size and high adsorption capacity at low cost with easy and rapid separation from aqueous solutions and promised to be better solution for water remediation.

2.3. SYNTHESIS OF MCM-41

Literature suggests two methods for synthesis of ordered mesoporous silica nanoparticles (MSN's) i.e. **Soft-templating** and **Hard-templating (nanocasting)** (Zhao et al., 2012). In soft templating, the ordered porous structure is attained by simultaneous cooperative assembly of both organic template and precursor whereas, in hard templating structure came from organic template only. Since organic template is responsible for structure of pores due to which sometimes mentioned as structure-directing agents (SDA). Strong interaction is necessary between the precursor and template to avoid macroscale phase separation (Zhao et al., 2012). Maximum studies follows the hard-templating method as it's easy to depict the pore structure on the basis of template used and can be modified by varying template as per requirement.

MCM-41 is ordered silica that is generally formed by self-assembly of sol-gel precursors (metal alkoxides) and structure directing surfactant. Maximum studies had reported use of combination of sol gel and hydrothermal techniques for synthesis of MCM-41 (Cai et al., 2001; Heidari et al., 2009). Surfactants when added to water forms rod like micelles that align themselves to hexagonal shape due to the template of surfactant itself. Then silica source is added that captures these rod like structures. The sample is then calcinated to remove this template to form mesoporous silica nanoparticles.

Detailed description of steps involved along with optimized condition found in literature (Zhao et al., 2012) for characteristic synthesis of MCM-41 has been tabulated in Table 2.1.

Table 2.1. Synthetic Characteristics of MCM-41

Steps involved	Materials/ conditions
Silica Precursors	Fumed silica, sodium silicate, silica gel, alkyloxyl silanes such as Tetra-ethyl-orthosilicate (TEOS) can be used as silica precursors.
Surfactants	Cationic surfactants generally ammonium salts with moderate chain length (C_8 to C_{22}) are generally used i.e. CTAB- Cetyl trimethyl ammonium bromide.
Synthesis media	Basic media is preferred with optimum pH 9.5-11.5 attained using NaOH or KOH or ammonia salt.
Temperature	-10 to 130 ℃ less than 130℃ because too high temperature can destroy mesostructure.
Pore size control	By increasing surfactant length, (C_8 to C_{22}) pore size can be increased from 1.6-4.2nm. or by adding organic additives TMB (tri-isopropyl-benzene) or poly(propylene glycol)
Template removal	Calcination 1-2 ℃/ min to 550 ℃.

Source: Zhao et al., 2012

2.3.1. Treatment of Aromatic Amines using Various MSNPs

Not much literature has been available for treatment of aromatic amines using MCM-41. First study reported in this area was to remove N-Boc group of aromatic amines using sodium hydrogen sulfate and HY-zeolite made on silica gel by Ravindranath et al., 2003. Study was very precise and didn't provide any information on percentage removal and adsorption capacity and effect of any parameter involved.

Three zeolites namely, Clinoptiolite, ZSM-5-88, ZSM-5-31 along with MCM-41 was successfully synthesized to adsorb phenol, benzene and toluene from aqueous solution by Ghiaci et al. (2004). Almost similar adsorption capacities were shown for benzene and toluene by all adsorbents. Equilibrium data was best fitted to Langmuir isotherm with maximum adsorption capacity of 641, 215, 88 mmol/g for clinoptiolite, ZSM-5-88 and ZSM-5-31 respectively for toluene. Further MCM-41 was synthesized and shows more absorption capacity as compared to previously used zeolites.

Alumino-silica nanoadsorbents (hexagonal and cubic) were synthesized by Safty et al. (2013) to remove *p*-nito-aniline aromatic amine with adsorption capacity of 0.117 mmol/g. Efficiency of the material depends largely on pore size, pore geometry and amount of loading. Theoretical model was established to duly explain the 3-D geometry of the pores and their orientation. Adsorbent was reused successfully several times without any structural damage.

Yang et al. (2011) reported the adsorption of aniline on to MCM-41 and concluded the adsorption capacity of 16.64 mg/g. Main emphasis was given on altering porosity of MCM-41 by studying the effect of the surfactant template and varying their extraction ratio and concluded that removal decreases with complete template removal. Adsorption was found to be exothermic with maximum removal in acidic pH of 2 with good ability to regenerate.

Recently, Liang et al. (2017) modified MCM-41 with different amounts of Fe to enhance removal and adsorption characteristics of aniline. It was found out that Fe enhances the affinity of MCM-41 towards aniline by deviating pore structure with maximum Fe loaded (8.76% by weight) results high adsorption capacity of 17.96 mg/g at pH-7. Physio-chemical adsorption and electrostatic interactions were the mechanisms involved behind adsorption.

2.3.2. Treatment of Heavy Metals using Various MSNPs

Simple MCM 41 was synthesized by Du et al., 2011 using clay (montmorillonite and kaolinite) as silica source by a hydrothermal method for Pb (II) ions removal and observes that adsorption process strongly depends on pH and is spontaneous and endothermic.

Similary, Tian et al. (2011) also reported efficient Cr (VI) treatment using synthesized MCM-41 giving detailed kinetic and adsorption mechanism. Hydrothermal method using tetra ethyl silicate as silica source and surfactant cetyl-trimethyl-ammonium bromide proved to provide high surface area of 1040 m^2/g which results high adsorption capacity of 904 mg/g using Langmuir isotherm. Thermodynamic study revealed endothermic and spontaneous nature of adsorption with positive ΔH^0 value of 40 kJ/mol and ΔS° value of 141 kJ/mol/K.

Recently, He et al. (2018) synthesized MCM-41 using co-condensation process for efficient removal of Ni^{2+} ions from real wastewater from electroplating industry with rapid initial uptake and adsorption of 90.9% at pH=6.

To improve the adsorption capacity, these mesoporous materials can be functionalized by huge number of organic, inorganic, polymeric, and ionic liquid based materials (Dinker and Kulkarni 2015).

Several research groups including Algarra et al. (2005); Benhamou et al. (2009); Heidari et al. (2009) ; Zhu et al.(2012); Benhamou et al.(2013); Fellenz et al.(2015) and Fellenz et al.(2017) functionalized MCM-41 by different amino groups to enhance heavy metals adsorption capacity. In all these studies synthesized MCM-41 was modified with different amino groups and characterized using various characterization techniques to confirm modification. Further adsorption of different metal ions was done at different conditions (Table 2.3) and concluded that adsorption capacity of respective metal ions increases with surface modification.

Iron oxide/mesoporous silica nanocomposites were functionalized using aminopropyl, and proved to be better adsorbents for Cr(III) and Cu(II) cations, however, showed lower affinities towards anions like chromate and arsenate (Egodawatte et al., 2015; Mehdinia et al., 2015). Li et al. (2011) functionalized Fe_3O_4 nanoparticles with MPTS using stober method onto MCM-41 whereas, Azizi et al. (2015) used chelating agent along with Fe_3O_4 to modify MCM-41 which along with high surface area shows super-paramagnetic character.

Wu et al. (2010) modified synthesized MCM-41 with Thiol using MPTS (3-mercapto-propyltrimthoxy-silane) salt using different molar ratios of TEOS and MPTS with optimum ratio 4, which as a result increases the surface area, pore size and pore volume of adsorbent enhancing adsorption capacity.

Only single study by Kumar et al. (2013), has been reported in literature so far for adsorption of Zn (II) ions from wastewater using MCM-41. They functionalized amino- MCM-41 with EDTA (Ethylenediamine-tetra-acetic acid) with high efficacy of 675.67 mg/g. Adsorption seems to follows second order kinetics and endothermic in nature.

Table 2.2 and 2.3 compares the work carried out by various researchers using MCM-41 as adsorbent for removal of different aromatic amines and heavy metal ions from wastewater respectively.

Table 2.2. MCM-41 for removal of aromatic amines from wastewater.

S. No.	Adsorbent	Pollutants Removed	Conditions	Adsorption Capacity	References
1.	Organic zeolites: Clinoptiolite, ZSM-5-88, ZSM-5-31	Benzene, toulene	pH- 7; Temperature- 25°C	641, 215, 88 mmol/g for clinoptiolite, ZSM-5-88 and ZSM-5-31, respectively, for toluene	(Ghiaci et al., 2004)
2.	Hexagonal, cubic alumino-silica	*p*-nitro-aniline	Adsorbent dose- 10g/L; Temperature- 45°C	0.117 mmol/g	(Safty et al., 2013)
3.	MCM-41	Aniline	pH- 7; dose -4 g/L; Temperature- 25°C; time- 2 h	16.64 mg/g	(Yang et al., 2011)
4.	Fe-MCM-41	Aniline	pH- 7; dose -1 g/L; Temperature- 25°C; time- 30 min; Pore size: 2.4 nm; Surface area: 1473.6 m^2/g	17.96 mg/g	(Liang et al., 2017)

Table 2.3. Functionalized MCM-41 for removal of heavy metals from wastewater.

S. No.	Adsorbent	Pollutants	Pore Size (nm)/ Surface Area (m^2/g)	Conditions	Adsorption Capacity	References
1.	MCM-41	Pb(II)	3.4; 512.3	pH- 5; dose -0.2 g/L; Temperature- 30°C; time- 24 h	117.0 mg/g	(Du et al., 2011)
2.	MCM-41	Cr (VI)	2.8; 1,040	pH- 4; dose -10 g/L; Temperature- 35°C; time- 2 h	904 mg/g	(Tian et al., 2011)
3.	MCM-41	Ni (II)	2.5; 856.4	pH- 6; dose -1 g/L Temperature- 30°C	20.8 mg/g	(He et al., 2018)
4.	Aminopropyl -Si MCM-41	Ni^{2+} , u^{2+}, Co^{2+}	4.3-4.8; 869	pH- 4; dose -1 g/L; contact time- 2 h; temperature- 30°C	------	(Algarra et al., 2005)
5.	Amino functionalized MCM-41	Ni(II), Cd(II), Pb(II)	1387; 42.22	pH- 5; dose -5 g/L; time- 2 h; temperature- 25°C	12.36, 8.25, 57.74, respectively	(Heidari et al., 2009)
6.	Amine-functionalized MCM-41 and MCM-48	Cd^{2+},Co^{2+}, Cu^{2+}, Pb^{2+}	3.42; 1207	Dose -1 g/L; time- 1h; temperature- 25°C	0.82 mmol/g (Cu)	(Benhamou et al., 2009)
7.	3-aminopropyl triethoxysilane MCM-41	Hg^{2+}	----; 648.53	pH- 6; dose -2 g/L; time- 2 h; temperature- 25°C	231.92 mg/g	(Zhu et al., 2012)

S. No.	Adsorbent	Pollutants	Pore Size (nm)/ Surface Area (m^2/g)	Conditions	Adsorption Capacity	References
8.	Amino-functionalized MCM-41 and MCM-48	Cr(VI) , As(V)	3.97; 1207	pH- 3.1; dose -0.1 g/L; time- 1.5 h; temperature- 25°C	134.6 ± 2.2, 95.2 ± 3 mg/g for Cr (VI), As (V)	(Benhamou et al., 2013)
9.	Amino-propyl functionalized mesoporous silica	Cr(VI)	2.5; 834	pH- 2.2; dose -1 g/L; time- 24 h; Temperature- 25°C	87.1 mg/g	(Fellenz et al., 2015)
10.	Amino-functionalized MCM-41	Cr (VI)	2.4; 517	pH- 2; dose -1 g/L; time- 24 h; temperature- 25°C	86.4 mg/g	(Fellenz et al., 2017)
11.	Fe_3O_4 coated MCM-41 (MMNPs)	Cu^{2+},Ni^{2+}, Co^{2+} ions	15; -----	pH- 7; dose -1 g/L; time- 3 min; temperature- 30°C	0.03, 0.03, 0.04 ng/ml, respectively	(Azizi et al., 2015)
12.	Fe_3O_4/ MCM-41/NH_2	Cr (III)	3.1; 540	pH- 5.4; time- 2h; Temperature- 25°C	2.08 mmol/g	(Egoedaw-ate et al., 2015)
13.	Magnetic di-thio functionalized MCM-41	Hg^{2+}	1.23; 830	pH- 6; dose – 0.3 g/L; time- 10 min; temperature- 25°C	538.9 mg/g	(Mehdinia et al., 2015)

S. No.	Adsorbent	Pollutants	Pore Size (nm)/ Surface Area (m^2/g)	Conditions	Adsorption Capacity	References
14.	Thiol-functionalized magnetic mesoporous silica material	Hg (II), Pb(II)	2.5; 321	pH- 5; dose -10 g/L; time- 2 h; Temperature- 30°C	260 and 91.5 mg/g, respectively	(Li et al., 2011)
15.	EDTA functionalized MCM-41	Cu(II), Zn(II) and Ni(II)	2.8; ----	pH- 5.5; dose -1 g/L; time- 45 min; temperature- 30°C	79.36, 74.07, 67.56 mg /g, respectively	(Kumar et al., 2013)
16.	Thiol-functionalized MCM-41	Cu(II), Pb(II), Ag(I), Cr(III)	5.27; 421.9	pH- 5; dose -1g/L; time- 1 h; temperature- 30°C	38.12, 66.04 , 92.08, 13.84 mg/g, respectivel.	(Wu et al., 2010)

2.4. RESEARCH GAPS

It is clear from literature review that most of the attention has been paid to the adsorption onto activated carbon for the removal of aromatic amines. A look into literature shows that there is no description regarding degradation of any aromatic amine including 4- Chloro-o- toluidine (4-COT) and 4- Aminobiphenyl (4-ABP) using mesoporous MCM-41.

If we consider heavy metal ions removal using silica based MCM-41 numerous work has been reported by adsorption onto MCM-41 and chemically modified MCM-41 (Table 2.1). However no research has been reported on Zinc removal using MCM-41 except Kumar et al., (2013), which treated Zn (II) ions using EDTA functionalized silica. However no description has been given by them regarding its removal using simple MCM-41 without any functionalization.

Also literature lacks study on simultaneous removal of two or more metal ions. No work has been reported so far our knowledge concerning the binary system for heavy metals removal using MCM-41 including Zn (II) and Cr (VI).

2.5. OBJECTIVES

The main aim of this study was to synthesize and characterize nanoadsorbents and evaluate their efficacy as adsorbents for the removal of aromatic amines and heavy metals from aqueous solution. In meeting the above goal, the following specific objectives are to be apprehended:

1. To synthesize and characterize MCM-41 for enhanced adsorption of aromatic amines (4- chloro-o-toluidine, 4- aminobiphenyl) and heavy metals (Cr^{6+}, Zn^{2+}).
2. To study effect of various adsorption parameters such as contact time, pH, adsorbent dose, adsorbate concentration and temperature on removal of above mentioned aromatic amines and heavy metals.
3. To perform kinetic and thermodynamic studies.

Chapter - 3

SYNTHESIS & CHARACTERIZATION OF MCM-41

3.0. GENERAL

In this chapter, synthesis of MCM-41 and its characteristics pursued using different characterization techniques have been discussed.

3.1. MATERIALS AND METHODS

3.1.1. Chemicals

Reagent grade analytical chemicals were used in this study. Tetraethyl-orthosilicate (TEOS), Cetyltrimethyl ammonium bromide (CTAB) were obtained from Sigma-Aldrich, India. NaOH was provided by Loba Chemie Pvt. Ltd., Mumbai, India.

3.1.2. Synthesis of MCM-41

MCM-41 nanoparticles were synthesized by hydrothermal method (Cai et al., 2001) using silica source, tetraethyl orthosilicate (TEOS), and surfactant, Cetyl trimethyl ammonium bromide (CTAB). 2M NaOH solution (3.5 ml) was mixed with 480 ml distilled water following the addition of 1.0 g of surfactant in stirring condition. This solution was heated up to 80° C, and 5 ml of TEOS was added in the homogeneous solution drop wise in stirring mode. Stirring was continued for 2 h, and ultimately white slurry was formed. Then after, the formed slurry solution was aged overnight at ambient temperature. This solution was further filtered, and collected white suspension was fully washed with distilled water and dehydrated in oven at 90 °C. Further, calcination was performed in muffle furnace in the presence of air at 550 °C at the fixed rate of 1°C per minute for 6 h to remove template.

3.1.3. Characterization Techniques

Characterization techniques are employed to measure material's structural, physical as well as chemical properties. Section 3.1.3.1 to 3.1.3.5 enclose the various characterization techniques used to investigate synthesized MCM-41 nanoparticles and results obtained.

3.1.3.1. BET Analysis*:* Surface area is a crucial parameter for optimizing the applicability of porous materials. BET surface area analyzer (BELSORP mini-II., Microtrac BEL Corp, Japan) yielded N_2- adsorption- desorption isotherms at 77K. In this technique, amount of nitrogen absorbed per unit mass of the solid (cm^3/g) and the relative pressure (P/P_0) at STP are used to determine the distribution of pore volume against pore size of adsorbent. Shape of this plot determines whether sample is microporous (pore size < 2nm; Type I isotherm); macroporous (pore size > 50 nm; Type II and Type III isotherms) or mesoporous (pore size 2-50 nm; Type IV isotherms). Before doing measurements, the samples were outgassed at 573K for 6h. It delivers significant information about material‘s surface area as well as porosity by using the BET (Brunauer-Emmett-Teller) equation. This obtained data also provides the BJH (Barret-Joyner- Halenda) plot which gives us pore size distribution of the mesoporous solid.

3.1.3.2. X- Ray Powder Diffraction (XRD): XRD is an analytical technique applied for the identification of the crystalline material. It provides useful information about the atomic and molecular structure of the crystal using Bragg’s law. The structure and crystallinity of synthesized MCM-41 was analyzed with XRD (Pan Alytical, Philips, Neatherlands) using Cu-Kα (λ=1.5418 Å). Sample was examined at 2θ: 0.5°-10°; step size: 0.02°; count time: 1 second; voltage: 40 kV; current: 40 mA.

3.1.3.3. Fourier transform infrared spectroscopy (FTIR): Identification of organic, inorganic and polymer materials can be done using FTIR by recording infrared spectrum of absorbance or transmittance of any material. Here in this study, it was done by FTIR spectrophotometer (Resolution Pro Carry 660, Agilent Technologies) in the range of 500–4000 cm^{-1}. The samples for FTIR were prepared via making its pellets with KBr (sample/ KBr = 1/100) by means of hydraulic press.

3.1.3.4. Scanning electron microscopy: Morphological information of prepared mesoporous MCM-41 was collected using scanning electron microscopy, FE-SEM (Hitachi X-650, Tokyo, Japan) and for the FE-SEM/ EDX, the homogeneous sample was spread on sample holders making a flat surface. To make them conductive, gold coating was done. Images were taken which provide us with nanoparticle size and shape. Elemental distribution of the synthesized material was confirmed using EDX.

3.1.3.5. Transmission Electron microscopy (TEM): High-resolution TEM was conducted on HR-TEM (Tecnai G^2, FEI Company, U.S.) 200 KV. Specimens for HR-TEM, which is capable of capturing fine details of material even as small as a single column of atom can be prepared simply by dissolving the sample in ethanol. Single drop of the obtained solution was placed on the copper grid coated with a transparent graphite and dried.

3.2. RESULTS AND DISCUSSION

3.2.1. BET Analysis

BET surface area of synthesized MCM-41 was found to be 502.77 $m^2 g^{-1}$. BJH model exhibited 0.85 $cm^3 g^{-1}$ pore volume with 3.21 nm pore size of MCM-41. Nitrogen adsorption/desorption isotherm plot (Fig. 3.1), obtained from BET analysis, was found to be of type IV along with hysteresis loop H1. The condensation step was found arising in the relative pressure range of 0.6–0.95 from condensation of nitrogen into the mesopores of MCM-41, indicating good structural order of MCM-41. This confirms the mesoporous nature of synthesized MCM-41 (Meléndez-Ortiz et al., 2013; Wu et al., 2012).

3.2.2. XRD plot

XRD spectra of MCM-41 exhibited a single peak at 0.98 (Fig.3.2), which is associated with the hexagonal mesophase structure (Santos et al., 2013; Monash et al., 2010; Zheng et al., 2000). Only one low-angle peak corresponding to the mesophase is observed. Since the material is not crystalline at the atomic level, no reflections were observed at the higher angles (Monash et al., 2010).

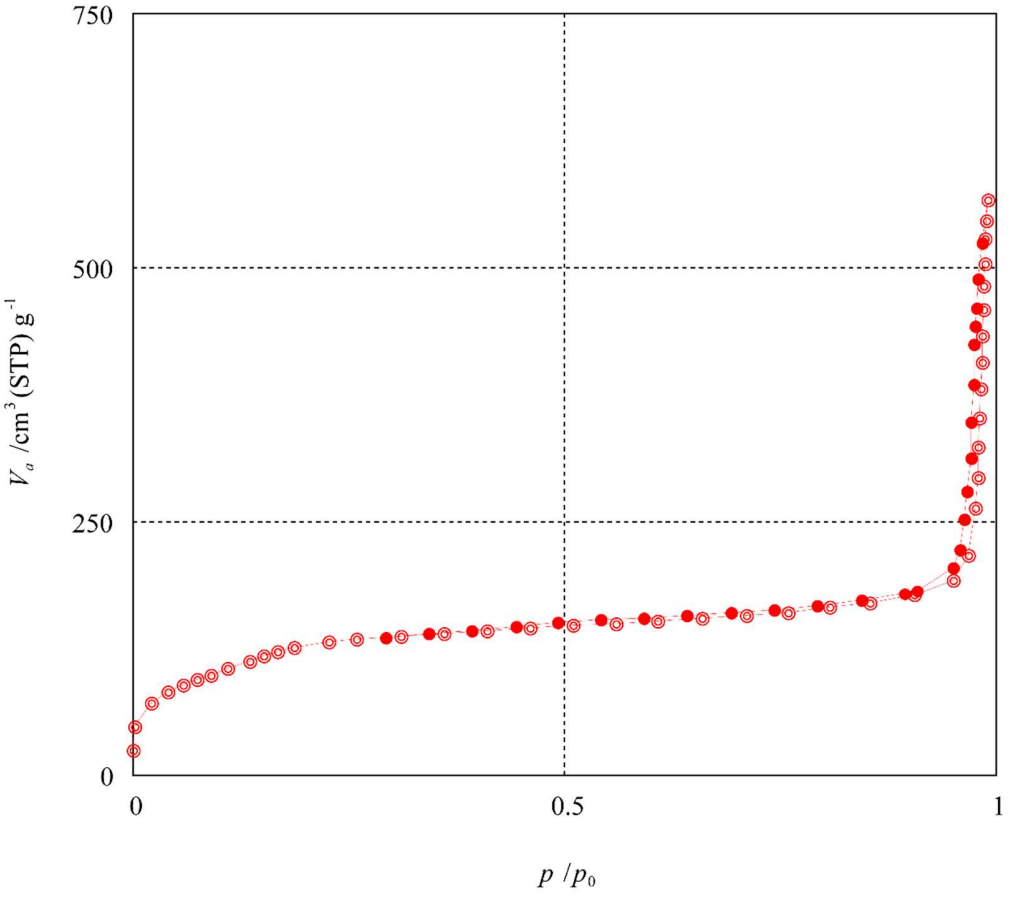

Fig. 3.1. Nitrogen adsorption-desorption isotherm for MCM-41.

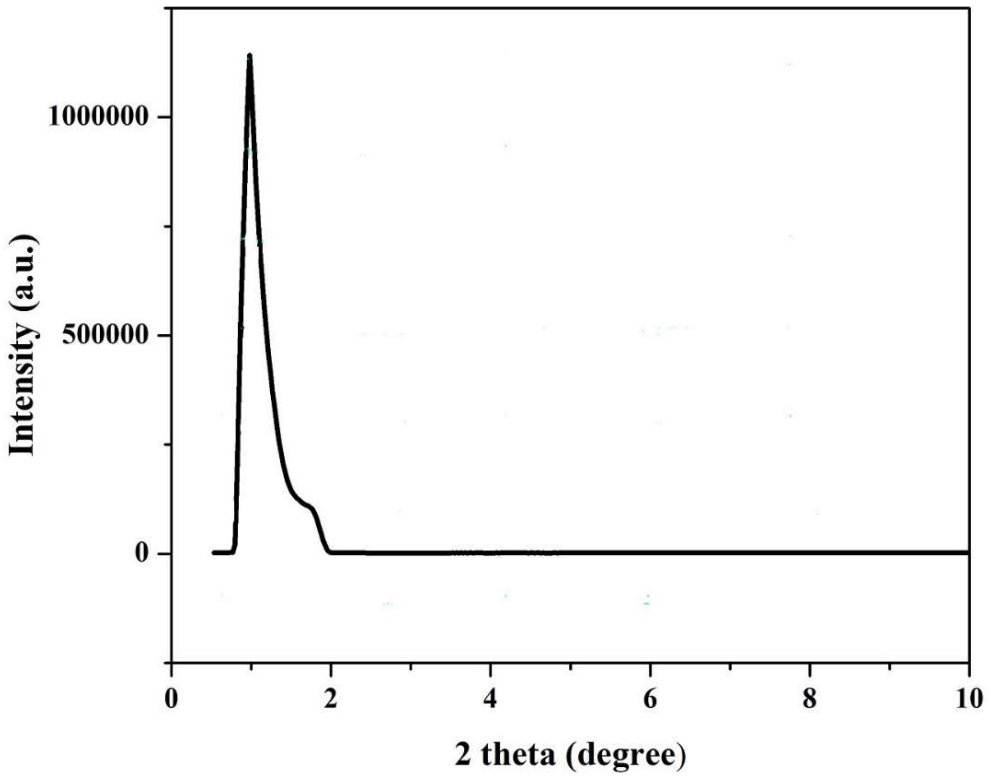

Fig. 3.2. XRD pattern of MCM-41.

3.2.3. FTIR spectra

Fig. 3.3 demonstrates the FTIR bands of synthesized MCM-41. Hydroxyl group and adsorbed water molecules on the surface appeared at 3410 cm^{-1} due to O–H stretching. Strong bands at 1057 cm^{-1} were observed due to asymmetric stretching vibrations of Si–O–Si. The vibration band at 961 cm^{-1} depicts vibrations between Si–OH. Free silica presence can be verified by band at 797 cm^{-1} (Santos et al., 2013; Kaur et al., 2015).

3.2.4. SEM and EDAX

The MCM-41 nanoparticles structure and morphology were analyzed by FE-SEM with bar length of 400nm at different magnifications of 100 000 X (Fig. 3.4 (a)) and 200 000 X (Fig. 3.4 (b)), which clearly revealed that MCM 41 possess spherical or elongated spherical particles of uniform structure within the size of 70-100 nm.

EDAX conducted for elemental analysis (Fig. 3.5) revealed presence of 51.39% silica and 31.82% oxygen. The Small amount of carbon (16.79 %) was also detected, which may be due to carbon tapping used during sample preparation.

3.2.5. TEM Micrographs

HR-TEM Micrographs (Fig.3.6) showed that the MCM-41 is hexagonal, and possesses evenly distrubuted pore system with a uniform mesoporous channels array (Mirzajani et al., 2016; Wu et al., 2012).

Results obtained reveals that MCM-41 was successfully synthesized and characterized with well-defined pore structure of high surface area and pore volume using various characterisation techniques which was further used as an efficient adsorbent for noxious aromatic amines and heavy metals adsorption from aqueous solution.

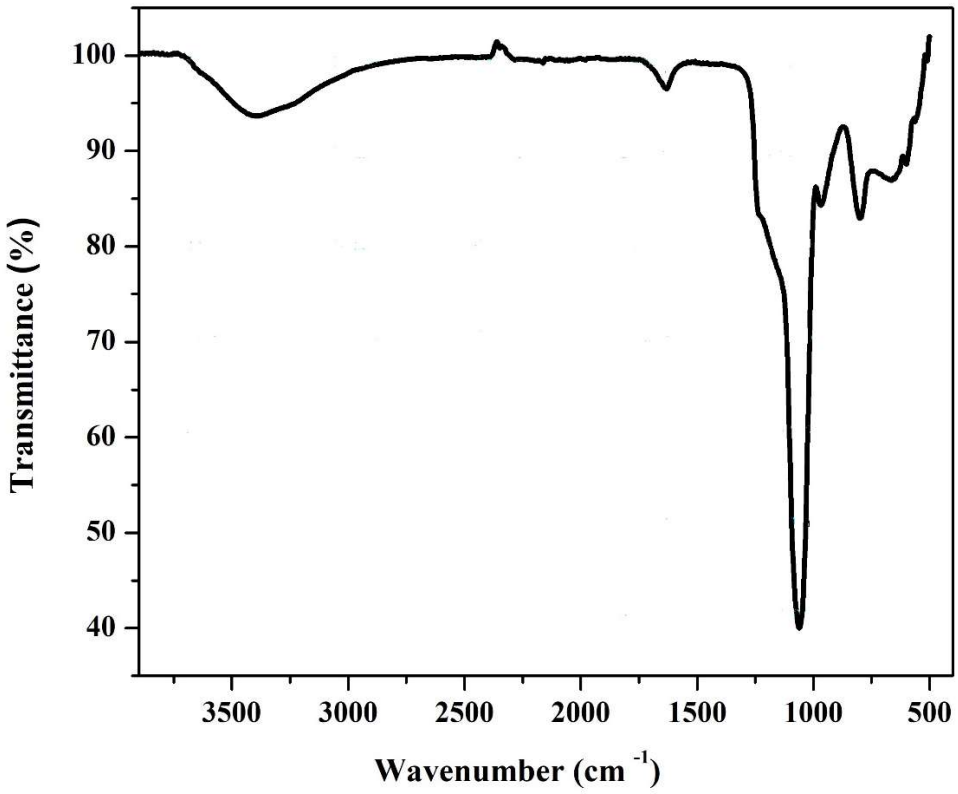

Fig. 3.3. FTIR spectra of MCM-41.

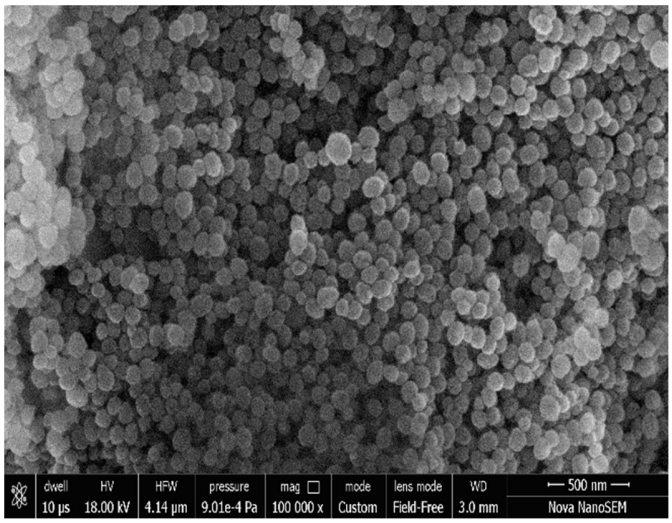

(a)

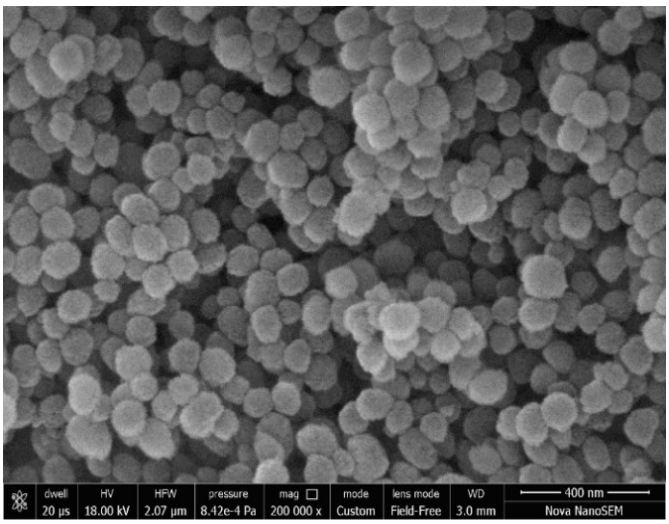

(b)

Fig. 3.4. FE-SEM image of MCM-41 at (a) 100 000 X magnification, (b) 200 000 X magnification.

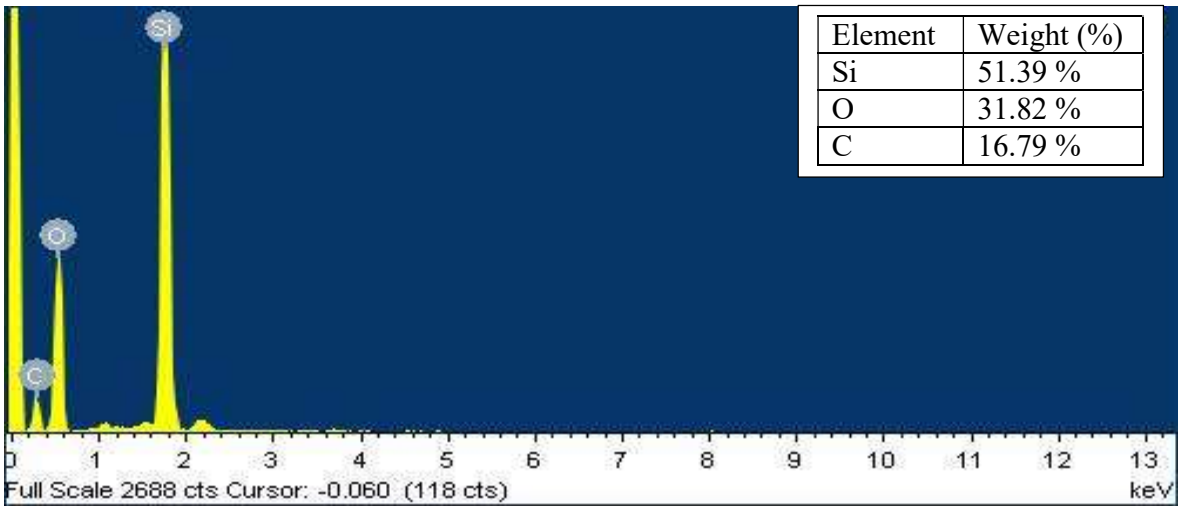

Element	Weight (%)
Si	51.39 %
O	31.82 %
C	16.79 %

Fig. 3.5. EDAX spectrum of MCM-41.

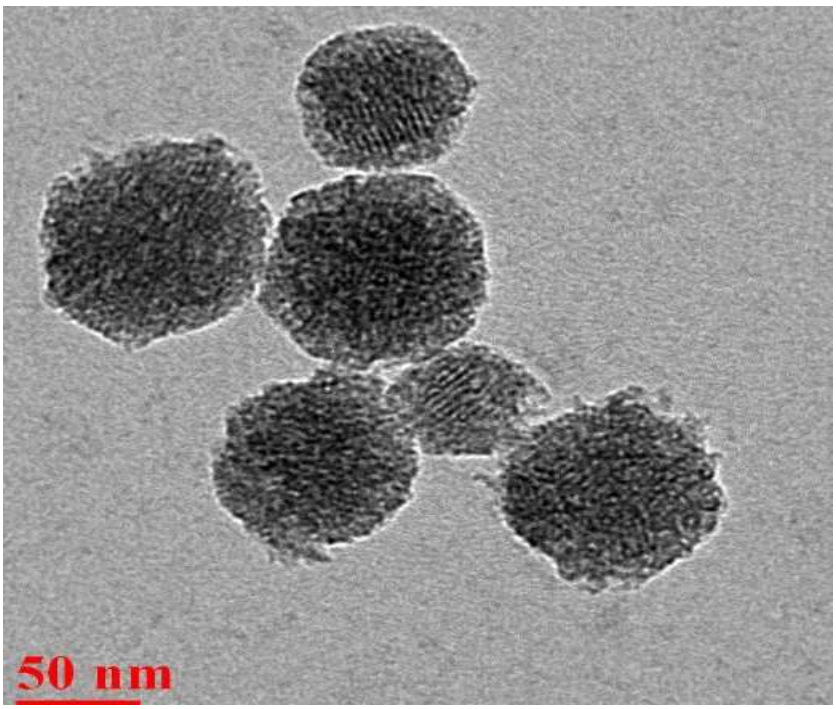

Fig.3.6. TEM Image of MCM-41.

Chapter – 4

AROMATIC AMINES ADSORPTION

4.0. GENERAL

This chapter deals with the adsorptive interaction characteristics of aromatic amines 4-chloro-*o*-toluidine (4-COT) and (4-aminobiphenyl (4-ABP) with MCM41.

4.1. MATERIALS AND METHODS

4.1.1. Chemicals and Wastewater

In the present study, analytical and reagent grade chemicals were used. 4-chloro-*o*-toluidine (4-COT) (CAS no. 95-69-2) and 4-aminobiphenyl (4-ABP) (CAS no. 92-67-1) were bought from Sigma-Aldrich, India. NaOH, Ethanol and HCl were supplied by Loba Chemie Pvt. Ltd., Mumbai, India.

To prepare stock solution of 4-chloro-*o*-toluidine (4-COT) and 4-aminobiphenyl (4-ABP), 0.1g of 4-ABP/4-COT was dissolved in 100 ml ethanol, and it was preserved at 4 °C (Jurado Sánchez et al., 2012). The working 4-COT/4-ABP aqueous solutions were obtained by diluting ostock solutions with suitable amount of distilled water.

4.1.2. Experimental Procedure

To conduct the experiments, 100 ml 4-COT/4-ABP solution of desired *pH* and concentration (C_0) was shaken in stoppered conical flask with suitable amount of the MCM-41 in an incubator shaker at constant speed of 180 rpm at required temperature (*T*). After desired time of adsorption, the adsorbent was separated by centrifuging the adsorbate and adsorbent system for 5 min at 6000 rpm. Clear 4-COT/4-ABP solution was then analysed for its residual concentration using double beam UV–VIS spectrophotometer (Prekin Elmer Lambda 35).

The % removal of 4-COT/4-ABP was calculated according to the equation:

$$\%Removal = \frac{(C_o - C_e)\, x100}{C_o} \qquad (4.1)$$

Where, C_o and C_e is the concentration of 4-COT/4-ABP in mg/L at t=0 and equilibrium, respectively.

The quantity of adsorbate adsorbed (adsorption capacity) q_t (mg/g) and q_e at any adsorption time, t and at equilibrium, respectively, were calculated by following equations:

$$q_t = \frac{(C_o - C_t)}{m} V \quad (4.2)$$

$$q_e = \frac{(C_o - C_e)}{m} V \quad (4.3)$$

Where, C_t (mg/L) is 4-COT/4-ABP concentration at any adsorption time (t), V is the 4-COT/4-ABP solution volume (L) and m is the adsorbent (MCM-41) mass (g).

To calculate the final concentration of aromatic amines (4-COT/4-ABP) after adsorption using UV-VIS spectrophotometer, calibration curve for each of 4-COT/4-ABP was plotted. For this purpose, first an absorbance was measured for 4-COT and 4-ABP solutions in UV-VIS spectrophotometer, and λ_{max} values of 238 nm and 272 nm, respectively, were obtained from the scan result (Fig. 4.1). Further at these λ_{max} values calibration curve for each of 4-COT/4-ABP was prepared (Fig. 4.2).

4.1.3. Adsorption Kinetics

In order to evaluate kinetic parameters for (4-COT/4-ABP) − MCM-41 system, pseudo-first-order/pseudo-second-order kinetic models (Equation 4.4 and 4.5, respectively) were applied and validated to the experimental kinetic data. Lagergren (1898) proposed a first-order rate equation to explain the kinetics of adsorption of liquid phase named as pseudo-first-order kinetics and is given by Equation 4.4:

$$q_t = q_e\left[1 - \exp\left(-k_f t\right)\right] \quad (4.4)$$

Ho and McKay (1999) proposed the pseudo-second order kinetic model on the basis of adsorption capacity and by assuming adsorption to be second order, presented as given below:

$$q_t = \frac{t k_S q_e^2}{1 + t k_S q_e} \quad (4.5)$$

where, k_f and k_s is the pseudo-first-order and pseudo-second-order rate constant. h (mg/g min), at $t \longrightarrow 0$, which is the rate of adsorption at initial stages, is defined as:

$$h = k_s q_e^2 \quad (4.6)$$

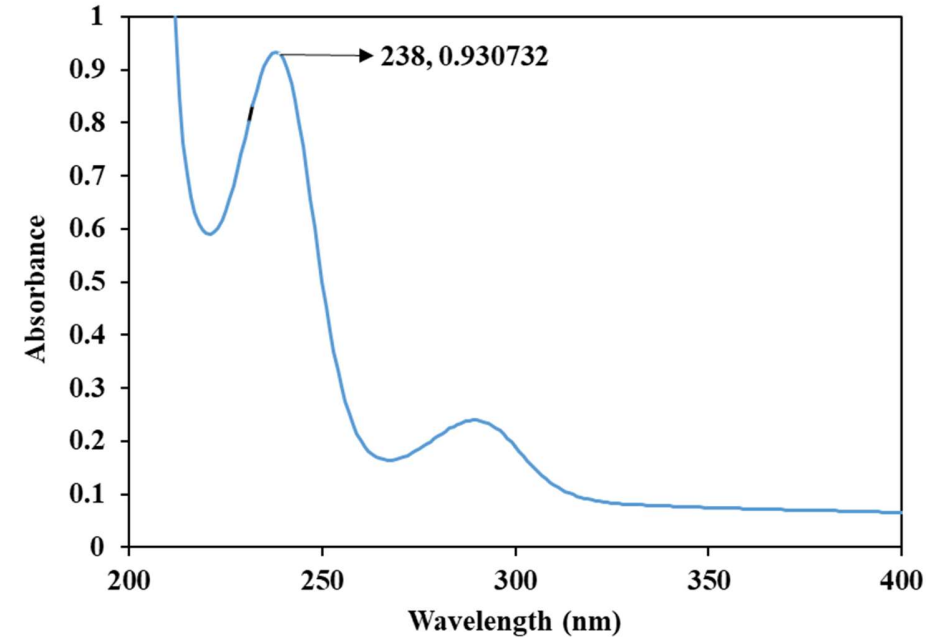

(a)

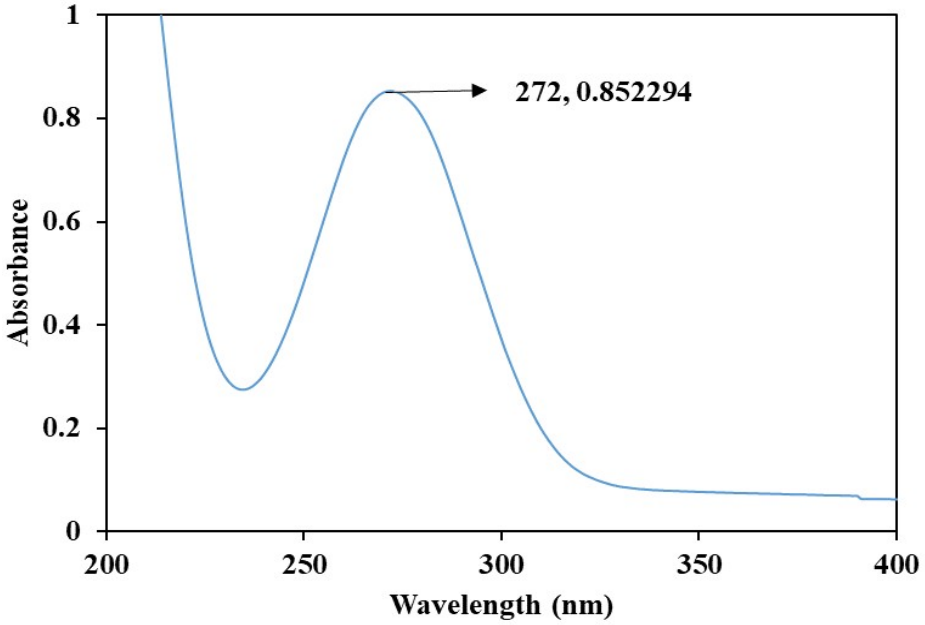

(b)

Fig. 4.1. UV Spectra of Amines (a) 4-COT (b) 4-ABP.

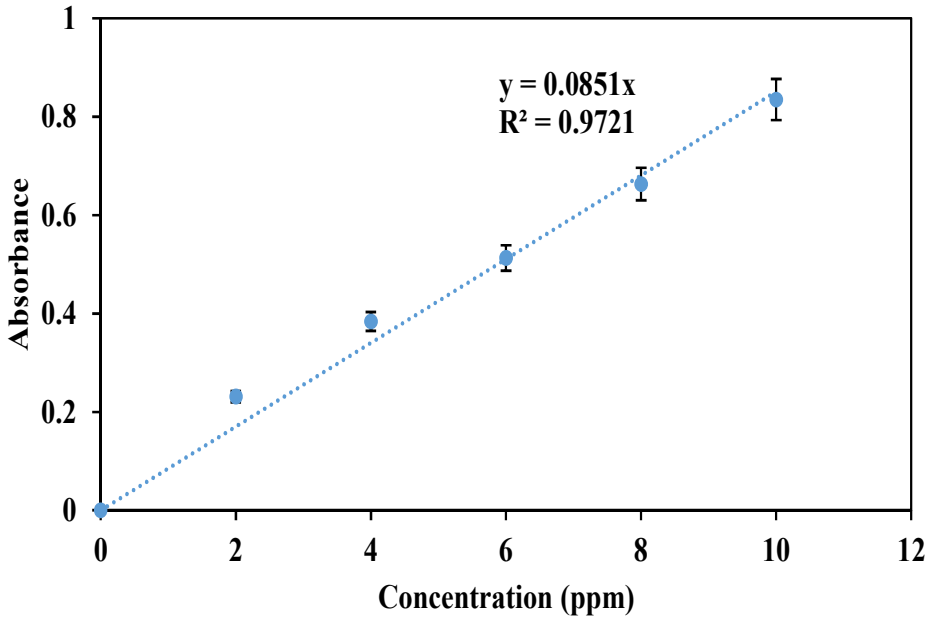

(a)

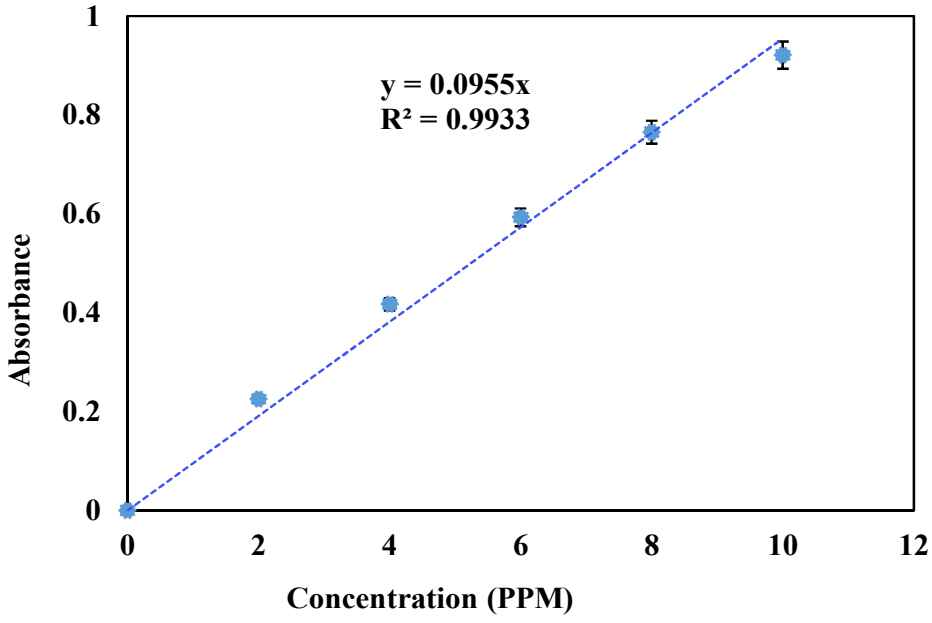

(b)

Fig. 4.2. Calibration Curve (a) 4-COT (b) 4-ABP.

Non-linear regression was performed with MPSD (Marquardt's percent standard deviation) error function (Marquardt, 1963) to validating experimental data with different kinetic models. The MPSD error objective function is given as:

$$MPSD = 100\sqrt{\frac{1}{n_m - n_p}\sum_{i=1}^{n}\left(\frac{q_{t,i,\exp} - q_{t,i,cal}}{q_{t,i,\exp}}\right)^2} \qquad (4.7)$$

Where, exp: experimental data values; cal: calculated data values; n_m: measurements number; n_p: number of parameters involved.

4.1.4. Adsorption Isothermal Study

Adsorption equilibrium isothermal data analysis with the adsorption capacity estimation provides important information for adsorption reaction pathway. Adsorption isothermal data were collected by conducting the adsorption experiments at different temperature (283, 293, 303 K). The experimental adsorption equilibrium isothermal data were then validated/fitted to Langmuir, Freundlich, Temkin and Dubinin-Radushkevich (D-R) isotherm models.

Langmuir isotherm is given by Equation 4.8:

$$\frac{C_e}{q_e} = \frac{C_e}{q_{max}} + \frac{1}{bq_{max}} \qquad (4.8)$$

Where, C_e = equilibrium adsorbate concentration (mg/L); q_e= adsorbent equilibrium adsorption capacity (mg/g); q_{max} = saturation adsorbent adsorption capacity (mg/g)

The Freundlich and Temkin isotherm model are given by the Equation 4.9 and 4.10, respectively (Freundlich, 1906; Temkin, 1940).

$$q_e = K_F C_e^{\frac{1}{n}} \qquad (4.9)$$

$$q_e = B \ln(A_T C_e) \qquad (4.10)$$

Equation 4.9 and 4.10, in linear form, can be written as:

$$\ln q_e = \ln K_F + \frac{1}{n}\ln C_e \qquad (4.11)$$

$$q_e = B \ln A_T + B \ln C_e \qquad (4.12)$$

where, K_F (mg/g)(L/mg)$^{1/n}$ is Freundlich constant that measures adsorption capacity and n as intensity of adsorption. $B = RT/b$, measures sorption heat (J/mol) and A_T (L/g) is constant.

Dubinin-Radushkevich (D-R) isotherm, which is also used in calculation of adsorption mean free energy (Dubinin-Radushkevich, 1947):

$$q_e = Q_{DR} \exp(-K_{DR}\,[RT \ln(1 + \frac{1}{C_e})]^2) \qquad (4.13)$$

Equation (4.13) in linear form is:

$$\ln(q_e) = \ln Q_{DR} - K_{DR}\,[RT \ln(1 + 1/C_e)]^2 \qquad (4.14)$$

Equation (4.14) can also be written as (Ozacan et al, 2006):

$$\ln(q_e) = lnQ_{DR} - K_{DR}\,(\acute{\varepsilon})^2 \qquad (4.15)$$

where, $\acute{\varepsilon}$ =Polanyi potential; Q_{DR} = adsorption capacity (mg/g) at saturated condition (theoretical); K_{DR} = D-R isotherm constant (mol^2/kJ^2) representing the mean free energy; R= Universal gas constant (8.314 kJ /mol); T= absolute temperature.

Further, the mean free energy of adsorption (E) (kJ/mol), can be obtained using the following expression:

$$E = \frac{1}{\sqrt{2K_{DR}}} \qquad (4.16)$$

4.1.5. Diffusion and Adsorption Controlling Mechanism

The adsorption kinetic models, as discussed in section 4.1.3 can't explicate the adsorption mechanism and the slowest adsorption process steps. Various adsorption steps are: film diffusion, pore or intra-particle diffusion and final adsorption on the adsorbent pore inner surface. The adsorption processes are controlled either by one or more of above steps. For adsorbate-adsorbent systems with high degree of mixing and high adsorbent surface area (as in the present study), film diffusion resistance becomes negligible. Therefore, surface/film diffusion of adsorbate molecule on the MCM-41 surface is very fast and cannot be the rate controlling. Adsorption through intra-particle diffusion may be the slowest adsorption step controlling the adsorption rate. Further, this was discovered using the Weber & Morris intra-particle diffusion model (Equation 4.17) (Weber & Morris, 1963).

$$q_t = K_{id} t^{1/2} + I \qquad (4.17)$$

Where, k_{id} (mg/g min$^{1/2}$) is the rate constant and I is intercept and represent the thickness of boundary layer formed over the adsorbent surface.

If the experimental data satisfy and linearly fitted to Weber & Morris equation (q_t vs $t^{1/2}$) and pass through origin, the intra-particle pore diffusion controls the adsorption rate. Otherwise, intercept (I) in the Equation (4.17) represent the boundary layer thickness (Gercel et al., 2007). Further, the experimental kinetic data were fitted to Boyd kinetic model (Boyd et al., 1947) to test, if adsorption of 4-COT on MCM-41 is controlled by the surface diffusion:

$$F = 1 - \frac{6}{\pi^2}\exp(-B_t) \qquad (4.18)$$

Where, $F = q_t/q_e$ at any t value, and B_t is dependent on F .

4.2. RESULTS AND DISCUSSION

4.2.1. Adsorption studies of 4-COT

Adsorption studies of 4-COT onto MCM-41 was performed to explore the effect of numerous adsorption process parameters including pH, adsorbent dose, adsorbate concentration, time and temperature. Obtained results are explained in detail in section 4.2.1.1 to 4.2.1.5.

4.2.1.1. Effect of Initial pH (pH_i): The effects of pH_i on 4-COT adsorption by MCM-41 was studied at T= 303 K by changing the pH_i from 2-9 with C_0= 50 ppm, m= 0.2g/L and t=2 h. Natural pH of 4-COT solution (50 mg/L) was found to be 7.5. To alter the pH of 4-COT solutions, 0.1 M HCl/NaOH solutions were used. It has been reported that UV light absorbance of some amine solution changes with change in pH of the solution (Thomas et al., 2007). Therefore, in the present study, it was verified, and found true for 4-COT. Hence, initial concentration (C_0) for calculation of % removal of 4-COT were obtained by subtracting the corresponding decrease in the C_o value due to change in absorbance value, after altering the pH of 4-COT solution.

Fig.4.3. illustrates the effect of pH for adsorption of 4-COT onto MCM-41. It can be seen that highest 4-COT removal efficiency of 51.99% was obtained at pH_i= 2. With increase in pH_i, 4-COT adsorption decreased sharply, and no removal was observed for $pH_i > 7$.

The interaction of 4-COT on surface of MCM-41 can be explained by change in charged state of 4-COT and MCM-41 with change in pH_i. The 4-COT gets protonated in the acidic solution (equation 4.19).

$$\text{4-COT} + H^+ \longleftrightarrow \text{(4-COT)-}H^+ \qquad (4.19)$$

An electrical charge may be attained by the MCM-41 materials. The FTIR analysis exhibited the presence of free silica with hydroxylated silica group (Si-OH) on the MCM-41 surface, due to which MCM-41 surface becomes negatively charged. It has been reported that point zero charge (pH_{PZC}) for hydroxylated surface of silica is about 2, and the *pKa* of Si-OH group on the MCM-41 surface is 6.5 (Meziani et al., 1997). Therefore, MCM-41 surface negative charge density is increased with increase in the solution *pH*. However, the protonation of 4-COT is decreased with increase in *pH*. Therefore, at highly acidic *pH* (*pH*=2), high electrostatic attraction of highly protonated 4-COT (4-COT-H^+) with the MCM-41 surface exhibited maximum 4-COT removal. With increase in the pH, due to the decrease in protonation of 4-COT, the electrostatic attraction becomes weaker and adsorption of 4-COT is decreased, and it becomes zero for the $pH \approx 6.5$ and above. Also, the hydrogen bonding between Si-OH of MCM 41 and 4-COT facilitated the adsorption of 4-COT. The schematic sketch of interaction of MCM 41 and 4-COT is shown in Fig. 4.4.

Final *pH* values (pH_f) as function of pH_i were also plotted (Fig. 4.3), which depicts no pH change after adsorption. No change in the pH values suggests absence of any chemical reaction during adsorption between the adsorbate and adsorbent, which, suggests physical adsorption. Maximum % removal of 4-COT were found at pH_i= 2, therefore, this was selected as optimum pH for further work.

Not much change in the FTIR spectra of loaded 4-COT was found as compared to that of bare MCM-41 (Fig. 4.5), confirming no new groups association between the adsorbate and adsorbent. Change in the peak height (decrease in the band) indicates that the functional groups present at these wavenumbers participate in the 4-COT adsorption. More the decrease in band, more is the adsorption (Rameshraja et al., 2012).

In FTIR, an increase in the peak intensity usually means an increase in the amount (per unit volume) of the functional group associated with the molecular bond, whereas a shift in peak position usually means the hybridization state or electron distribution in the molecular bond has changed. However, if the peak has broadened, then it could mean that some interaction has occurred. The decrease in band width after adsorption may be attributed to the occupancy of cations of the different characters on the same site. Decrease in both the peak intensities and band width, after 4-COT adsorption onto MCM-41 without any change in peak position indicates that 4-COT has been absorbed effectively on MCM-41 by weak electrostatic interations/ van der Walls interactions weak electrostatic 4-COT interations/ van der Walls interactions.Also, the absorption peak at 1630 cm^{-1} shows the presence of adsorbed water accumulated on the sample when it is mixed with KBr. The disappearance of this band after adsorption shows the presence of adsorbed water.

The morphology of the adsorbent after adsorption was analyzed by electron scanning microscopy (FE-SEM) at 15KV acting voltage with magnification of 120000 X. Fig. 4.6 (a) clearly revealed that the mesoporous MCM-41 preserved the uniform spherical structure, while Fig. 4.6 (b) illustrates that there is no change in shape after 4-COT adsorption, but textural change and hazy pores can be attributed to the loading of 4-COT on MCM-41.

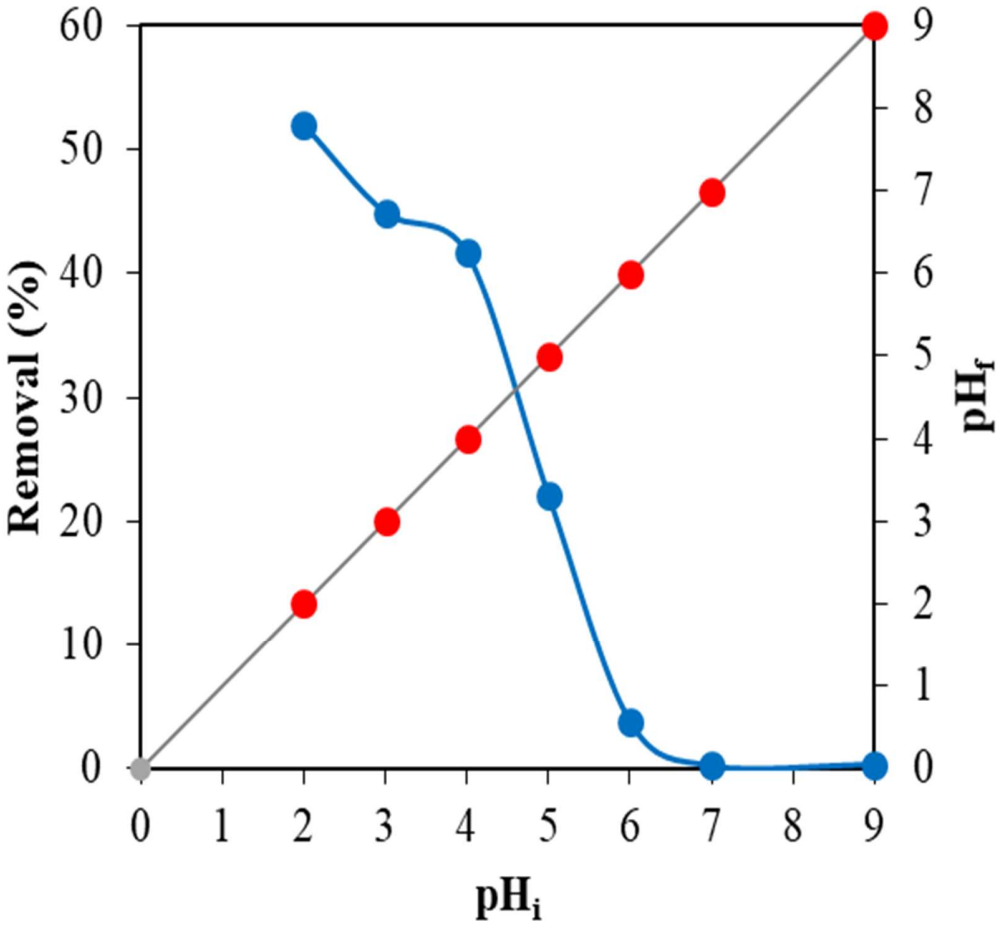

Fig. 4.3. Influence of initial pH on the 4-COT removal (C_0= 50 mg/L, T= 303 K, m= 0.2 g/L, t=2 h).

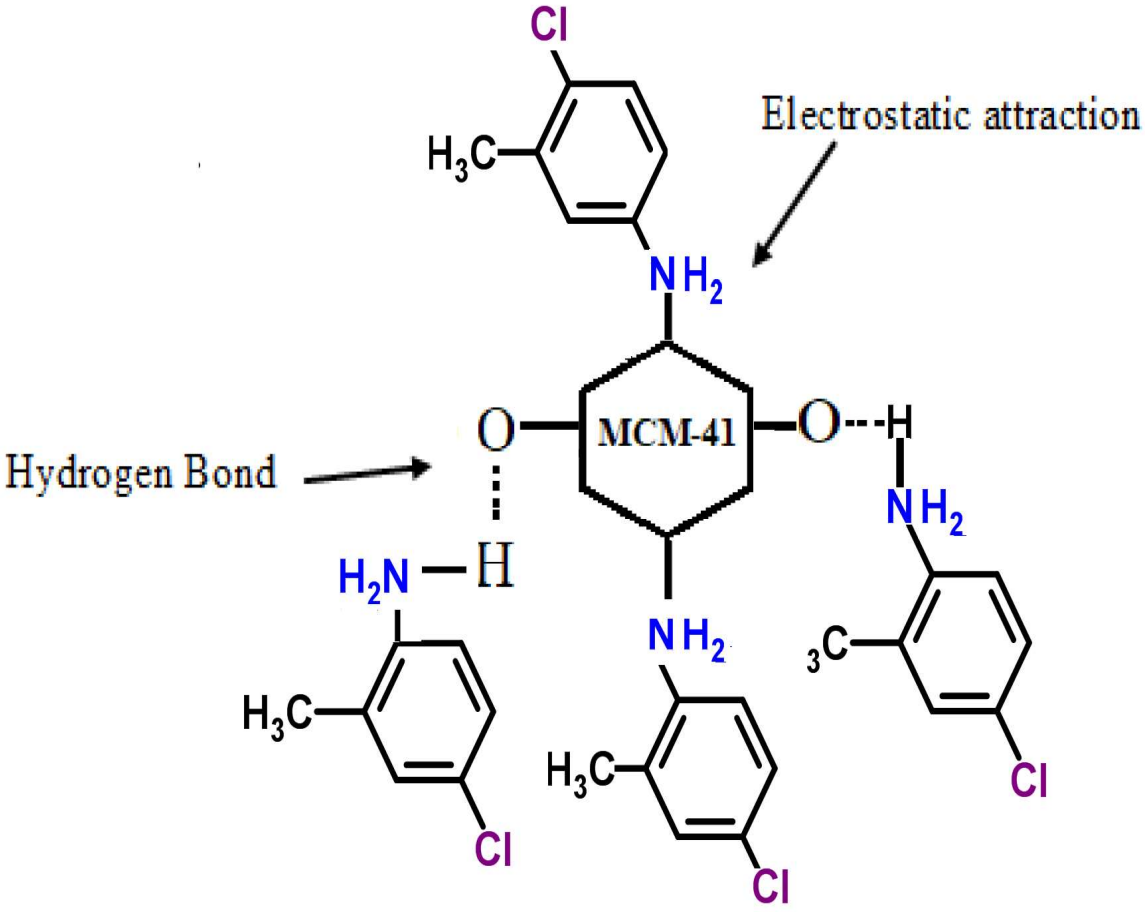

Fig. 4.4. Schematic interaction of 4-COT with MCM 41.

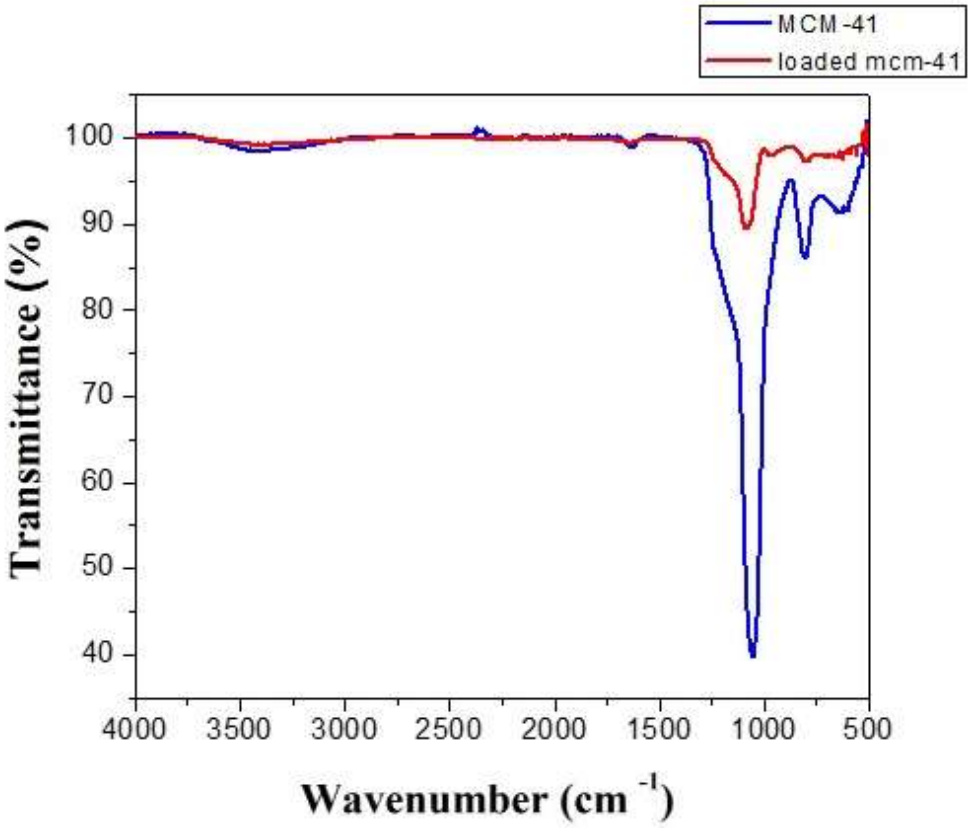

Fig. 4.5. FTIR spectra of MCM-41 and 4-COT loaded MCM-41.

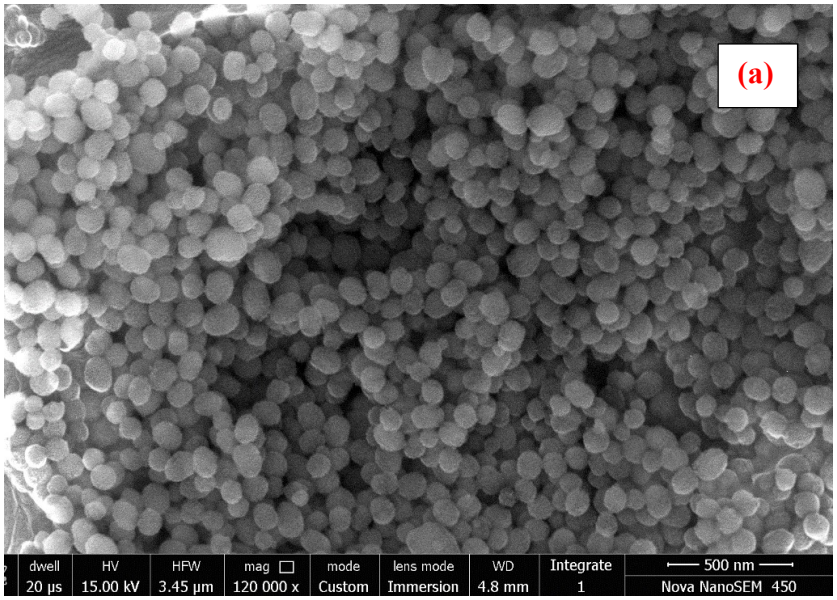

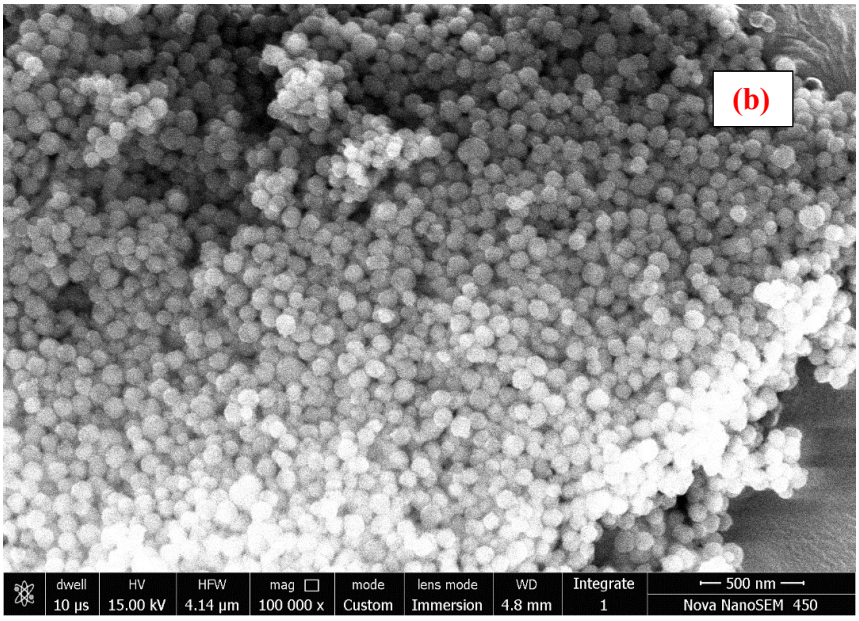

Fig 4.6. FE-SEM images (a) Bare MCM-41, (b) 4- COT loaded MCM-41.

4.2.1.2. Effect of adsorbent dose (*m*): The effect of *m* on the adsorption of 4-COT by MCM-41 was studied by varying *m* from 0.04 - 0.5g/L at T= 303 K, C_0= 50 mg/L, pH_i= 2 and t= 2h. An increase in *m* resulted in increased 4-COT removal onto MCM-41 up to m= 0.2 g/L, and remained unchanged for all m> 0.2 g/L (Fig. 4.7). At high *m* values, larger number of active sites availability for adsorption leads to increase in removal percentage. Further, at $m \geq 0.2$ g/L, constant removal efficacy of MCM-41 is due to the fact that adsorption is limited by the adsorbate concentration i.e. removal efficiency depends more upon the concentration of the solution and less upon the *m* . Thus, the optimum *m* (m_{opt}) for 4-COT removal by MCM-41 was selected as 0.2 g/L.

4.2.1.3. Effect of contact time (t*)* and adsorption Kinetics: Kinetic study was conducted in the C_0 range of 10-200 mg/L at T= 303 K, pH_i = 2, m_{opt}=0.2 g/L and t= 4h. Rapid uptake of 4-COT onto MCM-41 surface was observed within first five min followed by a slow adsorption phase. The equilibrium time was observed after 2 h. Fast initial surface adsorption of 4-COT onto MCM-41 owe to the presence of vast number of vacant sites, and the slower subsequent phase is due to diffusion of 4-COT molecule into inner pores surface of the MCM-41.

The best-fit values of Pseudo-first-order (Equation 4.4) and pseudo-second-order (Equation 4. 5) kinetic models parameters with the coefficient of determination (R^2) and MPSD error data are presented in Table 4.1. It was observed that Pseudo-second order kinetics best represented the kinetic experimental data with high R^2 value of 0.999 and low MPSD values (Fig. 4.8). The values of K_f, h and q_e increases, whereas k_S values decreases with increasing C_0 (Table 4.1). This may be due to the fact that an enhancement in C_0 increases the driving force between 4-COT solution and the surface of MCM-41.

Further, due to good mixing in this study, the external mass transfer from 4-COT bulk solution to MCM-41 surface was presumed to be completed in first 5 minutes letting the relationship C/C_o versus t for first 5 min as linear. The adsorption rate at initial adsorption time, K_S were determined as $(C_{5\min}/C_0)/5$, and the K_s values for C_o of 10, 20, 50, 100 and 200 mg/L were found to be 0.197, 0.136, 0.110, 0.114 and 0.092 min^{-1}, respectively.

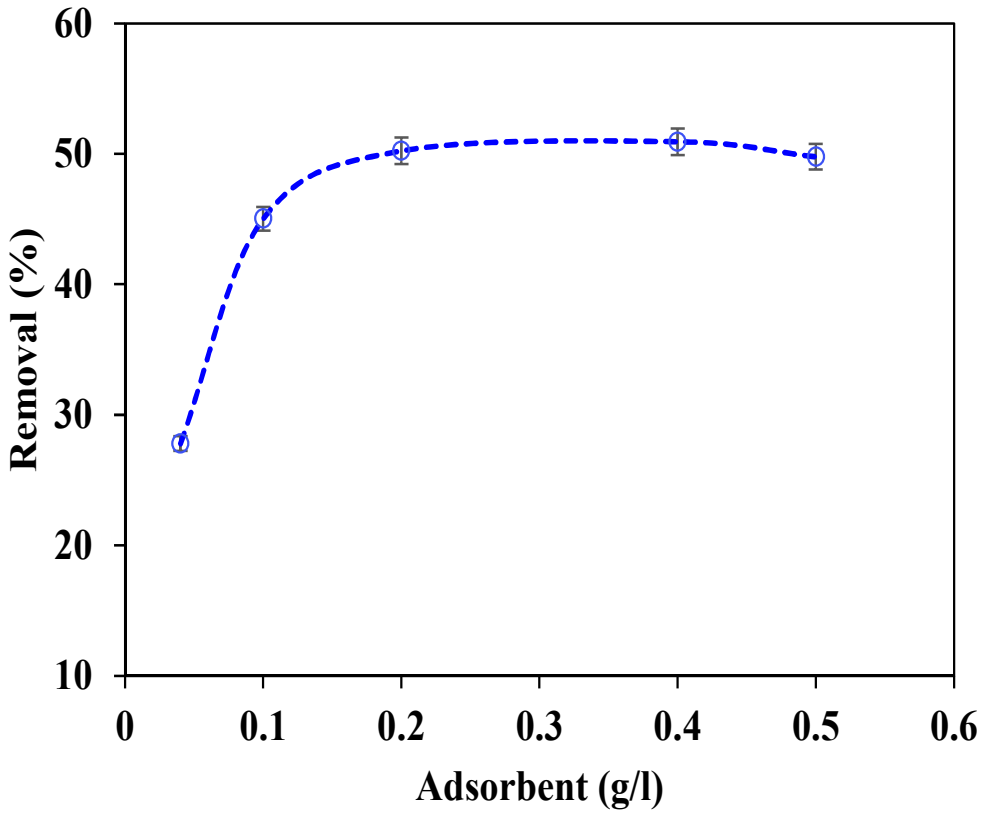

Fig. 4.7. Effect of adsorbent dose on the removal of 4-COT (C_0=50 mg/L, T= 303 K, pH_i=2, t= 2 h).

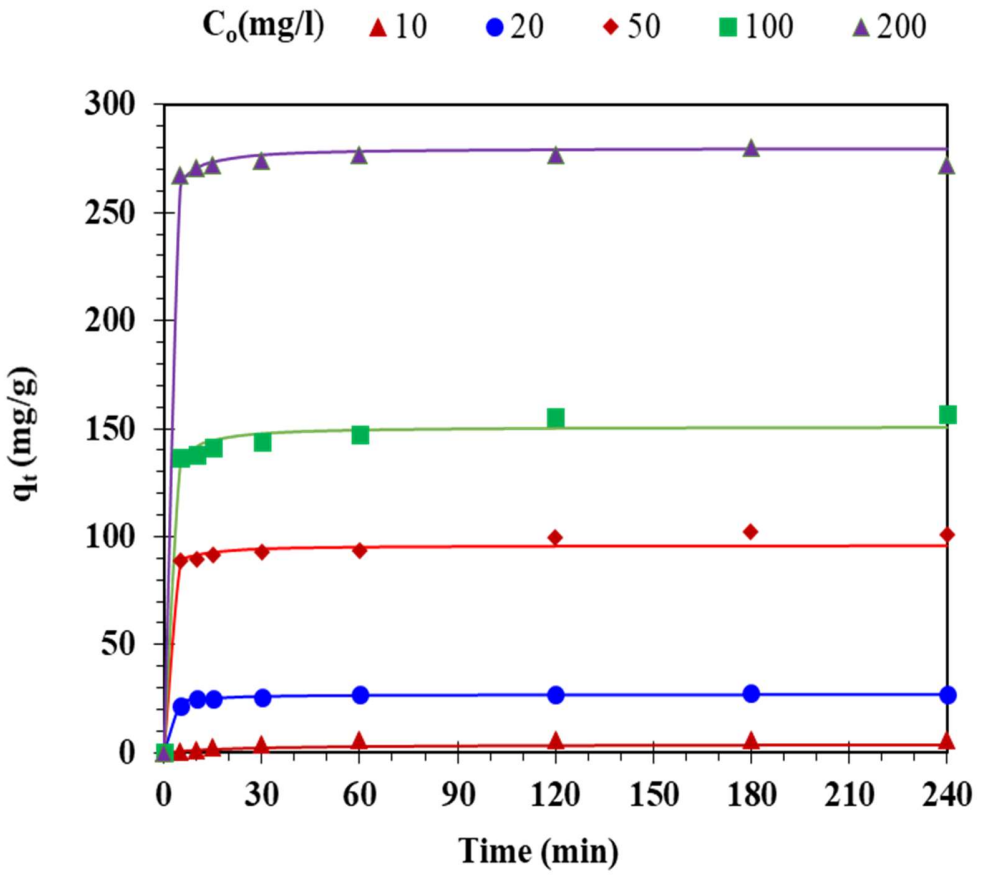

Fig. 4.8. Kinetics of 4-COT removal by MCM-41. Symbols represent the data from experiments, whereas the lines pseudo-second-order kinetic model prediction (T = 303 K, m_{opt}= 0.2 g/L, pH_i=2).

Table 4.1. Calculated kinetic parameters for the adsorption of 4-COT by MCM-41 (t= 4 h, C_0= 10–200 mg/L, m_{opt} = 0.2 g/L)

Pseudo-first-order model					
***C₀* (mg/L)**	$q_{e,exp}$ (mg/g)	$q_{e,cal}$ (mg/g)	K_f (min^{-1})	R^2	MPSD
10	5.817	4.5	0.01	0.906	150.64
20	27.086	27	0.2	0.980	14.38
50	101.11	96	0.4	0.989	14.14
100	156.93	151	0.5	0.979	16.51
200	271.96	270	0.6	0.999	5.92
Pseudo-second-order model					
***C₀* (mg/L)**	$q_{e,cal}$ (mg/g)	K_s(g/mg min)	h(mg/g min)	R^2	MPSD
10	4	0.03	0.16	0.975	148.88
20	27	0.03	24.76	0.999	3.74
50	96	0.02	184.32	0.994	9.30
100	151	0.01	228.01	0.987	12.09
200	280	0.01	784	0.999	3.25
Intra-particle diffusion					
***Co* (mg/L)**	K_{id} (mg/g $min^{1/2}$)		I (mg/g)		R^2
10	0.4		0.6743		0.759
20	0.303		23.418		0.663
50	1.049		86.679		0.951
100	2.156		132.16		0.794
200	0.961		267.4		0.895

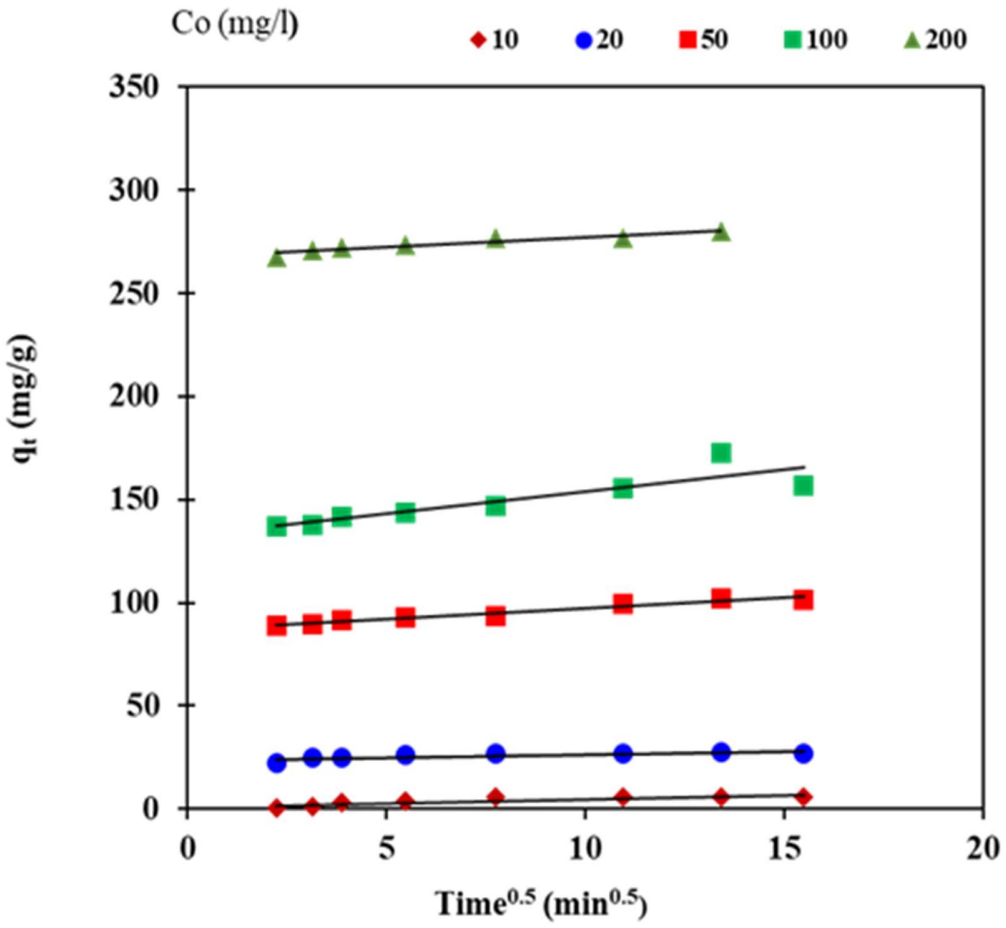

Fig. 4.9. Weber-Morris plot for the adsorption of 4-COT by MCM-41. (C_0 = 10–200 mg/L, m_{opt}= 0.2 g/L, t= 4h).

Fig. 4.9 represents plot of q_t *Vs* $t^{0.5}$ (Equation 4.17) in C_o range of 10-200 mg/L at T= 303 K, pH_i= 2, m_{opt}= 0.2 g/L and t= 4h. If the plot between q_t *Vs* $t^{0.5}$ is linear, then the process of adsorption is claimed to follow the intra-particle diffusion. However, experimental data exhibiting more than one linear plots indicates the involvement of more than one controlling steps in overall process.

In this study, q_t *Vs* $t^{0.5}$ plot (Fig. 4.9) were found linear over all the time but do not pass through the origin. This deviation of not passing through origin, may be owing to the difference in initial and final rate of adsorbate mass transfer on to the adsorbate surface (Kumar et al., 2014). This difference in rate of adsorbate mass transfer indicates the involvement of boundary layer in adsorption controlling. It further confirms that intra-particle diffusion is responsible in the rate control but is not the only factor involved. Also increment in value of I with increase in C_0 (Table 4.1.) results in the thicker boundary layers. Positive values of I indicates the rapid initial adsorption (Wu et al., 2009).

K_{id} values rises from 0.4 to 2.156 (mg/g $min^{1/2}$) for increase in C_o from 10 to 100 ppm respectively indicated accelerated diffusion of 4- COT through mesopores of MCM-41 due to higher driving force between 4-COT solution and surface of MCM-41 due to availability of more amine ions. K_{id} decreases with further increase in C_0, this may be due to the unavailability of vacant sites.

Further, to investigate the exact controlling step, the kinetic data were further fitted to Boyd kinetic model (Equation 4.18) and B_t values at various t values were calculated. B_t versus t plot was found non-linear (not shown here) with R^2 ranging from 0.94-0.97 values verified that adsorbate surface diffusion onto MCM-41 is not the only rate monitoring step, but the 4-COT adsorption on to MCM-41 was followed by some multifaceted mechanism with intra-particle diffusion.

4.2.1.4. Effect of temperature (*T*) and adsorption isothermal study: Temperature effect for adsorption of 4-COT onto MCM-41was studied at C_0 values ranging from 10-300 mg/L, pH_i= 2, m_{opt}=0.2 g/L and t= 2h by varying temperature (T) from 293-318 K. Increase in the adsorption of 4-COT onto MCM-41 with increase in temperature was observed due to enhanced movement of the 4-COT molecules to the MCM-41 surface (Kushwaha et al., 2010). The adsorption processes are generally exothermic, however intra-particle diffusion controlled

adsorption process are endothermic in nature. Further endothermic nature of adsorption onto MCM-41 was also reported in literature by various researchers (Juang et al., 2006; Chen et al., 2015; Tian et al., 2011).

Correlation of q_e with C_e in the aqueous phase was studied by validating the experimental isothermal data to Langmuir, Temkin and Freundlich isotherms. Langmuir isotherm showed very poor fitting to the experimental data (not shown here). The fittings of Freundlich and Temkin isotherms are presented in Fig. 4.10 and 4.11, and the calculated corresponding isotherms parameters are tabulated in Table 4.2.

High R^2 values for both the Temkin and Freundlich isotherms at all the temperatures studied indicates the suitability of these models for adsorption of 4-COT onto MCM-41. More is the value of *1/n* (Freundlich parameter), more is the affinity between 4-COT and MCM-41, and heterogeneous nature of the MCM-41. The K_F value were found increasing with increasing temperature (Table 4.2) revealed higher uptake of 4-COT at higher *T*. Increasing temperature increases the movement of 4-COT molecules, which incapacitates them to overcome the activation energy and boosts intra-particle diffusion (Aksu et al., 2004; Rameshraja et al., 2012; Singh et al., 2014; Srivastava et al., 2007). Parameters of Temkin isotherm, *B* and A_T were also found to increase with raised temperature revealing endothermic nature of adsorption (Table 4.2).

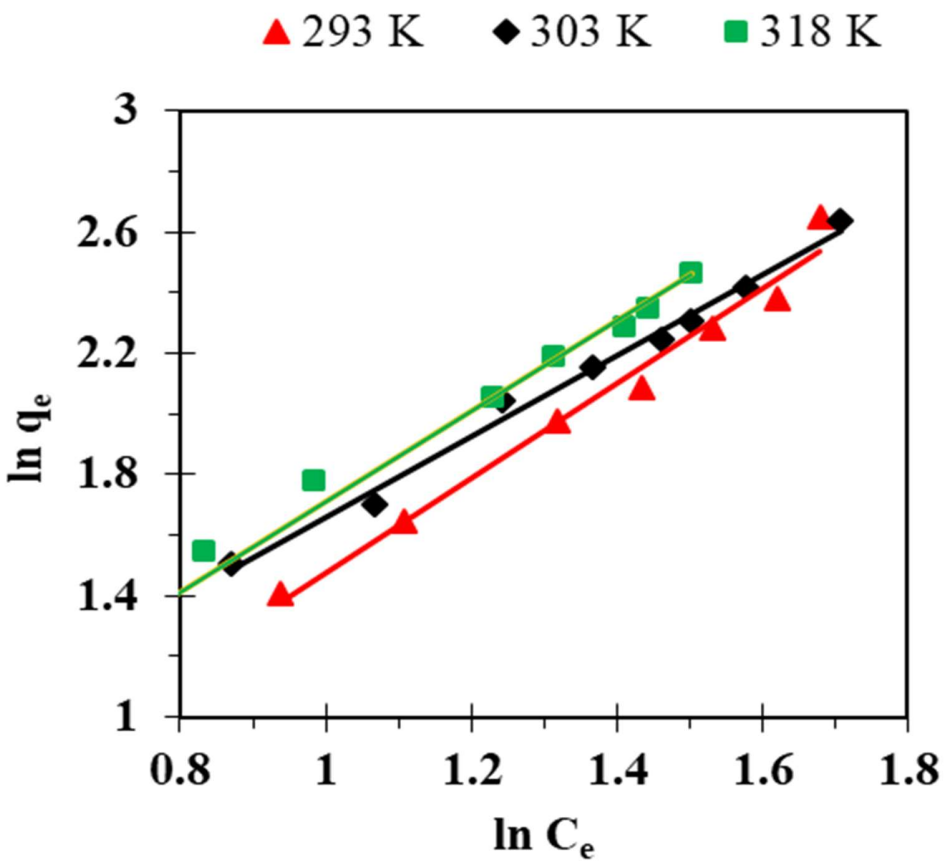

Fig. 4.10. Freundlich isotherm for the adsorption of 4-COT by MCM-41 (C_0 = 30–300 mg/L, m_{opt} = 0.2 g/L t = 2 h).

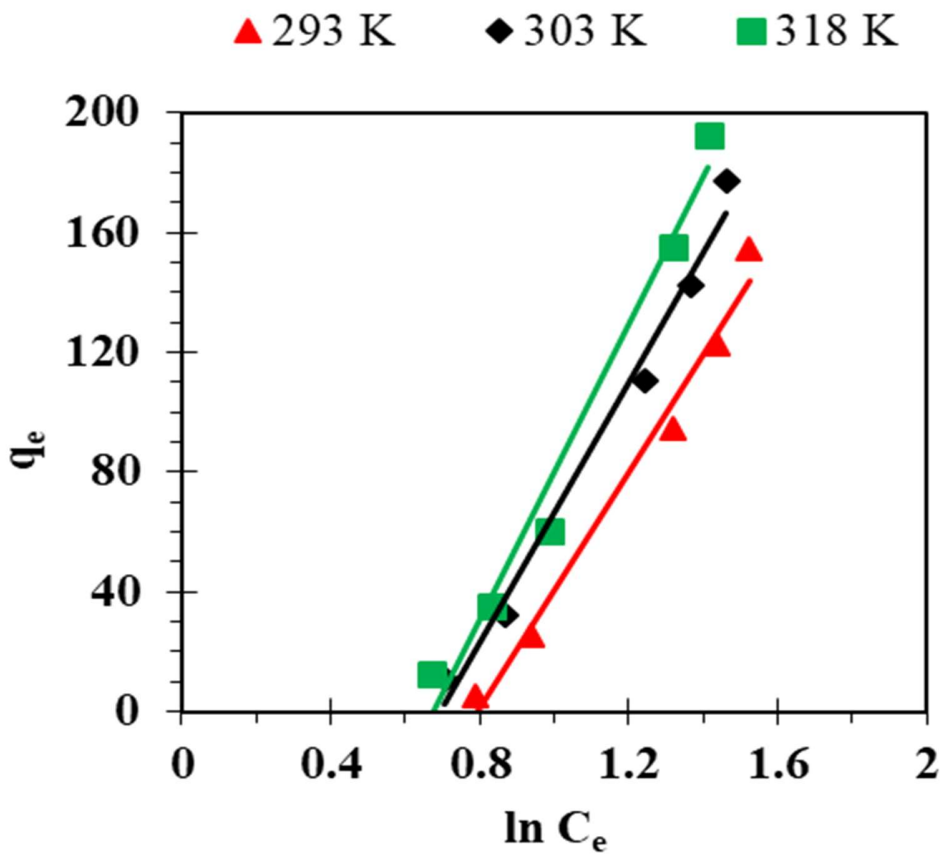

Fig. 4.11. Temkin isotherm for the adsorption of 4-COT by MCM-41 (C_0= 30–300 mg/L, m_{opt}= 0.2 g/L, t= 2 h).

Table 4.2. Isothermal parameters for the adsorption of 4-COT by MCM-41 (C_0= 10-300 mg/L, t= 2 h, pH_i =2, m_{opt} = 0.2 g/L)

Freundlich Isotherm			$q_e = K_F C_e^{1/n}$
T (K)	K_F ((mg/g)/(l/mg)$^{1/n}$)	*1/n*	R^2
293	0.923	1.557	0.98
303	1.382	1.33	0.991
318	1.050	1.278	0.997
Temkin Isotherm		$q_e = B \ln A_T + B \ln C_e$	
T (K)	B	A_T(L/g)	R^2
293	196.34	0.454	0.984
303	216.51	0.5	0.984
318	246.26	0.511	0.976

4.2.1.5. Estimation of thermodynamic parameters: Energetic changes linked to the adsorption/ removal of aromatic amines onto MCM-41 can be figured out with the help of thermodynamic parameters. These parameters are vital to determine spontaneity and feasibility of any adsorption process. Various thermodynamic variables include:

The entropy change (ΔS °): It measures the randomness or disorder of the adsorbed solute onto solid adsorbent.

The heat of adsorption (ΔH^0): The positive ΔH^0 value reveals the endothermic nature of adsorption.

Gibbs free energy change (ΔG°): It is given by the expression below:

$$\Delta G^0 = \Delta H^0 - T\Delta S^0 \qquad (4.20)$$

These thermodynamic variables can be calculated from eq. 4.20 by varying adsorption equilibrium constant (K_D) with T.

$$\ln K_D = \frac{-\Delta G^0}{RT} = \frac{\Delta S^0}{R} - \frac{\Delta H^0}{R}\frac{1}{T} \qquad (4.21)$$

Where, R: gas constant, universal (8.314 J/mol K); K_D: slope of plot of $l_n \frac{q_e}{c_e}$ *Vs* q_e (Srivastava et al., 2007).

Thermodynamic parameters attained from the linear plot between ln K_D and 1/T (Fig. 4.12) using eq. 4.20 and 4.21 have been summarized in Table 4.3. Value of K_D was found to decreases with raised T. The positive value $\Delta H°$ reveals the endothermic nature of adsorption. Physical adsorption is attributed to weak van der Walls forces between the adsorbate and adsorbent with low adsorption energy of 5-10 kJ/mol, whereas 30-70 kJ/mol $\Delta H°$ values indicates chemisorption (Kushwaha et al., 2010). In the present study, $\Delta H°$ value was found to be 16.37 kJ/mol. Therefore, it seems that 4-COT - MCM-41system follows some complex mechanism of physical and chemical adsorption.

High entropy value of 123.44 kJ/mol K was found which was similar to the investigation done by Parida et al., 2012, which reported high $\Delta S°$ value of 129.56 kJ/mol K for adsorption of Cr (VI) onto MCM-41. This positive value of $\Delta S°$ suggested high randomness at the adsorbent/adsorbate contact point (Mirzajani et al., 2016), and high affinity between the adsorbent and adsorbate during adsorption. Negative $\Delta G°$ values represent the 4-COT adsorption on to MCM-41 is feasible and spontaneous.

Table 4.3. Adsorption thermodynamic parameters of 4-COT on to MCM-41 (C_0= 10 -300 mg/L, pH_i=2, m= 0.2 g/L, t = 2 h)

Temperature (T) (K)	K x 10^{-3} (l/kg)	$\Delta G°$ (kJ/mol)	$\Delta H°$ (kJ/mol)	$\Delta S°$ (kJ/mol K)
293	3.4130	-19.725	16.37	123.44
303	3.3003	-21.155		
318	3.1447	-22.826		

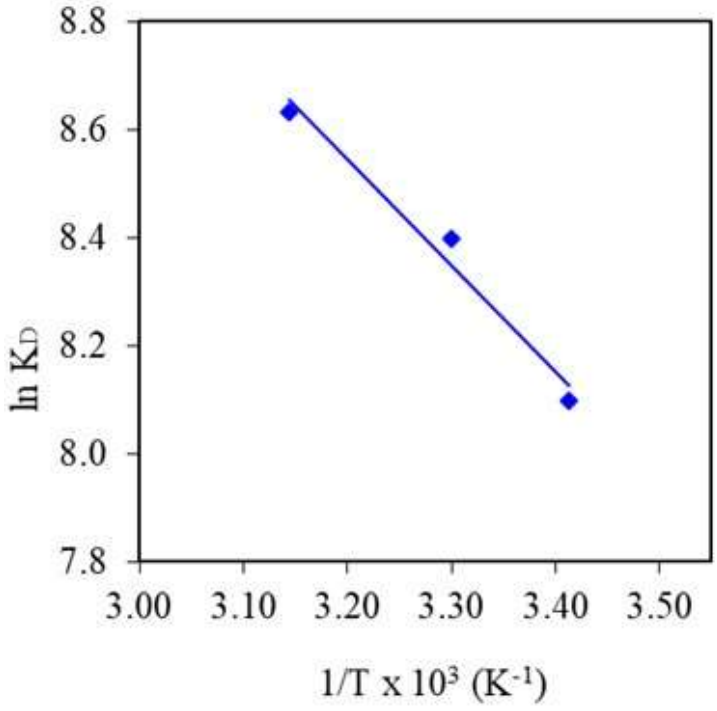

Fig. 4.12. ln K_D *vs* 1/T Plot to estimate the thermodynamic parameters for the adsorption of 4-COT

4.2.2. Adsorption studies of 4-ABP

Adsorption studies of 4-ABP onto MCM-41 was done to explore the effect of several parameters including pH, adsorbent dose, adsorbate concentration, time and temperature. Obtained results are explained in detail in section 4.2.2.1 to 4.2.2.5.

4.2.2.1. Effect of Initial pH (pH_i): The effects of pH_i on 4-ABP adsorption by MCM-41 was studied at T= 303 K by changing the pH_i from 2-9 with C_0= 50 ppm, m= 0.2g/L and t=2 h. 0.1 M NaOH/HCl solutions was used to alter the pH of the solution. Fig.4.13 shows the variation in 4-ABP adsorption (% removal) by MCM-41 with pH variation. Highest 4-ABP % removal of 64.73% was observed at $pH_i = 2$. Further, at $pH_i > 2$, a sharp decrease in 4-ABP removal was found, and no removal were observed for $pH_i > 6.5$.

This behavior of MCM-41 on 4-ABP adsorption can be explained with the help of altering charged state of 4-ABP and the surface characteristics of MCM-41 with pH_i alteration. In acidic solution, the 4-ABP is protonated via the following equation (equation 4.22).

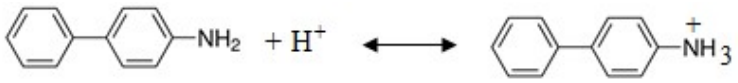

(4.22)

The MCM-41 surface is negatively charged due to the presence of hydroxylated silica group (Si-OH) with free silica on the MCM-41 surface (as identified in FTIR analysis in section 3.2.3). Further, point of zero charge (pH_{PZC}) for Si-OH on MCM-41 is ≈ 2, and its pK_a value is 6.5 which increases with the increase in degree of surface ionization. Due to this, in highly acidic pH (pH≈2), MCM-41 surface turns highly negative. For $pH > pH_{PZC}$, the negative charge density decreases and becomes very low at $pH \approx 6$ (Meziani et al., 1997). Therefore, highly acidic pH (pH_i=2) favoured the 4-ABP adsorption due to high electrostatic attraction between protonated 4-ABP and high negative charge surface of MCM-41, and maximum % removal was found. With the increase in pH_i, decrease in negative charge density on MCM-41 surface caused decreased 4-ABP % removal due to weaker electrostatic attraction. Also, the hydrogen bonding between Si-OH of MCM-41 and 4-ABP facilitated the adsorption of 4-ABP. The schematic sketch of interaction of MCM-41 and 4-ABP is shown in Fig.4.14.

The *pH* of the 4-ABP solution changes with the progress of adsorption of 4-ABP on to MCM-41. After the adsorption process, final *pH* (pH_f) values were plotted along with pH_i in Fig. 4.13. The pH_f values can be observed always being at higher side than the pH_i. However, very small change in pH_f value was observed at 2 pH_i. Presence of H^+ ions in excess to protonation of 4-ABP may be reason for this increased *pH*. Negligible change in *pH* was observed for highly basic pH_i. It can be interpreted that when the 4-ABP % removal is high, the change in the pH_f value is smaller, and it increases as the % removal is decreased up to neutral *pH* (*pH*=7). For pH_i >7, the change in the pH_f value is decreased, and becomes negligible at highly basic *pH*.

FTIR spectra of bare and 4-ABP loaded MCM-41 is depicted in Fig. 4.15 in the range 500-4000 cm^{-1}. No significant change in the FTIR spectra of 4-ABP loaded MCM-41 confirms that there is no chemical interaction between the adsorbate and adsorbent. Slight reduction in intensities were seen in 4-ABP loaded MCM-41 without change in peak position, which concludes that 4-ABP was adsorbed on MCM-41 by weak electrostatic interactions or van der Waals physical interaction (Kaur et el., 2015).

The morphology of MCM-41 was analyzed by electron scanning microscopy (FE-SEM) at 15KV acting voltage with magnification of 100000 X. Fig. 4.16 (a) clearly revealed that the mesoporous MCM-41 preserved the uniform spherical structure, while Fig. 4.16 (b) illustrates that there is no change in shape after 4-ABP adsorption, but textural change and hazy pores can be attributed to the loading of 4-ABP on MCM-41.

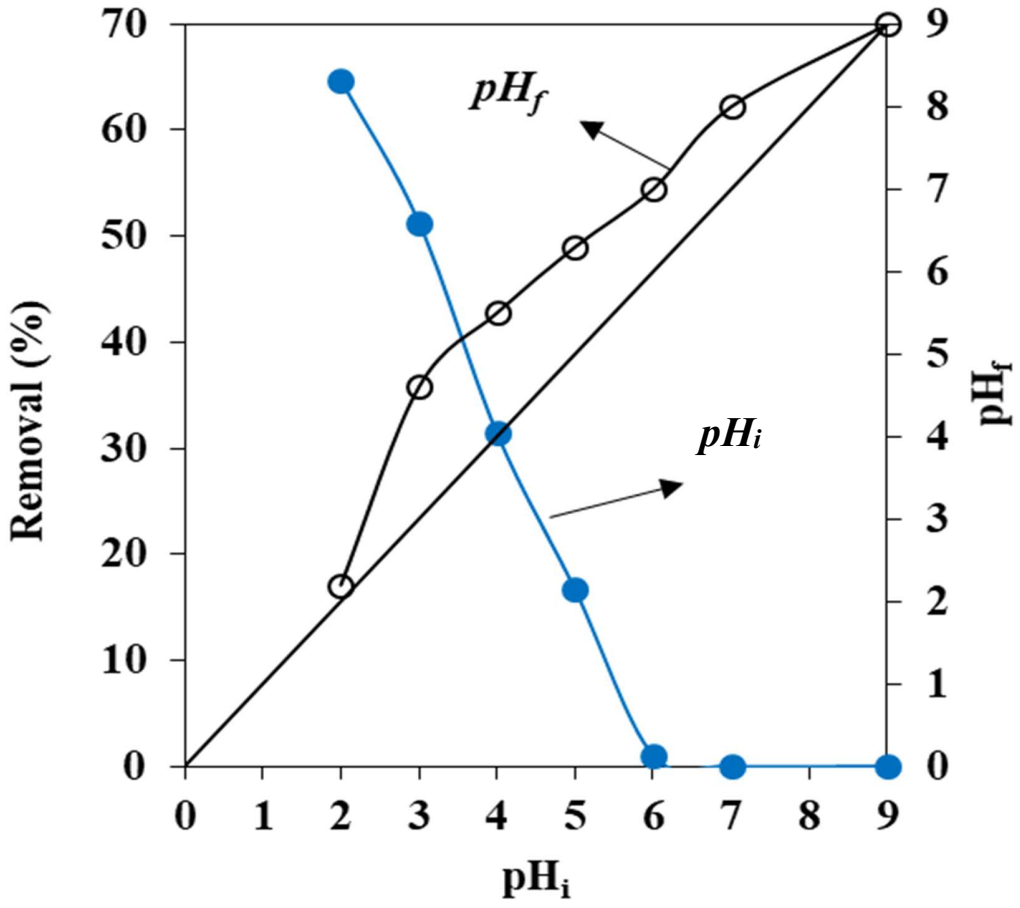

Fig. 4.13 Influence of initial pH on the 4-ABP removal by MCM-41 (C_0= 50 mg/L, T= 303 K, m= 0.2 g/L, t =2 h).

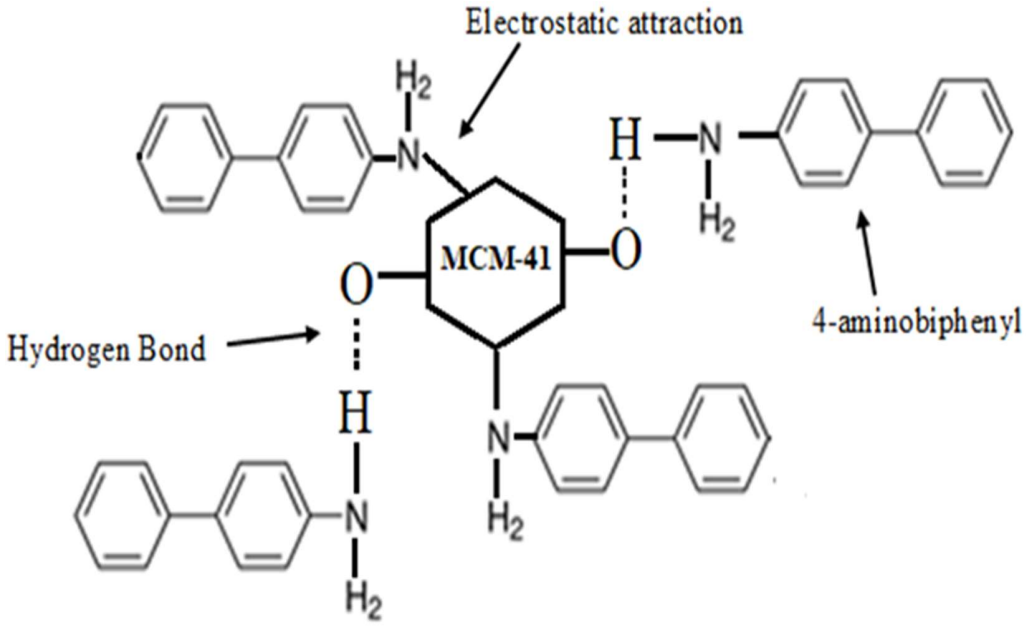

Fig. 4.14. Interaction of 4-ABP with MCM-41.

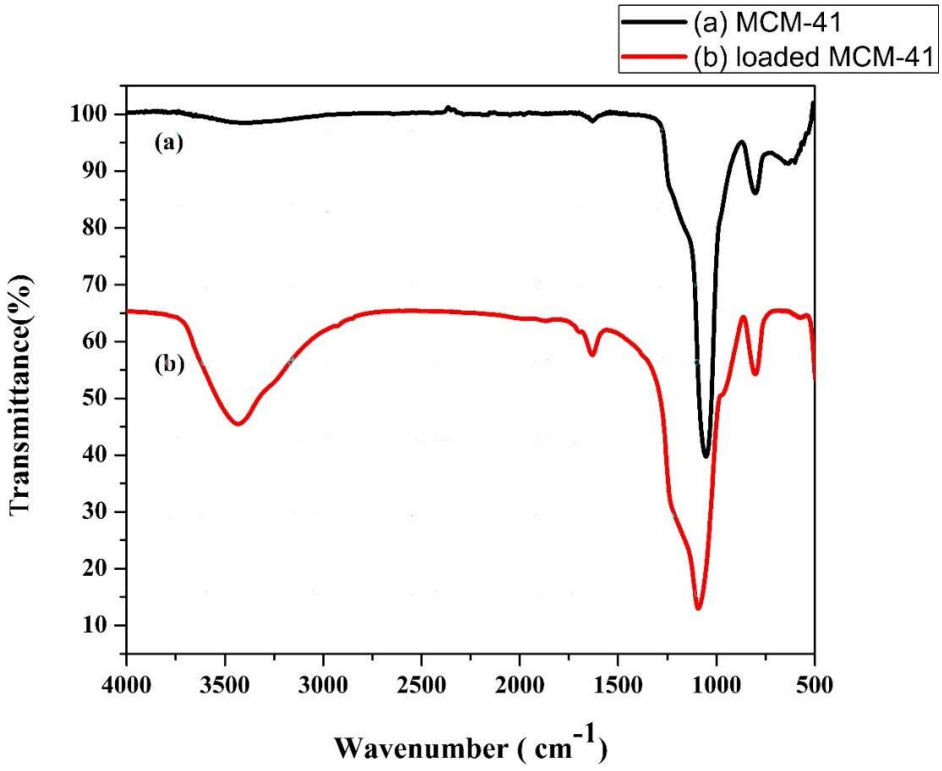

Fig. 4.15. FTIR spectra of MCM-41 and 4-ABP loaded MCM-41.

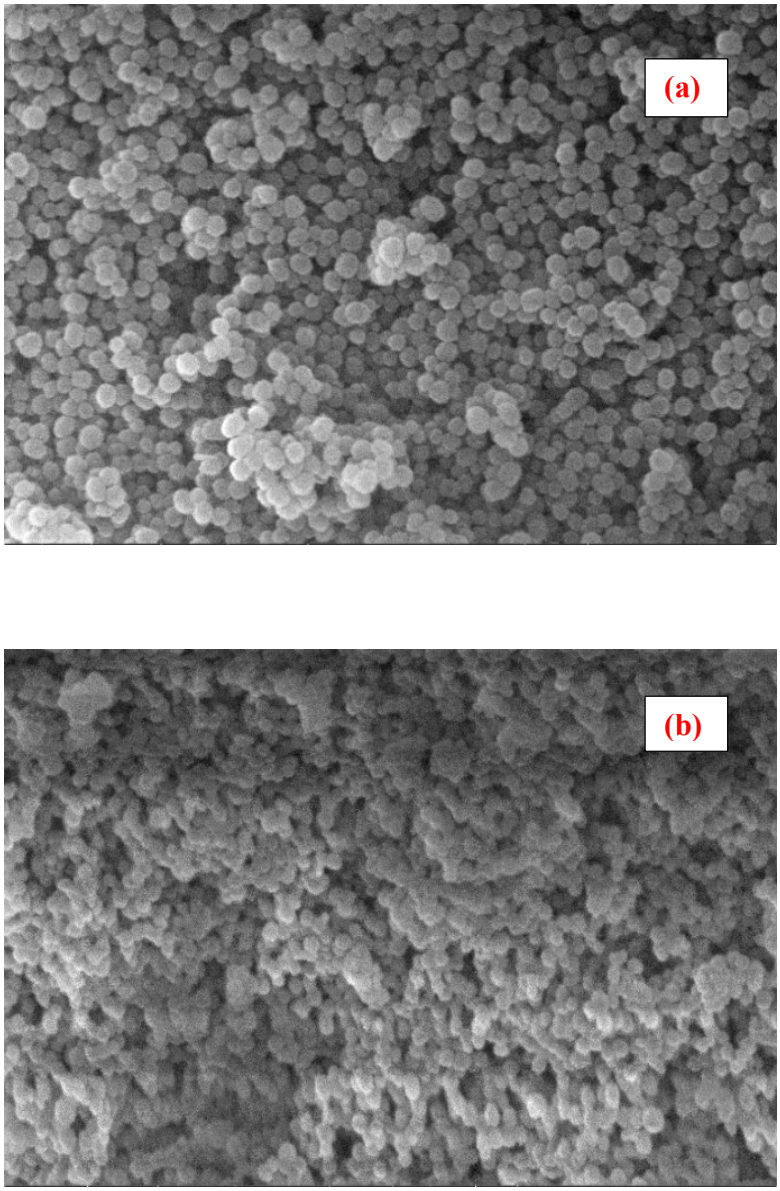

Fig. 4.16. FE-SEM images (a) Bare MCM-41, (b) 4- ABP loaded MCM-41.

4.2.2.2. Effect of adsorbent Dose (*m*): The effect of m on the adsorption of 4-ABP by MCM-41 was studied at C_0= 50 mg/L, optimum pH_i= 2 and T= 303 K by changing m from 0.04 to 0.5 g/L. An increase in m resulted in increased 4-ABP removal up to m= 0.2 g/L and remained consistent afterwards (Fig. 4.17). Increasing m provides large surface area for the adsorption, which in turn increases 4-ABP removal. Further, for $m \geq 0.2$ g/L, constant removal efficacy of MCM-41 imply that the adsorption process is adsorbate limiting (depending more on concentration of 4-ABP) not adsorbent. Thus, the optimum m (m_{opt}) for 4-ABP removal by MCM-41 was taken as 0.2 g/L.

4.2.2.3. Effect of contact time (*t*) and adsorption Kinetics: Experiments for the kinetic study was conducted by varying the C_0: 10-200 mg/L at T= 303 K, optimum pH_i= 2.0, m_{opt}= 0.2 g/L and t= 4 h. The collected kinetic data were then validated to pseudo-first-order (Equation 4.4) and pseudo second-order kinetic model (Equation 4.5) using non-linear regression, and adsorption time effect on 4-ABP removal by MCM41 were explored with kinetic parameter calculation.

Effect of t and adsorption kinetics of 4-ABP adsorption on to MCM-41 is shown in Fig. 4.18. Rapid initial adsorption (within 5 minutes) followed by a slower period was observed and ultimately adsorption rate becomes constant after 2 h (Fig. 4.18). It was observed true at all the C_o values. At initial stage of adsorption, fast initial removal may be due to the surface adsorption of 4-ABP onto enormous empty sites of MCM-41surface. After occupying all surface sites, diffusion of 4-ABP onto inner pores of the MCM-41, slows down the adsorption rate (Mangrulkar et al., 2008). The fittings of calculated q_t values by applying pseudo-second-order kinetic model have also been shown in Fig. 4.18 with continuous line, however, experimental data points are shown by symbols. The kinetic models parameters values along with the R^2 and MPSD values for both the kinetic models is illustrated in Table 4.4. It can clearly be understood that experimental kinetic data are generally best validated by pseudo-second order kinetic model with high R^2 (0.99) and smaller MPSD values. Values of k_S decreases, while h and q_e increases with increasing C_0 values. Since, the mass transfer coefficient for the diffusion of 4-ABP molecules to the surface as well as pores of MCM-41 controls the adsorption of 4-ABP on to MCM-41 surface. Therefore, with enhancement in C_0, rise to driving force to the adsorbate resulted higher mass transfer, which in turn increased of q_e and h.

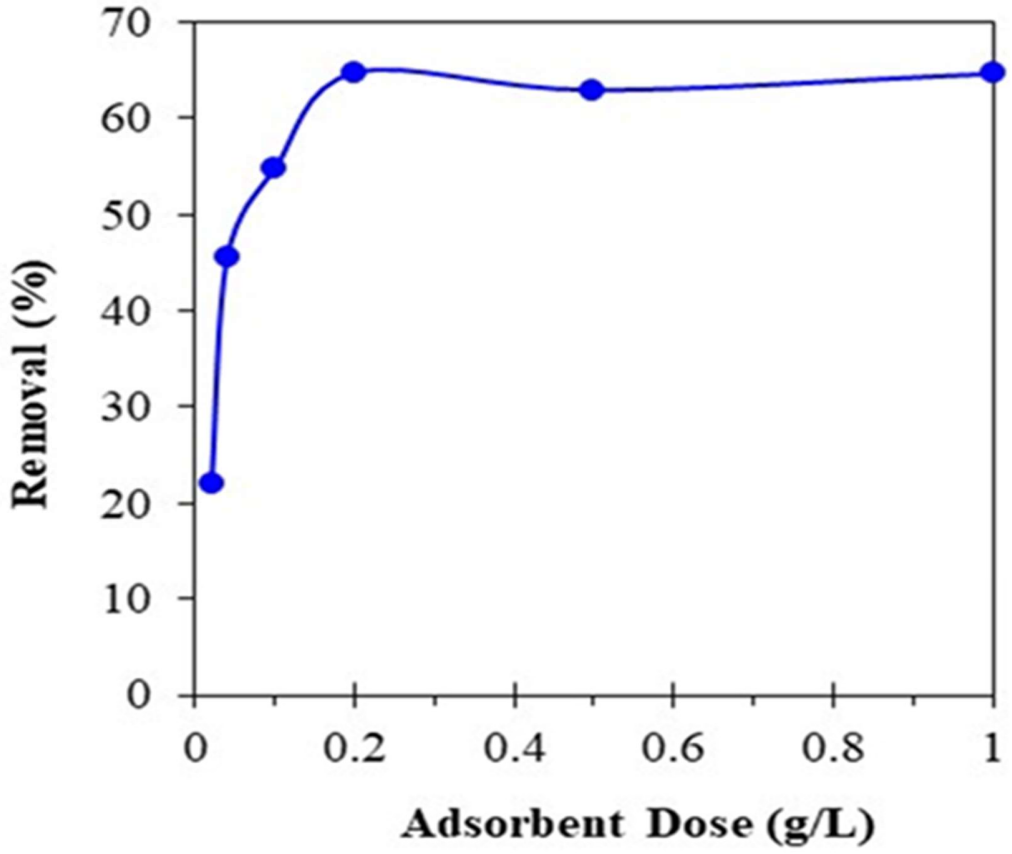

Fig. 4.17. Effect of adsorbent dose on the removal of 4-ABP by MCM-41 (C_0=50 mg/L, T= 303 K, *pHi*=2, t = 2 h).

Various adsorption steps are: film diffusion, pore or intra-particle diffusion and surface adsorption. The adsorption processes are controlled either by one or more above steps. For adsorbate-adsorbent systems with high degree of mixing and high adsorbent surface area (as in the present study), film diffusion resistance becomes negligible. Therefore, the intra-particle diffusion and surface diffusion may be the adsorption rate controlling steps.

Fig. 4.19 shows multilinear graph of q_t Vs $t^{0.5}$ of 4-ABP adsorption on MCM41. If rate controlling step is intra-particle pore diffusion, the q_t Vs $t^{0.5}$ graph must be linear and should pass through origin point. However, in present study multilinear graph of q_t Vs $t^{0.5}$ was obtained, therefore, it can be concluded that more than one rate controlling steps are involved in the process. First linear portion explains the gradual reach to equilibrium stage for 4-ABP adsorption with the intra-particle diffusion as rate-limiting step. Subsequently, extremely low 4-ABP concentrations decrease the intra-particle diffusion, and finally equilibrium stage is reached (second linear portion) (Rameshraja et al., 2012). Rate constants K_{i1} and K_{i2} are the slopes of the linear portions, and their values were found increasing with increase in C_o (Table 4.4) due to increased driving force at higher C_o.

Further, to investigate the actual rate controlling step, kinetic data obtained were further fitted to Boyd kinetic model (Equation 4.18). If the plot of B_t Vs t is linear and passes through origin, the rate controlling step can be represented by surface diffusion. It was seen that the plot of B_t versus t (not shown here) was non-linear with R-squared = 0.760- 0.975 at all C_i values studied. This implies that surface diffusion is not only the adsorption rate controlling step, but intra-particle diffusion may also be involved.

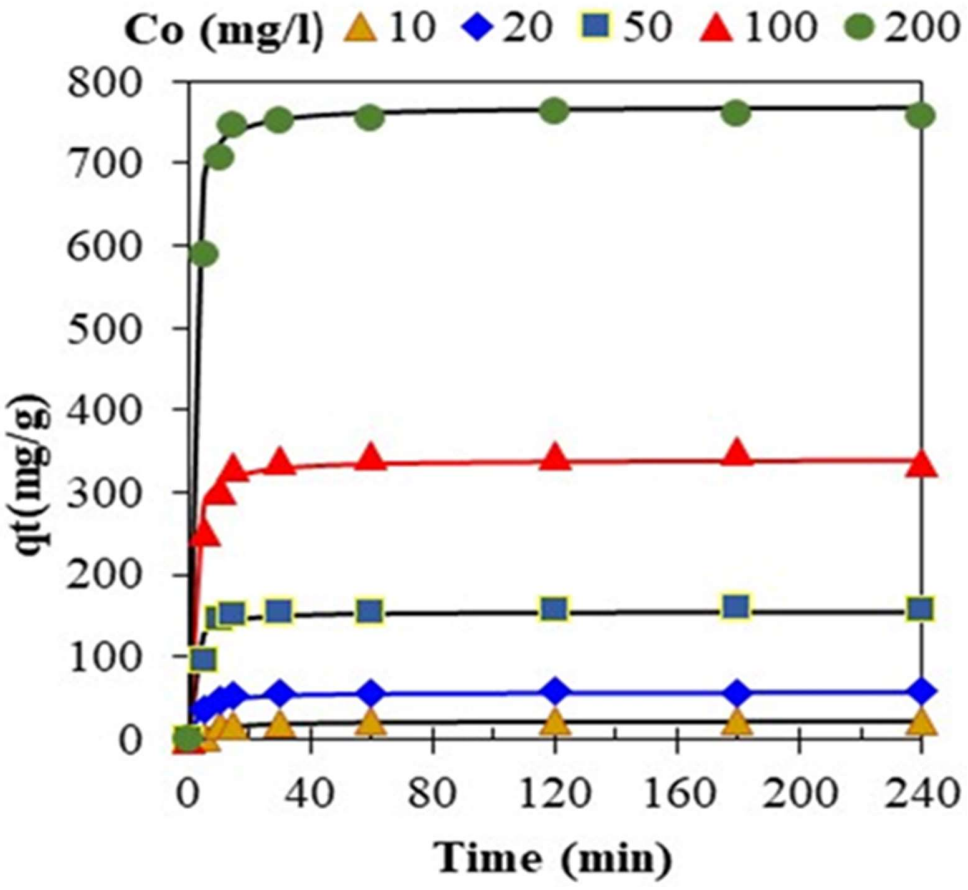

Fig. 4.18. Kinetics of 4-ABP removal by MCM-41. Symbols represent the data from experiments, whereas the lines pseudo-second-order kinetic model prediction (T = 303 K, pH_i =2, m_{opt} = 0.2 g/L).

Table 4.4. Kinetic parameters for removal of 4-ABP by MCM-41 (C_0 = 10–200 mg/L, t = 4 h, pH_i =2, m_{opt} = 0.2 g/L)

Pseudo-first-order model					
C_0 **(mg/L)**	$q_{e,exp}$ (mg/g)	$q_{e,cal}$ (mg/g)	K_f (min^{-1})	R^2	MPSD
10	21.09	21.50	0.1	0.96	97.25
20	57.59	57.75	0.3	0.98	24.04
50	157.63	153	0.4	0.96	20.94
100	337.18	338	0.4	0.98	13.28
200	757.28	752.21	0.5	0.99	10.23
Pseudo-second-order model					
C_0 **(mg/L)**	q_e, cal(mg/g)	K_s(g/mg min)	h (mg/g min)	R^2	MPSD
10	22	0.007	3.38	0.946	117.86
20	57	0.007	22.74	0.99	12.40
50	155	0.006	144.15	0.97	20.38
100	340	0.003	346.8	0.99	11.45
200	770	0.002	1185.8	0.99	8.62
Intra-particle diffusion					
C_0 **(mg/L)**	K_{i1} (mg/g $min^{1/2}$)	I_1(mg/g)	R^2	K_{i2} (mg/g $min^{1/2}$)	I_2 (mg/g)	R^2
10	1.547	11.338	1	0.2026	18.718	0.511
20	10.433	12.714	0.941	0.2539	53.962	0.567
50	35.557	20.331	0.894	0.4911	151.28	0.800
100	48.738	144.7	0.990	0.0918	342.08	0.540

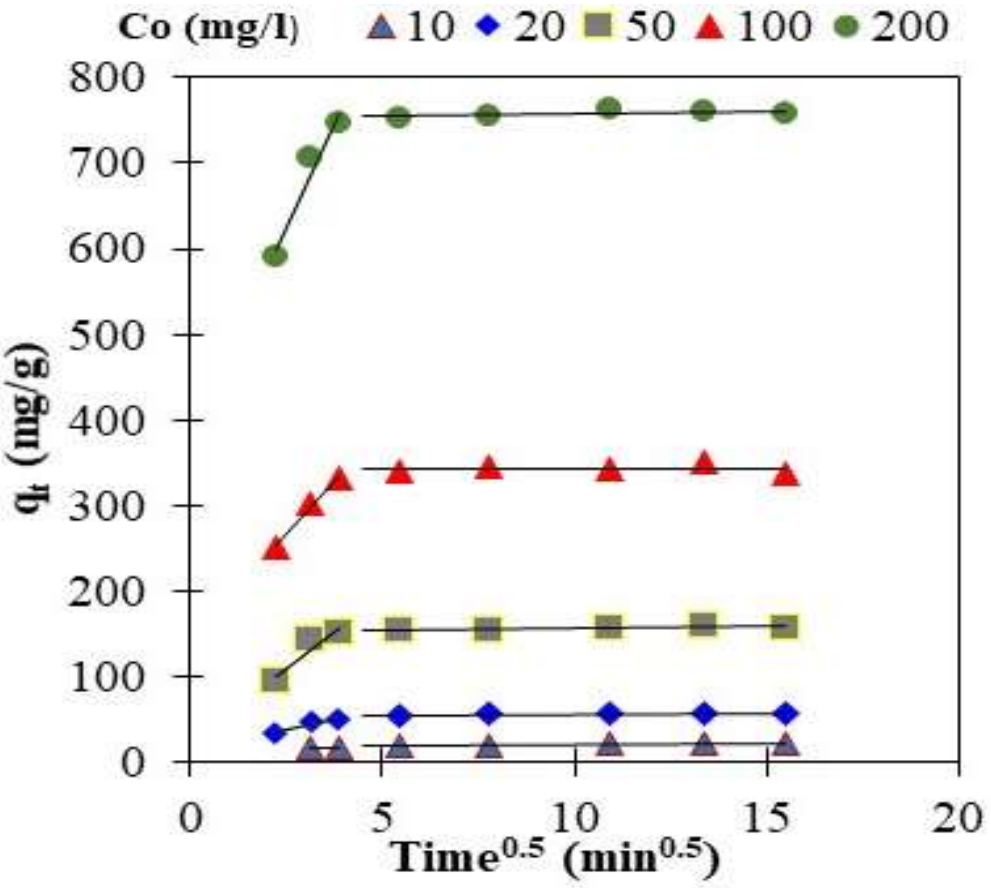

Fig. 4.19. Weber-Morris plot for the adsorption of 4-ABP by MCM-41 (C_0 = 10–200 mg/L, m_{opt} = 0.2 g/L, t = 4h).

.

4.2.2.4. Effect of temperature and adsorption isothermal study: Isothermal adsorption data of 4-ABP adsorption onto MCM-41were collected by conducting experiments at different temperatures (*T*) 283 K, 293 K and 303 K with C_0 values of 10-500 mg/L at optimum pH_i= 2.0, m_{opt}= 0.2 g/L and *t*= 4 h. The fitting of experimental data are graphed in the Fig. 4.20 and 4.21, and calculated isothermal parameters are listed in Table 4.5. High R-squared values for all isotherms studied implies their suitability to represent the adsorption of 4-ABP on to MCM-41. However, Freundlich and D-R isotherm both with high R^2 value well suits the equilibrium adsorption data of 4-ABP onto MCM-41 at all the temperatures.

Fig.4.20 demonstrates the fitting of Freundlich isotherm of experimental data at different temperatures. Increasing value of K_F with increase in temperature reveals more uptake of 4-ABP at increased temperature. This may be the result of increased kinesis of 4-ABP ions and enhanced intra-particle diffusion rate. High *1/n* values indicates the high affinity between 4-ABP and MCM-41, and heterogeneity of the adsorbent. Endothermic nature of the adsorption can be justified by increasing A_T value with increase in temperature (Table 4.5).

The fitting of experimental isotherm data on D-R isotherm model is shown in Fig. 4.21, and the values of D-R isotherm parameters are listed in Table 4.5. The value of K_{DR} decreases with increase in temperature, while that of Q_{DR} values increases. This indicates that higher temperature comprises high adsorption capacity. The mean free energy (*E*) values describes nature of adsorption (physical adsorption or chemisorption) (Ozcan et al., 2006). If the value of *E* lies below 8 kJ/mol, adsorption owe to weak van der Waals interaction (physical adsorption) and it is chemisorption for *E* ranging 8–16 kJ/mol. Obtained *E* values are limited within the range of 5.81–8.06 kJ/mol (Table 4.5). It suggests that physical adsorption play a major role followed by chemisorption at eminent temperatures.

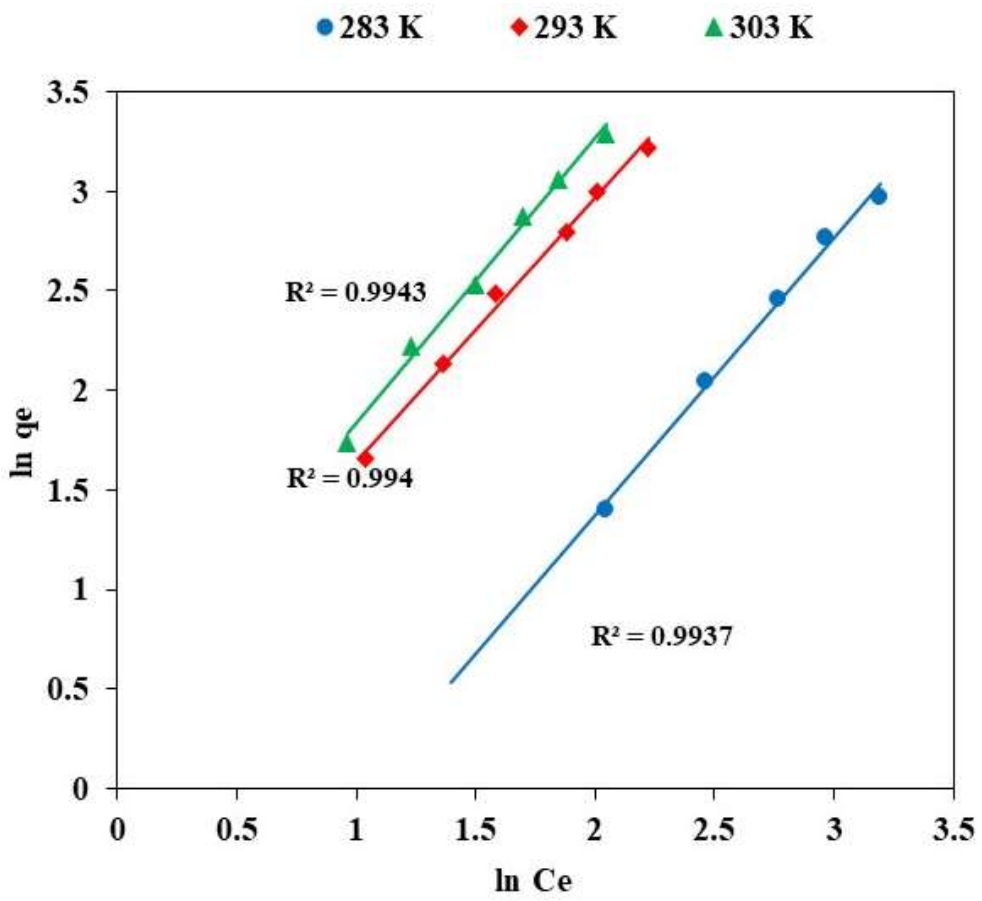

Fig. 4.20. Freundlich isotherms for the adsorption of 4-ABP by MCM-41 (C_0 = 10–500 mg/L, m_{opt} = 0.2 g/L, t = 2 h).

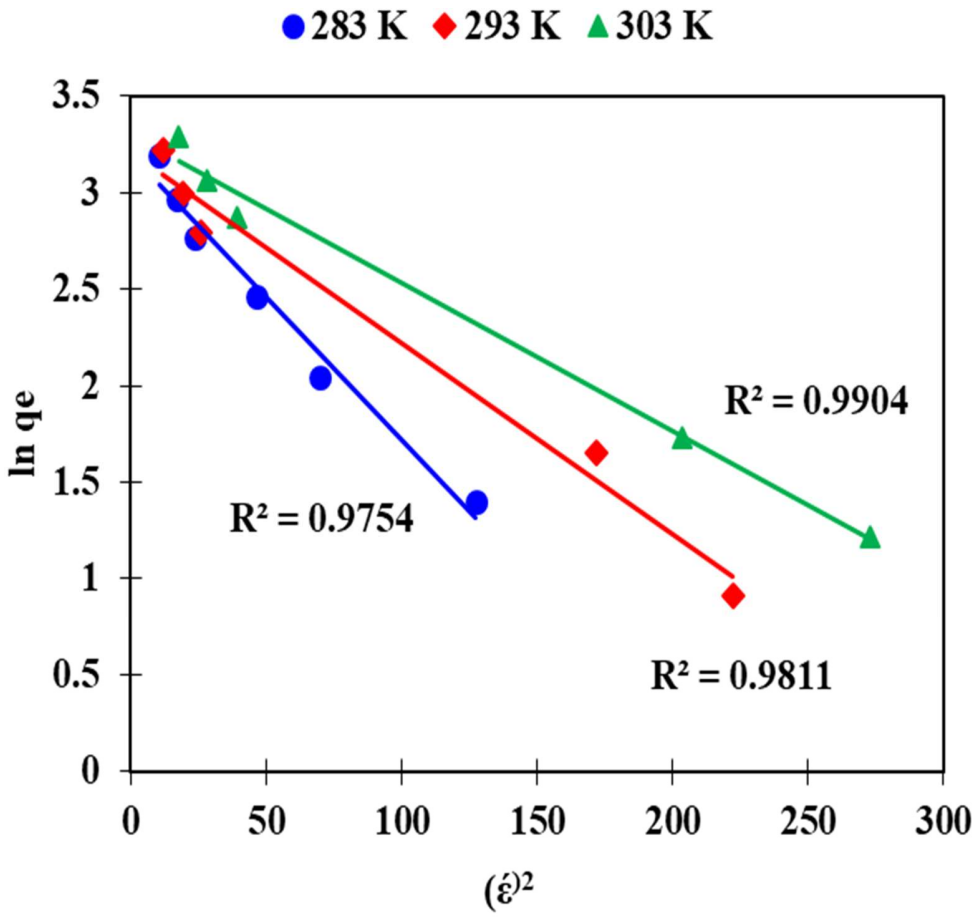

Fig. 4.21. D-R isotherms for the adsorption of 4-ABP by MCM-41 (C_0 = 10–500 mg/L, m_{opt} = 0.2 g/L, t = 2 h).

Table 4.5. Isotherm parameters for the treatment of 4-ABP by MCM-41 (C_0= 10 -500 mg/L, t = 2 h, pH_i =2, m_{opt} = 0.2 g/L)

Freundlich Isotherm			$q_e = K_F C_e^{1/n}$
T (K)	K_F ((mg/g)/(l/mg)$^{1/n}$)	*1/n*	R^2
283	0.244	1.391	0.993
293	1.497	1.431	0.994
303	1.3861	1.319	0.994
Temkin Isotherm		$\boldsymbol{q_e = B \ln A_T + B \ln C_e}$	
T (K)	B	A_T(L/g)	R^2
283	986.41	0.2856	0.919
293	822.46	0.3840	0.946
303	1080.8	0.3997	0.928
D-R Isotherm		$\boldsymbol{\ln(q_e) = lnQ_{DR} - K_{DR}\ (\varepsilon)^2}$	
T (K)	K_{DR} (mol^2 /kJ^2)	Q_{DR} (mg/g)	E (kJ/mol)	R^2
283	0.0148	24.459	5.8123	0.9754
293	0.0099	24.657	7.1073	0.9811
303	0.0077	26.966	8.0645	0.9904

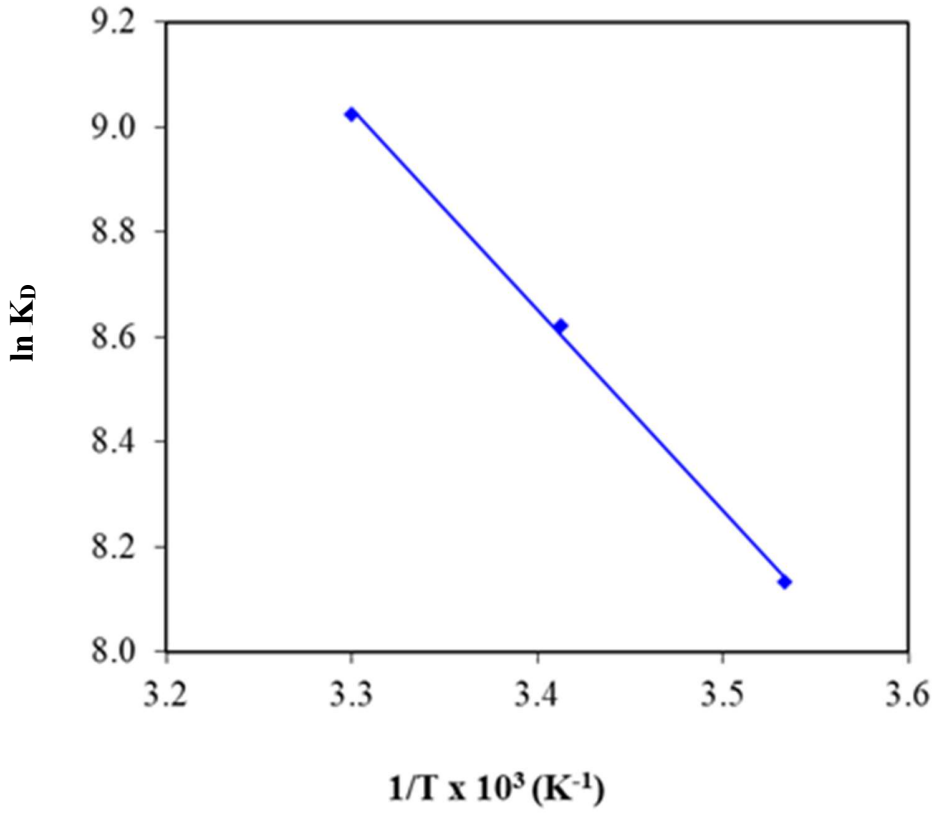

Fig. 4.22. ln K_D *vs* 1/T Plot to estimate the thermodynamic parameters for the adsorption of 4-ABP.

Table 4.6. Thermodynamics parameters for the adsorption of 4-ABP by MCM-41 (C_0= 10-500 mg/L, t = 2 h, pH_i =2, m_{opt}= 0.2 g/L)

T (K)	ΔG° (kJ/mol)	ΔH° (kJ/mol)	ΔS° (kJ/mol K)
283	-19.21	30.579	175.87
293	-20.91		
303	-22.73		

4.2.2.5. Estimation of Thermodynamic Parameters: Detailed theoretical background for the calculation of thermodynamic parameters has been discussed in section 4.2.1.5. Thermodynamic parameters were estimated from ln K_D Vs $1/T$ plot (Van't Hoff) (Fig. 4.22) and values obtained are summarized in Table 4.6. ΔS° and ΔH° were obtained to be 175.87 KJ/mol K and 30.579 kJ/mol, respectively. The positive ΔH° indicates the endothermic characteristic of 4-ABP adsorption on to MCM-41. However, the positive ΔS° values suggested increased randomness at the interface at increased temperature (Mirzajani et al., 2016). Due to this affinity of the 4-ABP is increased towards MCM-41. Negative ΔG° values implies that process of adsorption is feasible and spontaneous. Increase in its negativity with increased temperature indicates accelerated 4-ABP adsorption at higher temperature. This is due to lowered viscosity of solution at elevated temperature which boosts the rate of mass transfer from the liquid to solid phase.

From the data obtained in sections 4.2.1 and 4.2.2., we conclude that the adsorption of both the aromatic amines shows almost similar behavior. q_e of MCM-41 were found to increase with increase in C_0 and T. pH study and FTIR analysis revealed high electrostatic attraction between amines and MCM-41 and no chemical change of MCM-41 surface was observed. Kinetic study concluded that both 4- COT and 4-ABP adsorption by MCM-41 follows pseudo-second order kinetics. Intra-particle diffusion with surface diffusion were found involved in adsorption rate controlling. Increasing Temkin isotherm parameter, A_T, with temperature concluded endothermic nature of adsorption. Negative ΔG° with increasing magnitude at increased temperature depicted the feasible and spontaneous adsorption.

Chapter – 5

HEAVY METALS ADSORPTION

5.0 GENERAL

This chapter deals with the adsorptive interaction characteristics of heavy metals [Zn(II) and Cr(VI)] with MCM-41 from their synthetic Single/binary aqueous solution.

5.1. MATERIALS AND METHODS

5.1.1. Chemicals and Wastewater

Analytical and reagent grade chemicals were used. Potassium dichromate ($K_2Cr_2O_7$) and 1000 ppm standard Zinc stock solution were supplied by Sigma (Aldrich). Loba Chemie supplied NaOH and HCl. Throughout the study, aqueous solutions were prepared in double distilled water. Cr(VI) solution was prepared by mixing 2.8287 g (99.9%) $K_2Cr_2O_7$ in 1 L distilled water (Parida et al., 2012). Synthetic working solution used in this study was prepared in double distilled water with addition of required amount of respective Zn(II) and Cr(VI) stock solutions.

5.1.2. Experimental Procedure

For each experiment, the adsorbent (MCM-41) of known fixed quantity was added into 100 ml conical flasks containing Zn (II) and/or Cr (VI) solutions of known concentration (C_o) and initial pH (pH_i), and shaken in an temperature controlled incubator at controlled temperature and uniform speed of 180 rpm. After adsorption, the adsorbent was separated out by centrifuging at 6000 rpm for 5 min, and final pH (pH_f) and residual Zn (II) and Cr (VI) concentration was determined. The residual solution concentration was analyzed by atomic adsorption spectrophotometer (AA500, Lab India). The equilibrium concentration (C_e) was calculated using equation 4.1 and the adsorption capacity at time t, (q_t) and at equilibrium (q_e) is calculated using equation 4.2 and 4.3.

5.1.3. Adsorption Kinetics

The kinetic parameters for (Zn(II)/Cr(VI)) adsorption on to MCM-41 were evaluated by pseudo-first-order/pseudo second-order kinetic models (equation 4.4 and 4.5, respectively) and

validated to the experimental kinetic data and MPSD error function was calculated using equation 4.7. (Section 4.1.3.)

5.1.4. Adsorption Isothermal Study

Investigation of adsorption equilibrium and adsorption capacities at adsorption equilibrium delivers vital information regarding adsorption pathway reactions. To explore the effect of Cr (VI) presence on Zn (II) adsorption from Zn (II)–Cr (VI) binary aqueous solution, Cr (VI) concentration (C_o) was varied from 0–95mg/L in Zn (II) presence from 0–75mg/L concentration. Isothermal experiments were piloted at 288, 298, 308 K temperatures. The values of equilibrium adsorption capacity ($q_{e,i}$), single component adsorption (Ad_i) and all components adsorption (Ad_{Tot}) were obtained by utilizing the equations 5.1 to 5.3.

$$q_{e,i} = \frac{\left(C_{o,i} - C_{e,i}\right)}{m} V \tag{5.1}$$

$$A_{di} = \frac{\left(C_{o,i} - C_{e,i}\right)}{Co,i} * 100 \tag{5.2}$$

$$A_{dTot} = \frac{\left(\sum (C_{o,i} - C_{e,i}\right)}{\sum Co,i} * 100 \tag{5.3}$$

The obtained equilibrium data were then correlated to various competitive multicomponent isotherm models (Langmuir (extended), Sheindorf–Rebuhn–Sheintuch (SRS) model, Freundlich isotherm and modified R–P isotherm). Difference between the experimental and calculated q_e values obtained from various multi-component isotherms were calculated using MPSD (equation 4.7).

5.1.4.1 Multicomponent isotherm equations: The behavior of adsorption of two or more components is totally different from that of single component adsorption which can't be explained by above mentioned isotherm equations. Therefore, to judge multicomponent adsorption mechanism various researchers have modified the isotherm equations explained below.

5.1.4.1.1. Non-modified competitive Langmuir model: For simultaneous adsorption of *i* component in a N component system using basic Langmuir model (equation 4.4), we get, (Srivastava et al., 2006)

$$q_{e,i} = \frac{q_{mi} K_{L,i} C_{e,i}}{1 + \sum_{j=1}^{N} K_{L,j} C_{e,j}} \tag{5.4}$$

Where $q_{m,i}$ and $K_{L,i}$ is assessed by Langmuir isotherm equations 's fitting.

5.1.4.1.2. Modified competitive Langmuir isotherm: Constants obtained from isotherm equations for single system may not be able to describe the specific metal ions interaction and among that specific metal ions and combined mixture. By diving the specific adsorbate concentration by interaction term η_i, we get the modified competitive Langmuir isotherm equation to study the interactive effect of different components as shown in equation 5.4 (Srivastava et al., 2006).

$$q_{e,i} = \frac{qm,iK_{L,i}(C_{e,i}/ni)}{1 + \sum_{j=1}^{N} K_{Ll}(C_{e,j}/ni)} \tag{5.5}$$

5.1.4.1.3. Extended Langmuir isotherm: Yang et al. (1987) extended the simple Langmuir equation for multi-component system on the assumption that all sites present on the surface are uniform and every single adsorbate molecule compete for the very same site. It is given by equation 5.6:

$$q_{e,i} = \frac{q_{\max} K_i C_{e,i}}{1 + \sum_{j=1}^{N} K_j C_{e,j}} \tag{5.6}$$

Here q_{max} and K_i are parameters attained from the fitting of this equation with the experimental values.

5.1.4.1.4. Extended Freundlich isotherm: For any binary mixture, Fritz (1974) proposed the extended Freundlich equations given as equation 5.7 and 5.8.

$$q_{e,1} = \frac{K_{F,1} C_{e,1}^{n_1 + x_1}}{C_{e,1}^{x_1} + y_1 C_{e,2}^{z_1}} \tag{5.7}$$

$$q_{e,2} = \frac{K_{F,2} C_{e,2}^{n_2 + x_2}}{C_{e,2}^{x_{21}} + y_2 C_{e,1}^{z_2}} \tag{5.8}$$

Values of $K_{F,1}$; $K_{F,2}$ and n_2 are taken from simple Freundlich isotherm equation for single system, and other six parameters such as x_1; y_1; z_1 and x_2; y_2; z_2 are the multicomponent Freundlich constants for respective components.

5.1.4.1.5. Sheindorf–Rebuhn–Sheintuch (SRS) equation: On the basis of Freundlich isotherm equation Sheindorf et al. (1981) derived an equation for multicomponent system given as SRS equation (Equation 5.9):

$$q_{e,i} = K_{F,i} C_{e,i} \left(\sum_{j=1}^{N} a_{ij} C_{e,j} \right)^{n_i - 1} \tag{5.9}$$

Values of n_i and $K_{F,i}$ should be taken from simple single-component Freundlich equation. a_{ij} is competitive coefficient (adsorption inhibition of component i owing to the presence of component j) determined from experimental data of multi-component system.

5.1.4.1.6. Modified competitive Redlich–Peterson isotherm: Modified R-P model consists of only one interaction parameter η, as in the case of modified Langmuir model, which depicts the intensity of interaction between the adsorbate and the adsorbent (Srivastava et. al., 2006) given as:

$$q_{e,i} = \frac{K_{R,i} \left(C_{e,i} / \eta_{R,i} \right)}{1 + \sum_{j=1}^{N} a_{R,j} \left(C_{e,j} / \eta_{R,j} \right)^{\beta,j}} \tag{5.10}$$

5.2. RESULT AND DISCUSSION

5.2.1. Adsorption studies of Zn (II) and Cr (VI)

Adsorptive studies of Zn (II) and Cr (VI) with MCM-41 was done to inspect the effect of pH, adsorbent dose, adsorbate concentration, time and temperature in individual system (Zn (II)/Cr (VI) − MCM-41), and optimum condition was obtained. Further, simultaneous adsorptive interaction of binary solution of Zn (II) and Cr (VI) with MCM-41 was performed at the optimized condition were examined.

5.2.1.1. Effect of initial pH (pH_i): pH values of heavy metal solution not only governs adsorbent surface chemistry but also significantly affects the kinetics of adsorption along with equilibrium. The effect of pH_i on Zn (II) and Cr (VI) adsorption by MCM-41 was explored by altering the pH_i 2 to 9 with C_0 = 50 ppm and m =0.1g/L at T=298K (Fig.5.1). Natural pH of Zn (II) aqueous solution (50 mg/L) was found to be pH=1.3, whereas for the Cr (VI) solution it is 4. HCl/NaOH solutions of 0.1 M were used to change the pH of the solution to desired level.

In case of Zn(II), no removal was observed up to pH 5.0. At all 5< pH≤ 7 the Zn (II) % removal was found increasing, and becomes nearly constant to 82.0% beyond pH=7.0 (Fig.5.1). This behavior of MCM-41 on Zn (II) adsorption can be clarified by adsorbent surface characteristic modification with pH_i variation. In an acidic solution, MCM-41 surface is protonated via the reaction taking place shown in equation 5.11.

$$[\text{Si-OH}] + [\text{H-OH}] \xrightarrow{H^+} \text{Si-OH}^{2+} + 2\text{OH}^- \qquad (5.11)$$

This protonated adsorbent surface at pH< 5 is responsible for electrostatic repulsion between MCM-41 surface and the cationic metal ion resulting no removal (Srivastava et al., 2006). Also, higher concentration of H^+ in highly acidic pH, and competitive adsorption between H^+ and metal ions, MCM-41 shows higher affinity towards H^+ to adsorb causing protonation of active sites, and thus decreasing the available adsorption sites for metal ions (Kara et al., 2017). Hence, the adsorption capability of MCM-41 for Zn (II) was found lower at lower pH.

As pH_i of the solution is increased, the positively charged active sites on MCM-41are reduced and the negatively charged active sites are increased (shown in equation 5.12 and 5.13) which favored the cationic Zn (II) ions adsorption due to electrostatic attraction (Srivastava et al., 2006).

$$\text{Si-OH} + \text{OH}^- \longrightarrow \text{SiO}^- + \text{H}_2\text{O} \qquad (5.12)$$

$$\text{SiO}^- + \text{Zn}^{2+} \longrightarrow \text{Si-O-Zn} \qquad (5.13)$$

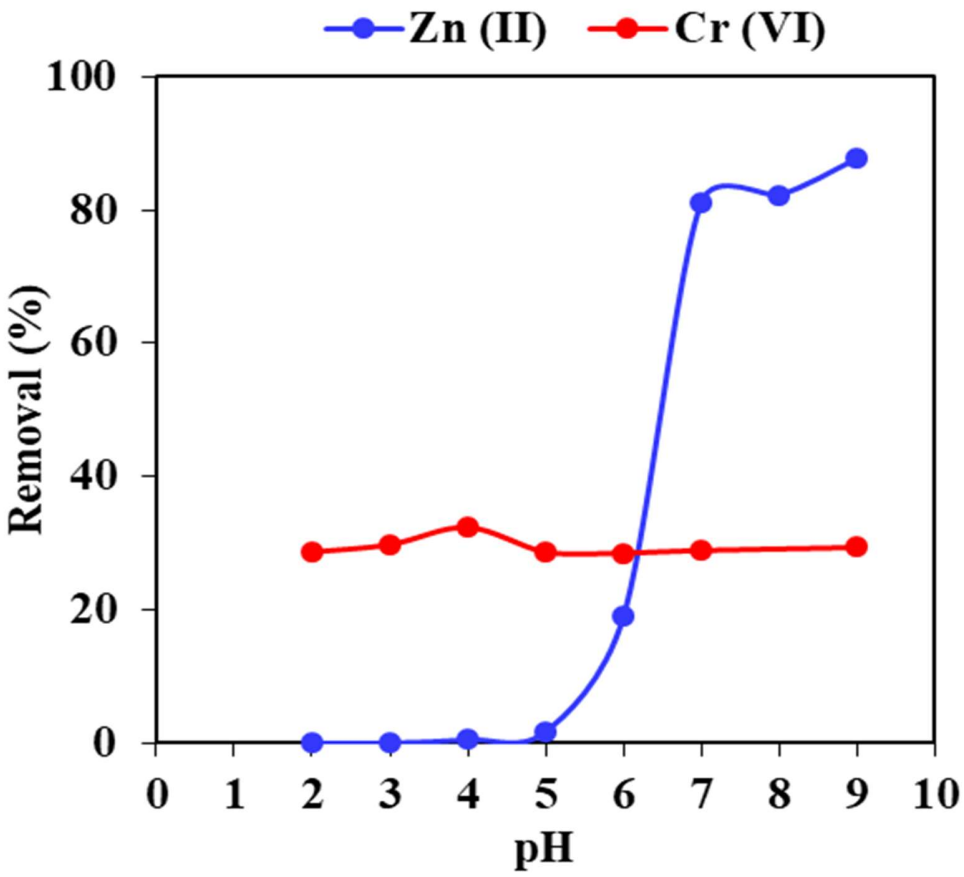

Fig. 5.1. Influence of initial pH on the Zn (II) and Cr (VI) adsorption (C_0= 50 mg/L, T=298 K, m=0.1 g/L, t= 2h).

In case of Cr (VI), removal increases with rise in solution pH and attains maxima at pH 4.0 and then deteriorates and becomes almost constant beyond pH > 5. This behavior was observed as a result of different forms of Cr (VI) ions formation at distinct pH's. At pH 4–5 Cr (VI) exists as anions $HCr_2O_7^-$ and $Cr_2O_7^{2-}$ at pH 4–5 (Tian et al., 2011). Protonated MCM-41 easily adsorbs the anions that are highly active and polar. On the other hand, MCM-41become negatively charged with increase in pH which resists the further adsorption of anions in the form $HCr_2O_7^-$ and $Cr_2O_7^{2-}$ beyond pH > 5 and removal % remains constant (Tian et al., 2011). Schematic probable mechanism for Cr (VI) and Zn (II) adsorption on MCM-41 is demonstrated in Fig 5.2.

Since, it's difficult to maintain basic pH as Zn^{2+} ions forms $Zn(OH)_2$ at higher pH with OH^- ions, therefore, it's preferable to perform further studies at the natural pH_i =7, which can be considered as optimum *pH*.

Samples were characterized after adsorption of heavy metals using different characterization techniques such as XRD, FTIR and SEM/EDX. No change was observed in the XRD spectra of the adsorbent after the adsorption reveals that no damage of the adsorbent occurs during the process of adsorption. The surface functional groups were further characterized by FT-IR spectroscopy (Fig. 5.3). It Clarifies that the surface functional groups of the adsorbents remains same after the adsorption. However, one low-frequency region peaks owe to metal−oxygen−metal vibrations (Wang et al. 2017).. The EDX result showed 40.3% and 59.7% Silica (Si) and oxygen (O), respectively, in the bared MCM-41. However, the loaded MCM-41 (after binary adsorption) revealed 36.5%, 57.4%, 2.3% and 3.8% Si, O, Cr and Zn, respectively.

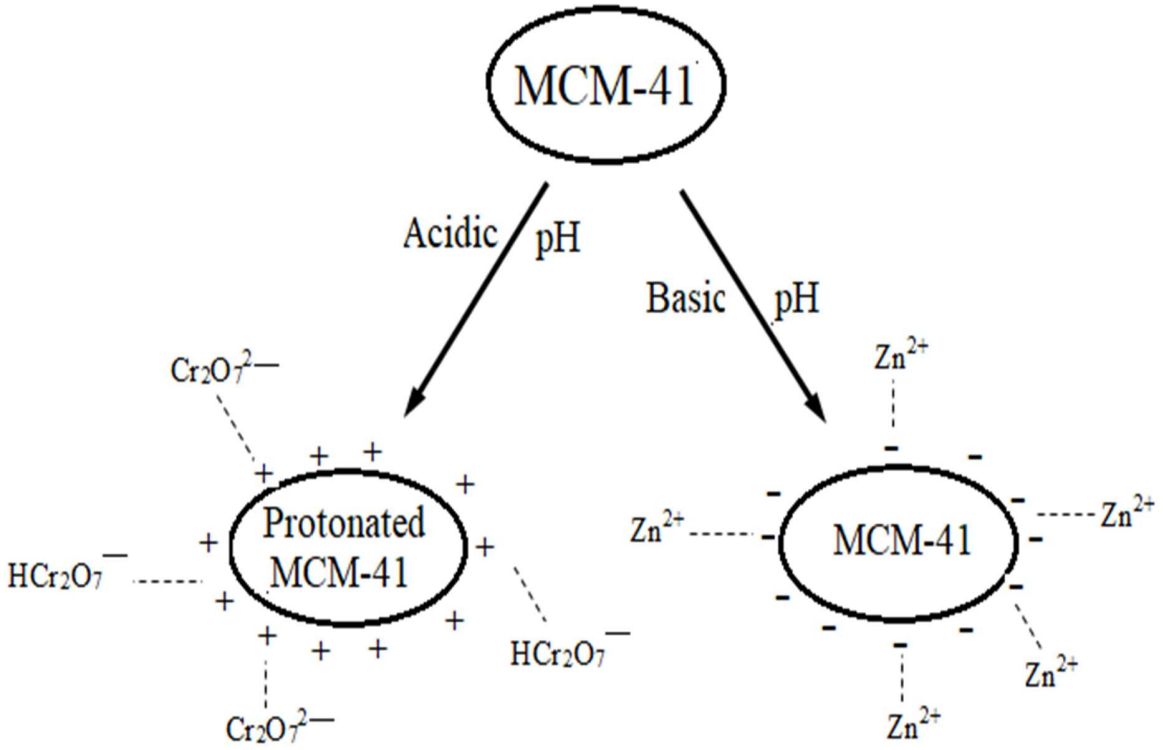

Fig.5.2. Schematic probable mechanism for Cr (VI) and Zn (II) adsorption on MCM-41 ($HCr_2O_7^-$ and $Cr_2O_7^{2-}$ are the Cr (VI) forms at lower pH).

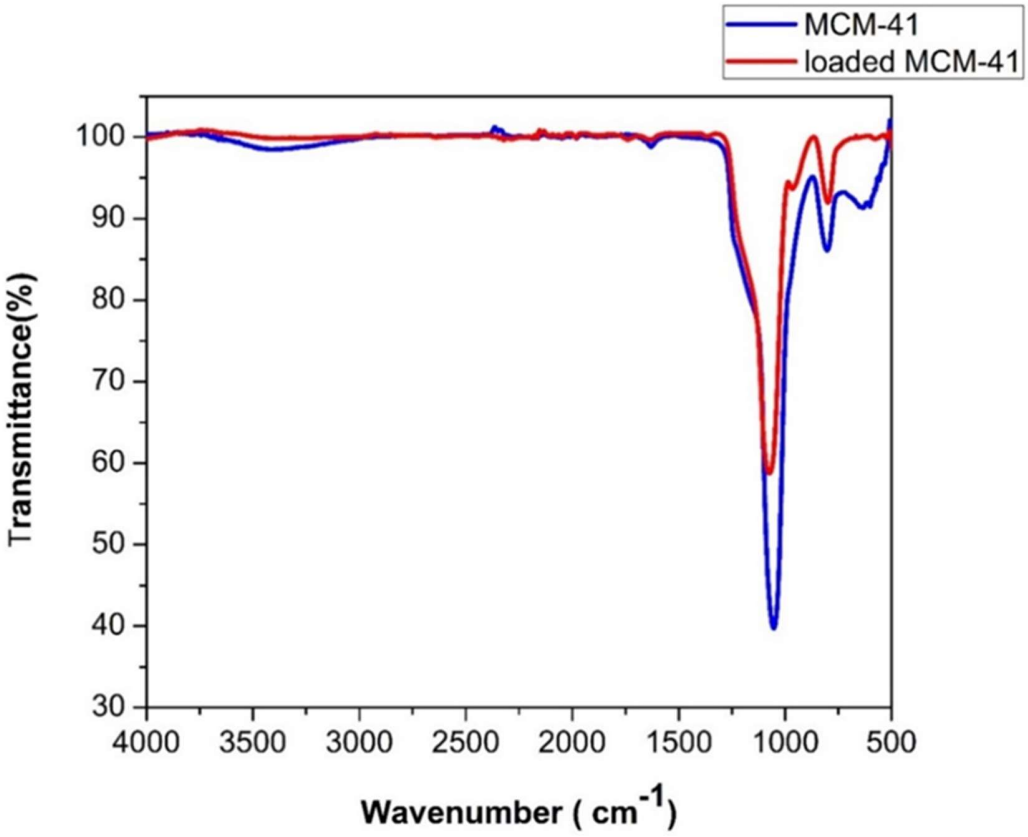

Fig. 5.3. FTIR spectra of MCM-41 and Cr (VI) and Zn (II) loaded MCM-41.

5.2.1.2. Effect of adsorbent dose (*m*): The outcome of MCM-41 dose (*m*) on Zn (II) as well as Cr (VI) removal was studied by changing *m* from 0.01- 0.3g/L. Other parameters were: C_0 = 50 mg/l; optimum pH_i = 7; and T = 298 K. Fig. 5.4 manifest that by increasing *m* up to 0.1 g/L, an upsurge in the Zn (II) and Cr (VI) adsorption was observed. But beyond *m* = 0.1 g/L, it remained nearly unaffected.

For *m*>= 0.1 g/L adsorption remains constant due to "very low concentration of adsorbate i.e. "limited adsorbate" present in the solution. Adsorbate limiting adsorption means that the adsorption depends more upon the concentration of the solution and less upon the *m* . These results may be attributed to the poor access to the available vacant sites of the adsorbent for m >= 0.1 g/L due to overcrowding/ agglomeration of adsorbent particles. Moreover, the high adsorbent dosage could impose a screening effect of the dense outer layer of the adsorbate, thereby shielding the binding sites from metal. Therefore, at this stage concentration dominates by enhancing the driving force between the heavy metal ions and adsorbent with enhancement of C_0. Thus, the optimum *m* (m_{opt}) for Zn (II) as well as Cr (VI) adsorption by MCM-41 was considered as 0.1 g/L.

5.2.1.3. Effect of contact time (*t*) and adsorption Kinetics: Adsorbate-adsorbent contact time effects and kinetics was conducted for C_0= 50 mg/L at 298 K, pH_i=7.0, m_{opt}=0.1 g/L. The kinetic data were collected up to 4h.The obtained experimental kinetic data were further fitted to pseudo-first-order (Equation 4. 4) and pseudo second-order kinetic model (Equation 4. 5) using non-linear regression technique, and the consequence of time on heavy metal ions adsorption by MCM-41 were found out with kinetic parameter calculation.

Obtained kinetic parameters and MPSD values along with R^2 squared values calculated from the experimental kinetic data fitting to pseudo-first-order and pseudo second-order kinetic models for both Zn(II) and Cr(VI) are shown in Table 5.1. High R-squared values (0.99) and smaller MPSD values shows that it follows pseudo second-order kinetics. Rapid uptake by adsorbent was observed within first ten min followed by a slow phase with constant removal after 2h showing equilibrium clearly depicted in Fig.5.5. Fast initial removal is owing to the vacant sites availability in hefty number at surface of adsorbent indicating surface adsorption, and the lethargic next stage is dedicated to Zn^{2+} and Cr^{2+}ions diffusion onto inner pores of the adsorbent after filling of all surface sites (Mangrulkar et al., 2008), meeting much larger

confrontation ensuing in slow adsorption in second phase (Srivastava et al., 2006; Santos et al., 2013).

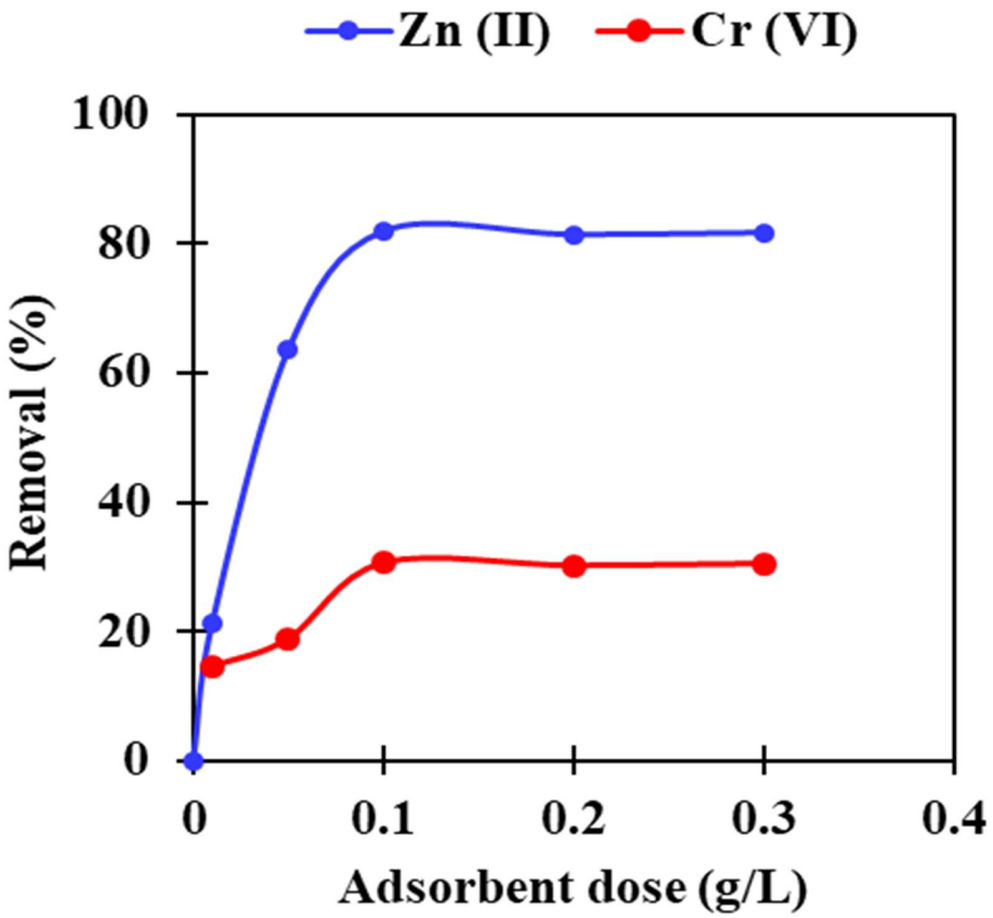

Fig 5.4. Effect of adsorbent dose on removal of Zn (II) (C_0=50 mg/L, T= 298 K, t = 2 h).

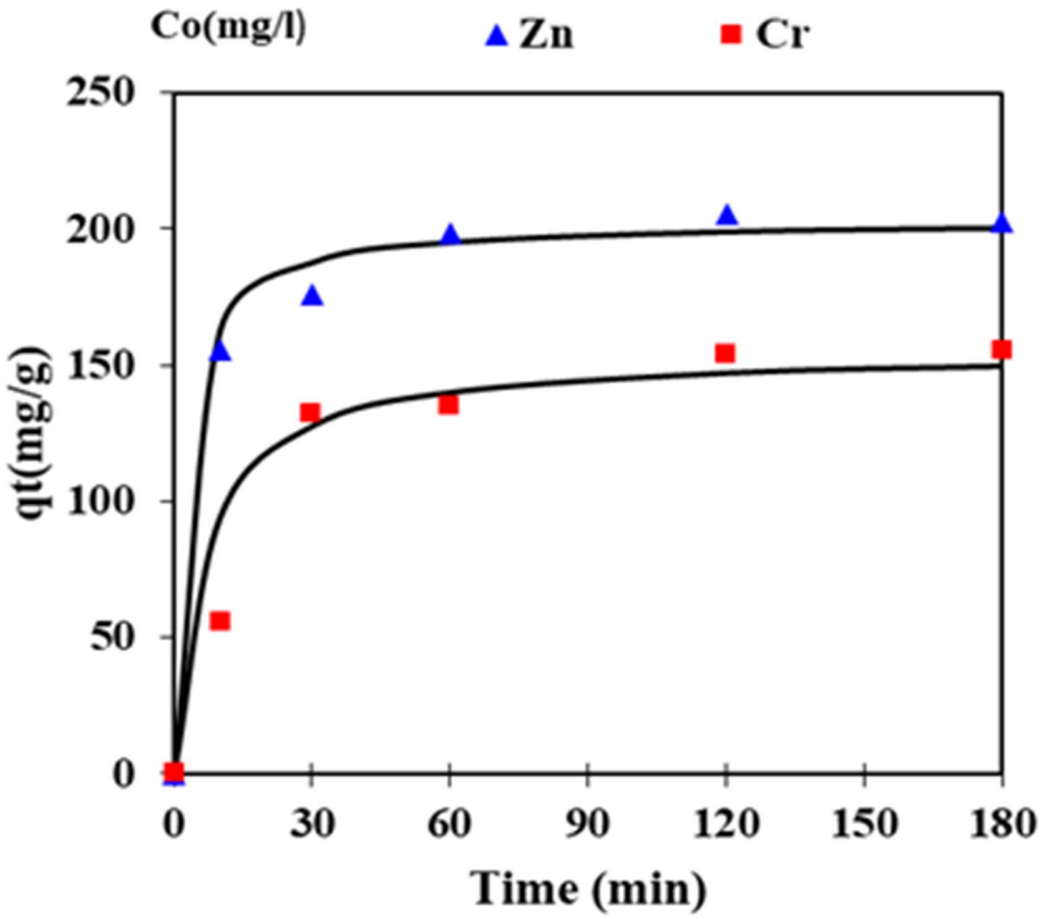

Fig. 5.5. Kinetics of Zn (II) and Cr (VI) adsorption by MCM-41. Symbols represent the data from experiments, whereas the lines pseudo-second-order kinetic model prediction (C_0=50 mg/L, T= 298 K, m = 0.1 g/L).

5.2.1.4. Estimation of Thermodynamic Parameters: Various thermodynamic parameters like Gibbs free energy change *(ΔG°),* the entropy change *(ΔS°)* and the heat of adsorption (ΔH°) were obtained from the linear plot of ln K_D versus $1/T$ (Fig. 5.6) using Equation 4.20 and 4.21 and have been summarized in Table 5.3. Value of K_D was found to decreases with raised T. The positive value ΔH° reveals the endothermic nature of adsorption. In physical adsorption, weak van der Walls forces are involved among the adsorbate and adsorbent interaction with low adsorption energy of 5-10 kJ/mol, whereas it is 30-70 kJ/mol for chemisorption (Kushwaha et al., 2010). In the present study, positive value of ΔH° of 54.20 kJ/mol for Zn (II) and 9.43 kJ/mol for Cr (VI) was attained. Therefore, it seems that the adsorption of Cr (VI) follows physical adsorption whereas Zn (II) adsorption onto MCM-41 follows chemical adsorption.

High entropy value for Cr (VI) of 100.281 kJ/mol K was found which was similar to the investigation done by Parida et al. (2012), which reported high ΔS° value of 129.56 kJ/mol K for adsorption of Cr (VI) onto MCM-41. However, the positive ΔS° values suggested increased randomness at the interface at increased temperature (Mirzajani et al., 2016). Due to this affinity of heavy metal ions is increased towards MCM-41. Negative ΔG° values implies spontaneous and feasible nature of adsorption. Increase in its negativity with increased temperature indicates accelerated adsorption at higher temperature. This is due to lowered viscosity of solution at elevated temperature which enhances the rate of mass transfer from the aqueous adsorbate to solid adsorbent.

Table 5.1. Kinetic parameters for removal of Zn (II) and Cr (VI) by MCM-41 (C_0 = 50 mg/L, t = 4 h, pH_i =7, m_{opt} = 0.1 g/L)

Pseudo-first-order model [Zn (II)]					
C_0 (mg/L)	$q_{e,\ exp}$ (mg/g)	$q_{e,\ cal}$ (mg/g)	K_f (min^{-1})	R^2	MPSD
50	203	196	0.2	0.98	14.76
Pseudo-second-order model [Zn (II)]					
C_0 (mg/L)	$q_{e,\ cal}$(mg/g)	K_s (g/mg min)	H (mg/g min)	R^2	MPSD
50	203	0.002	82.418	0.996	8.89

Pseudo-first-order model [Cr (VI)]					
C_0 (mg/L)	$q_{e,\ exp}$ (mg/g)	$q_{e,\ cal}$ (mg/g)	K_f (min^{-1})	R^2	MPSD
50	155	156	0.1	0.96	52.80
Pseudo-second-order model [Cr (VI)]					
C_0 (mg/L)	$q_{e,\ cal}$(mg/g)	K_s (g/mg min)	h (mg/g min)	R^2	MPSD
50	155	0.001	24.025	0.96	41.61

Table 5.2. Adsorption thermodynamic parameters of Zn (II) and Cr (VI) adsorption by MCM-41 (C_0= 10 -300 mg/L, t = 2 h, pH_i=2, m= 0.2 g/L)

Temperature (T) (K)	**Kx 10^{-3} (l/kg)**	**ΔG° (kJ/mol)**	**ΔH° (kJ/mol)**	**ΔS° (kJ/mol K)**
Zn (II)				
288	3.4722	-17.1881	54.2082	247.8487
298	3.3557	-19.5997		
308	3.3003	-20.9251		
Cr (VI)				
288	3.4722	-19.4542	9.4329	100.2818
298	3.3557	-20.4320		
308	3.3003	-20.9656		

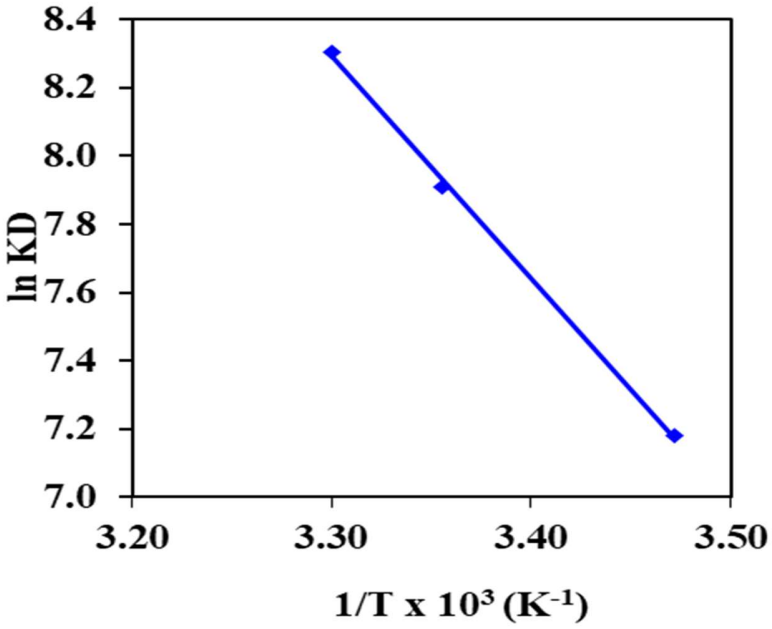

(a)

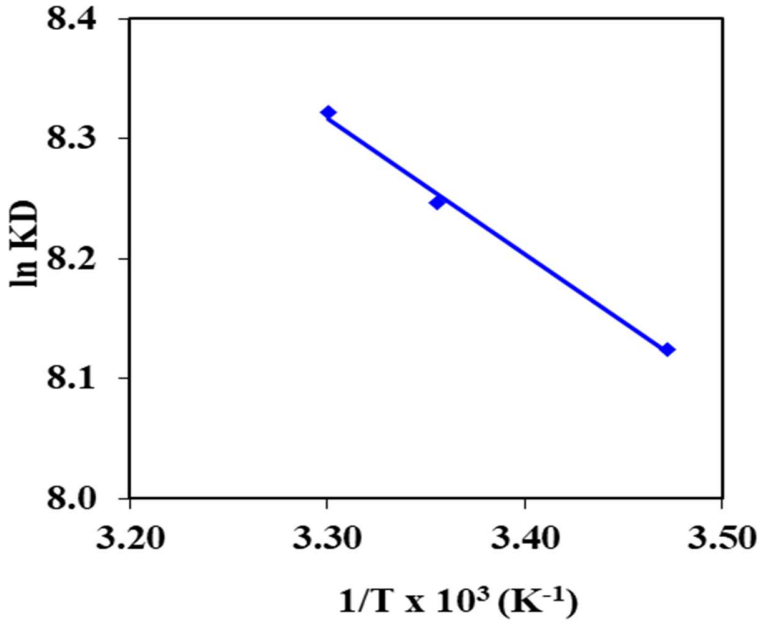

(b)

Fig. 5.6. Plot of ln K_D versus *1/T* for ln K_D *vs* 1/T Plot to estimate the adsorption thermodynamic parameters of (a) Zn (II) and (b) Cr (VI).

5.2.2. Simultaneous Multicomponent Adsorption of Zn (II) and Cr (VI)

Binary adsorption was studied by altering Zn (II) concentration in the presence of various concentration of Cr (VI) and vice-versa. The experimental equilibrium adsorption data were collected at various temperatures 288, 298, 308 K, and fitted to various multicomponent adsorption isotherms (Equations 5.4-5.10).

Isotherms (non-linear) of Zn (II) with the Cr (VI) increasing concentration, and vice-versa are compared and shown in Fig. 5.7 and 5.8, respectively. For each initial concentration (C_o) of Zn (II): 10, 20, 50, 75 mg/L, C_0 of Cr (VI) was varied from 10-95 mg/L (Table 5.3-5.9).

It was observed that for entire temperature range, $q_{e,\ Zn\ (II)}$ increases with increase in $C_{0,\ Zn(II)}$ of at constant Cr (VI) concentration, whereas, it decreases uninterruptedly with increasing the Cr(VI) concentration (Fig.5.7). Analogous behavior was observed for Cr (VI) for increasing concentration of Zn (II) (Fig.5.8). Thus, the initial concentration of one adsorbate affects the adsorption uptake of another, because of the interface amongst the cationic metal ions and the adsorbent MCM-41.

The equilibrium uptake of Zn (II) onto MCM-41 was found to be 33.6 mg/g for $C_{0,\ Zn}$ = 10 mg/L and $C_{0,\ Cr}$ = 0.0 mg/L. Whereas, for same $C_{0,\ Zn}$= 10 mg/L but in the presence of $C_{0,Cr}$ = 95 mg/L, it was decreased to 24.6 mg/g (Table 5.3). Therefore, it was witnessed that as Cr (VI) concentration is increased, Zn (II) individual component adsorption and total adsorption (for both the components) decreases, and was observed true at all temperatures (288, 298, 308 K) studied (Table 5.3-5.5). Identical observation were obtained for Cr (VI) adsorption at increasing concentration of Zn (II) (Table 5.6-5.9). Correspondingly, for $C_{0,\ Cr}$ = 10 mg/L and $C_{0,\ Zn}$= 0 mg/L, adsorption capacity of 43.6 mg/g was achieved, which decreased to 26.4 mg/g for $C_{0,\ Cr}$ = 10 mg/L at $C_{0,\ Zn}$= 75 mg/L (Table 5.6). It revealed that Zn (II) ions occurrence restricts the equilibrium uptake of Cr (VI) ions from the aqueous solution and vice versa.

In general, multicomponent adsorption shows three types of effects: synergism, antagonism and non-interaction (Srivastava et al., 2006). **(a)** ***Synergism:*** the adsorption yield of the mixture is more than that of each single adsorbates present in it. **(2)** ***Antagonism***: the adsorption yield of all the components of mixture lesser than each of the individual component. **(3)** ***Non-interaction:*** the adsorption yield of each of the adsorbates remains unaffected.

For example, from Table 5.3, it was predicted that the total adsorption yield (Ad_{Tot}%) must be Ad_{Tot}% = 41.8% [calculated using equation 5.3; Ad_{Tot}%= 100×[(75- 44.4)+ (95-54.9)/ (75+95)]]. However, experimentally calculated Ad_{Tot}%, including both Zn (II) and Cr (IV) adsorption, was found lower i.e. 17.29% [(100×[(75- 69.8)+ (95-70.8)/ (75+95)]]. Thus, above calculation revealed the antagonistic nature of adsorption. Therefore, in this study, the Zn (II) and Cr (IV) adsorption from their binary aqueous solution mixture was found antagonistic type.

Adsorption capacity for Zn (II) and Cr (VI) removal obtained in this work has been compared with the data available in literature for removal of Cr (VI) and Zn(II) using functionalized MCM-41 (Table 2.3). By comparing data, it can be concluded that $q_{e,Cr\ (VI)}$ and $q_{e,\ Zn\ (II)}$ for present study is 392, 554 mg/g for Cr (VI) and Zn (II), respectively. The reported data in the present study is much higher than that of reported earlier except Tian et al. (2011), who reported adsorption capacity of 904 mg/g for single component adsorption of Cr (VI).

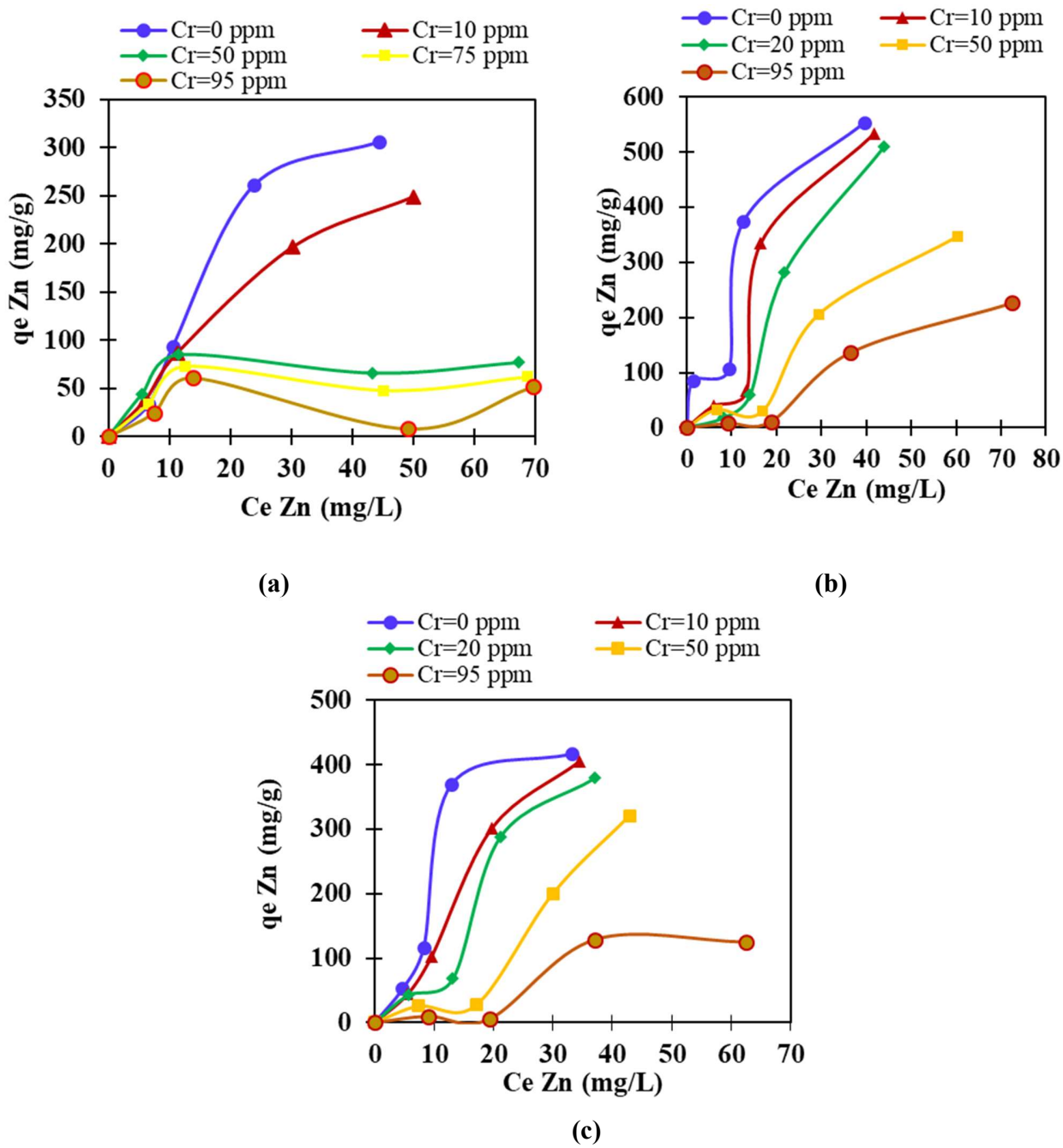

Fig. 5.7 Non-linear adsorption isotherms comparison for Zn (II) adsorption in the presence of increasing concentration of Cr (VI) onto MCM-41 at (a) 288, (b) 298 and (c) 308 K (pH_i = 7, t = 2 h, m = 0.1 g/L, Relative uncertainty in adsorption capacity (q_e) = ±0.004).

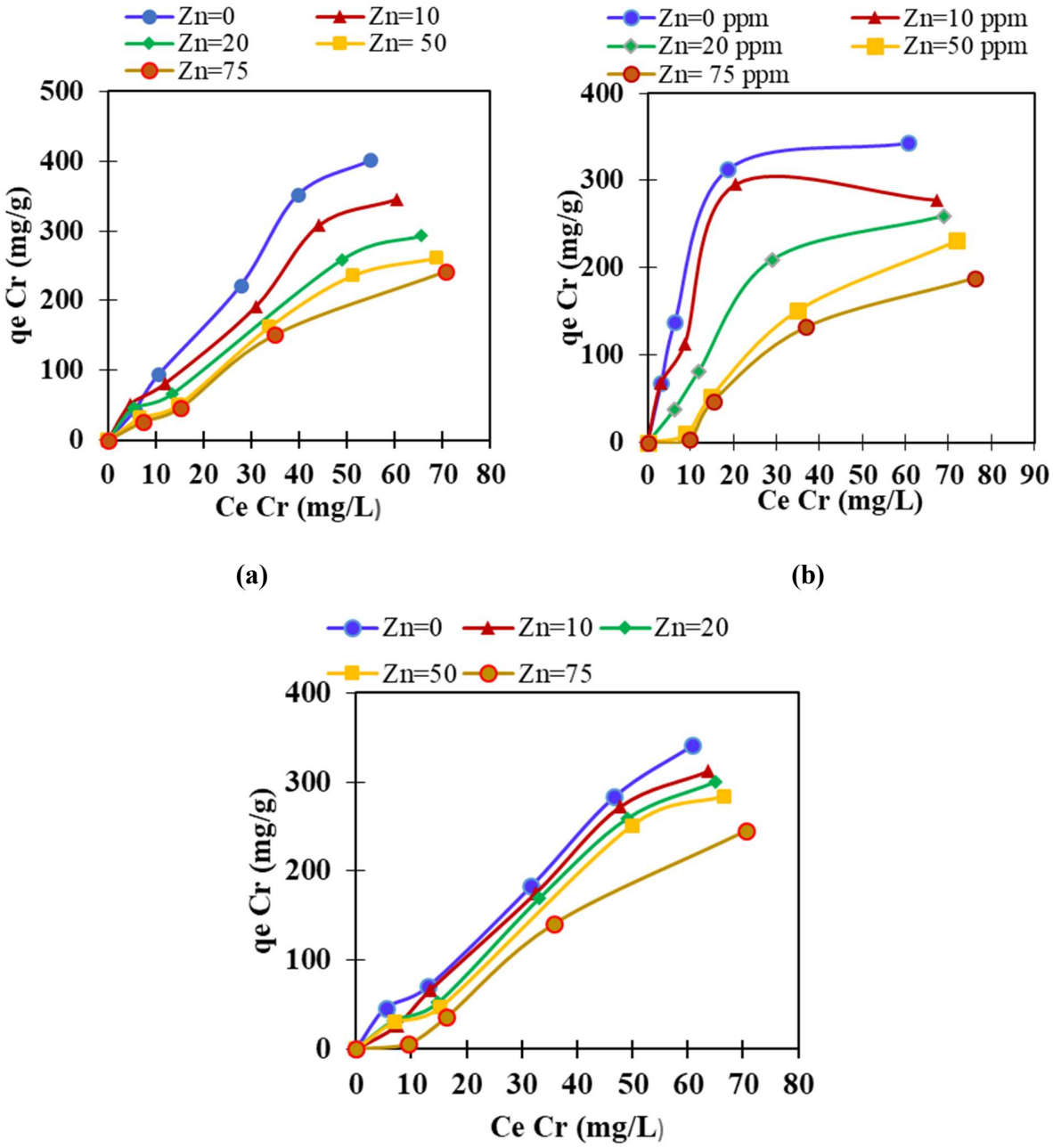

Fig. 5.8. Non-linear adsorption isotherms comparison for Cr (VI) adsorption in the presence of increasing concentration of Zn (II) onto MCM-41 at (a) 288, (b) 298 and (c) 308 K (pH_i = 7, t = 2 h, m = 0.1 g/L, Relative uncertainty in adsorption capacity (q_e) = ±0.004).

Table 5.3. Individual, total adsorption equilibrium uptakes and yields at different Zn (II) concentration in the presence of increasing concentration of Cr(VI) onto MCM-41 at 288K (pH_i =7, m_{opt} = 0.1 g/L, t = 2h)

C_0, Zn mg/L	C_0, Cr mg/L	Ce, Zn mg/g	Ce, Cr mg/g	q_e, Zn mg/g	q_e, Cr mg/g	Ad_{Zn} %	Ad_{Cr} %
0	0	0	0	0	0	0.00	0.00
10	0	6.64	0	33.6	0	33.60	0.00
20	0	10.6	0	94	0	47.00	0.00
50	0	23.9	0	261	0	52.20	0.00
75	0	44.4	0	306	0	40.80	0.00
0	10	0	5.64	0	43.6	0.00	43.60
10	10	5.43	4.79	45.7	52.1	45.70	52.10
20	10	13.3	5.36	67	46.4	33.50	46.40
50	10	25.6	6.83	244	31.7	48.80	31.70
75	10	40.8	7.36	342	26.4	45.60	26.40
0	20	0	10.6	0	94	0.00	47.00
10	20	6.12	11.9	38.8	81	38.80	40.50
20	20	11.3	13.4	87	66	43.50	33.00
50	20	30.3	14.9	197	51	39.40	25.50
75	20	50.1	15.3	249	47	33.20	23.50
0	50	0	27.8	0	222	0.00	44.4
10	50	5.54	30.9	44.6	191	44.60	38.20
20	50	11.5	32.4	85	176	42.50	35.20
50	50	43.4	33.8	66	162	13.20	32.40
75	50	67.3	34.9	77	151	10.27	30.20
0	75	0	39.8	0	352	0.00	46.93
10	75	6.58	44.2	34.2	308	34.20	41.06
20	75	12.7	49.1	73	259	36.50	34.53
50	75	45.2	51.4	48	236	9.60	31.46
75	75	68.8	55.4	62	196	8.27	26.13
0	95	0	54.9	0	401	0.00	42.21
10	95	7.54	60.5	24.6	345	24.60	36.31
20	95	13.9	65.7	61	293	30.50	30.84
50	95	49.2	68.9	8	261	1.60	27.47
75	95	69.8	70.8	52	242	6.93	25.47

Table 5.4. Individual, total adsorption equilibrium uptakes and yields at different Zn (II) concentration in the presence of increasing concentration of Cr(VI) onto MCM-41 at 298K (pH_i =7, m_{opt} = 0.1 g/L, t = 2h)

C_0, Zn mg/L	C_0, Cr mg/L	C_e, Zn mg/g	C_e, Cr mg/g	q_e, Zn mg/g	q_e, Cr mg/g	Ad $_{Zn}$ %	Ad $_{Cr}$ %
0	0	0	0.00	0	0.00	0.00	0.00
10	0	1.4	0.00	86	0.00	86.00	0.00
20	0	9.4	0.00	106	0.00	53.00	0.00
50	0	12.6	0.00	374	0.00	74.80	0.00
95	0	39.6	0.00	554	0.00	58.32	0.00
0	10	0	3.19	0	68.14	0.00	68.14
10	10	6	3.15	40	68.20	40.00	68.50
20	10	13.33	6.22	66.7	37.84	33.35	37.80
50	10	16.5	9.06	335	9.40	67.00	9.40
95	10	41.7	9.66	533	3.40	56.11	3.40
0	20	0	6.28	0	137.16	0.00	68.58
10	20	8.2	8.68	18	113.20	18.00	56.60
20	20	14.1	11.86	59	81.40	29.50	40.70
50	20	21.8	14.76	282	52.40	56.40	26.20
95	20	44	15.26	510	47.40	53.68	23.70
0	50	0	18.71	0	312.88	62.58	62.58
10	50	6.7	20.46	33	295.42	33.00	59.08
20	50	16.94	29.04	30.6	209.64	15.30	41.92
50	50	29.4	34.92	206	150.84	41.20	30.16
95	50	60.3	36.80	347	132.04	36.53	26.40
0	95	0	55.71	0	392.91	0.00	39.29
10	95	8.2	62.26	18	327.40	18.00	34.46
20	95	15	64.03	50	309.70	25.00	32.60
50	95	49	66.92	10	280.76	2.00	29.56
95	95	85.6	71.16	94	238.40	9.89	25.09

Table 5.5. Individual, total adsorption equilibrium uptakes and yields at different Zn (II) concentration in the presence of increasing concentration of Cr(VI) onto MCM-41 at 308K (pH_i =7, m_{opt} = 0.1 g/L, t = 2h)

C_0, Zn mg/L	C_0, Cr mg/L	Ce, Zn mg/L	Ce, Cr mg/L	q_e, Zn mg/g	q_e, Cr mg/g	Ad_{Zn} %	Ad_{Cr} %,
0	0	0	0	0	0	0.00	0.00
10	0	4.73	0	52.70	0	52.70	0.00
20	0	8.30	0	117.00	0	58.50	0.00
50	0	13.00	0	370.00	0	74.00	0.00
75	0	33.30	0	417.00	0	55.60	0.00
0	10	0	5.37	0	46	0.00	46.30
10	10	5.57	7.40	44.30	26	44.30	26
20	10	9.66	6.81	103.40	32	51.70	31.90
50	10	19.80	6.95	302.00	31	60.40	30.50
75	10	34.50	9.40	405.00	6	54.00	6.00
0	20	0	13.0	0	70	0.00	35.00
10	20	5.70	13.40	43.00	66	43.00	33.00
20	20	13.20	14.80	68.00	52	34.00	26.00
50	20	21.20	15.30	288.00	47	57.60	23.50
75	20	37.10	16.40	379.00	36	50.53	18.00
0	50	0	31.70	0	183	0.00	36.60
10	50	7.42	32.50	25.80	175	25.80	35.00
20	50	17.20	33.10	28.00	169	14.00	33.80
50	50	30.00	33.10	200.00	169	40.00	33.80
75	50	42.90	35.90	321.00	141	42.80	28.20
0	75	0	46.70	0	283	0.00	37.73
10	75	8.70	47.80	13.00	272	13.00	36.27
20	75	8.60	49.10	114.00	259	57.00	34.53
50	75	42.90	49.90	71.00	251	14.20	33.47
75	75	42.90	49.90	321.00	251	42.80	33.47
0	95	0	60.90	0	341	0.00	35.89
10	95	8.99	63.80	10.10	312	10.10	32.84
20	95	19.40	65.00	6.00	300	3.00	31.58
50	95	37.10	66.60	129.00	284	25.80	29.89
75	95	62.50	70.50	125.00	245	16.67	25.79

Table 5.6. Individual, total adsorption equilibrium uptakes and yields at different Cr (VI) concentration in the presence of increasing concentration of Zn(II) onto MCM-41 at 288K (pH_i =7, m_{opt} = 0.1 g/L, t = 2h)

C_0, Cr mg/L	C_0, Zn mg/L	Ce, Cr mg/L	Ce, Zn mg/L	q_e, Cr mg/g	q_e, Zn mg/g	Ad_{Cr} %	Ad_{Zn} %
0	0	0	0	0	0	0	0.00
10	0	5.64	0	43.6	0	43.60	0.00
20	0	10.6	0	94	0	47.00	0.00
50	0	27.8	0	222	0	44.40	0.00
75	0	39.8	0	352	0	46.93	0.00
95	0	54.9	0	401	0	42.21	0.00
0	10	0	6.64	0	33.6	0	33.60
10	10	4.79	5.43	52.1	45.7	52.10	45.70
20	10	11.9	6.12	81	38.8	40.50	38.80
50	10	30.9	5.54	191	44.6	38.20	44.60
75	10	44.2	6.58	308	34.2	41.06	34.20
95	10	60.5	7.54	345	24.6	36.31	24.60
0	20	0	10.6	0	94	0	47
10	20	5.36	13.3	46.4	67	46.40	33.50
20	20	13.4	11.3	66	87	33.00	43.50
50	20	32.4	11.5	176	85	35.20	42.50
75	20	49.1	12.7	259	73	34.53	36.50
95	20	65.7	13.9	293	61	30.84	30.50
0	50	0	23.9	0	261	0	52.20
10	50	6.83	25.6	31.7	244	31.70	48.80
20	50	14.9	30.3	51	197	25.50	39.40
50	50	33.8	43.4	162	66	32.40	13.20
75	50	51.4	45.2	236	48	31.46	9.60
95	50	68.9	49.2	261	8	27.47	1.60
0	75	0	44.4	0	306	0	40.80
10	75	7.36	40.8	26.4	342	26.40	45.60
20	75	15.3	50.1	47	249	23.50	33.20
50	75	34.9	67.3	151	77	30.20	10.27
75	75	55.4	68.8	196	62	26.13	8.27
95	75	70.8	69.8	242	52	25.47	6.93

Table 5.7. Individual, total adsorption equilibrium uptakes and yields at different Cr (VI) concentration in the presence of increasing concentration of Zn(II) onto MCM-41 at 298K (pH_i =7, m_{opt} = 0.1 g/L, t = 2h)

C_0, Cr mg/L	C_0, Zn mg/L	C_e, Cr mg/L	C_e, Zn mg/L	q_e, Cr mg/g	q_e, Zn mg/g	$A_{d\ Cr}$ %	$A_{d\ Zn}$ %
0	0	0.00	0	0.00	0	0.00	0.00
10	0	3.19	0	68.14	0	68.14	0.00
20	0	6.28	0	137.16	0	68.58	0.00
50	0	18.71	0	312.88	0	62.58	0.00
95	0	55.71	0	392.90	0	41.36	0.00
0	10	0.00	1.4	0.00	86	0.00	0.00
10	10	3.15	6	68.20	40	68.50	40.00
20	10	8.68	8.2	113.20	18	56.60	18.00
50	10	20.46	6.7	295.42	33	59.08	33.00
95	10	62.26	8.2	327.40	18	34.46	18.00
0	20	0.00	9.4	0.00	106	0.00	53.00
10	20	6.22	13.33	37.84	66.7	37.84	33.35
20	20	11.86	14.1	81.40	59	40.70	29.50
50	20	29.04	16.94	209.64	30.6	41.92	15.30
95	20	64.03	15	309.70	50	32.60	25.00
0	50	0.00	12.6	0.00	374	0.00	74.80
10	50	9.06	16.5	9.40	335	9.40	67.00
20	50	14.76	21.8	52.40	282	26.20	56.40
50	50	34.92	29.4	150.84	206	30.16	41.20
95	50	66.92	49	280.76	10	29.55	2.00
0	95	0.00	39.6	0.00	554	0.00	58.32
10	95	9.66	41.7	3.40	533	3.40	56.11
20	95	15.26	44	47.40	510	23.70	53.68
50	95	36.80	60.3	132.04	347	26.42	36.53
95	95	71.16	85.6	238.40	94	25.09	9.89

Table 5.8. Individual, total adsorption equilibrium uptakes and yields at different Cr (VI) concentration in the presence of increasing concentration of Zn(II) onto MCM-41 at 308K (pH_i =7, m_{opt} = 0.1 g/L, t = 2h

C_0, Cr mg/L	C_0, Zn mg/L	C_e, Cr mg/L	C_e, Zn mg/L	q_e, Cr mg/g	q_e, Zn mg/g	Ad $_{Cr}$ %	Ad$_{Zn}$%
0	0	0.00	0.00	0	0.00	0.00	0.00
10	0	5.37	0.00	46	0.00	46.30	0.00
20	0	13.00	0.00	70	0.00	35.00	0.00
50	0	31.70	0.00	183	0.00	36.60	0.00
75	0	46.70	0.00	283	0.00	37.73	0.00
95	0	60.90	0.00	341	0.00	35.89	0.00
0	10	0.00	4.73	0	52.70	0.00	52.70
10	10	7.40	5.57	26	44.30	26.00	44.30
20	10	13.40	5.70	66	43.00	33.00	43.00
50	10	32.50	7.42	175	25.80	35.00	25.80
75	10	47.80	8.70	272	13.00	36.27	13.00
95	10	63.80	8.99	312	10.10	32.84	10.10
0	20	0.00	8.30	0	117.00	0.00	58.50
10	20	6.81	9.66	32	103.40	31.90	51.70
20	20	14.80	13.20	52	68.00	26.00	34.00
50	20	33.10	17.20	169	28.00	33.80	14.00
75	20	49.10	8.60	259	114.00	34.53	57.00
95	20	65.00	19.40	300	6.00	31.58	3.00
0	50	0.00	13	0	370.00	0.00	74.00
10	50	6.95	19.80	31	302.00	30.50	60.40
20	50	15.30	21.20	47	288	23.50	57.60
50	50	33.10	30.00	169	200.00	33.80	40.00
75	50	49.90	42.90	251	71.00	33.47	14.20
95	50	66.60	33.30	284	167.00	29.89	33.40
0	75	0.00	33.30	0	417.00	0.00	55.60
10	75	9.40	34.50	6	405.00	6.00	54.00
20	75	16.40	34.50	36	405.00	18.00	54.00
50	75	35.90	42.90	141	321.00	28.20	42.80
75	75	49.90	42.90	251	321.00	33.47	42.80
95	75	70.50	62.50	245	125.00	25.79	16.67

5.2.2.1. Adsorption isotherm modelling for binary adsorption of Zn (II) and Cr (VI): The correlation of experimental equilibrium adsorption data to the multicomponent adsorption isotherm models and their parameters are necessary to design any adsorption system. Various calculated isotherm parameters and estimated MPSD values for the q_e values from the experiments and predicted data at temperatures 288, 298 and 308 K, for the simultaneous adsorption of Zn (II) and Cr (VI) are tabulated in Table 5.9. By comparing experimental and the calculated q_e values and along with respective MPSD error values, we can conclude that the modified R-P isotherm model suits the experimental data for binary adsorption of Zn (II) and Cr(VI) onto MCM-41 with lowest MPSD value of 74.47 followed by extended-Freundlich isotherm model and SRS model with MPSD values of 99.95 and 105.61, respectively.

Basic Langmuir model for single component adsorption is modified and extended for multi-component systems. Langmuir model is applicable for monolayer adsorption, whereas, Freundlich isotherm model could be related to multilayer adsorption. Due to unsuitability of basic Langmuir model for representation of multicomponent adsorption equilibrium, modified Langmuir coefficient n_i was introduced by Bellot and Condoret, (1993), which is an interaction term that depicts the suitability of the model. For best suitability, the value of n_i should be close to 1.0 (Rameshraja et al., 2018). The use of this interaction term in this study marginally improved the Langmuir fitting with experimental data. In this work, values of n_i were found to be much higher than 1.0 at all the three temperatures (288, 298 and 308 K) indicating the unsuitability of the Modified Langmuir model. Similar results were confirmed for extended-Langmuir model by the parity plot shown in Fig. 5.9 as maximum data points are distant from the 45◦ line. However, at lower temperature of 288 K, low MPSD values of 80.94, suggests its suitability. Extended-Langmuir model shows low value of K_{EL} i.e. 0.65 and 0.992 with small MPSD values of 80.94, suggesting better fittings of extended-Langmuir at lower temperatures.

Freundlich constant K_F was observed increasing with increase in temperature from 9 to 9.5 for Zn (II) and 9 to 9.6 for Cr (VI) (Table 5.9). This rise in K_F with temperature reveals more uptake of heavy metals at higher temperature due to increased kinesis of the heavy metal ions which beaten the activation energy obstacle and boosts the intra-particle diffusion (Bellot and Condoret, 1993).

Based on the Freundlich isotherm model, SRS model was proposed by Sheindorf et al. (1981), which fitted the data from experiments following to extended-Freundlich model. In SRS model there are two competition coefficients: a_{12}, which describes the adsorption reticence of component 1 [Zn (II)] due to the presence of component 2 [Cr (VI)], and a_{21}, which describes the adsorption reticence of component 2 [Cr (VI)] due to the presence of component 1 [Zn (II)] (Rameshraja et al., 2018). In this study, the competition coefficient a_{12} and a_{21} were found to be 8.8 and 12.5, respectively, at T= 308 K indicating the inhibition of Zn (II) in presence of Cr (VI) is less as compared to the inhibition in the adsorption of Cr (VI) in the presence of Zn (II). However, opposite results were revealed at low temperatures of 288 K and 298 K (Table 5.9).

Modified R-P models also consists of only one interaction parameter η as in the case of modified Langmuir model which depicts the intensity of interaction between the adsorbate and the adsorbent. As compared to non-modified R-P model with MPSD values of 118.71, modified R-P model fits the data more efficiently with low MPSD values of 74.47 at 308 K.

The parity plots of experimental and calculated q_e data points for both Zn (II) and Cr (VI) were shown in Fig. 5.9-5.11 at 288 K, 298 K and 308 K, respectively. The optimum depiction of the binary adsorption data at 308 K was well presented by modified R-P model, where maximum of the data points were distributed around 45° line. It is followed by SRS model and extended-Freundlich isotherm model. Extended- Langmuir model illustrates poor fitting for the same data points as maximum of them are far apart from the 45° line.

A 3-D demonstration of the binary adsorption isotherm plots of Zn (II) and Cr (VI) onto MCM-41 is shown in Fig. 5.12-5.14 for modified R-P model at 288 K, 298 K and 318 K respectively and for extended-Freundlich model is shown in Fig. 5.15-5.17 at 288 K, 298 K and 318 K respectively. The 3-D plots better symbolizes the fitting of experimental data to calculated data. It also signifies the interaction of one component in the existence of another during adsorption. In these 3-D graphs, the surfaces are predicted by the modified R-P model (Fig.5.12-5.14) and extended-Freundlich model (Fig. 5.15-5.17) and the symbols depicts the experimental data in all the figures. By looking into these pictures, we found both modified R-P model and extended-Freundlich model to be suitable with best fit for modified R-P model at 308 K (Fig.5.17) where almost all experimental data points lies within the surfaces depicted by the modified R-P model.

Table 5.9. Estimated isotherm parameters for simultaneous adsorption of Zn(II) and Cr(VI) by MCM-41 in binary system (pH_i =7, m_{opt} = 0.1 g/L, t = 2h)

288 K					**298 K**					**308 K**				
Non-modified Langmuir model														
Adsorbate	q_m		K_L		Adsorbate	q_m	K_L			Adsorbate	q_m		K_L	
Zn (II)	50		0.9		Zn (II)	50	0.9			Zn (II)	50		0.8	
Cr (VI)	210		0.99		Cr (VI)	70	0.09			Cr (VI)	70		0.04	
MPSD	84.84				MPSD	94.03				MPSD	106.05			
Modified Langmuir model														
Adsorbate	n_i	q_m	K_L		Adsorbate	n_i	q_m	K_L		Adsorbate	n_i	q_m	K_L	
Zn (II)	2	50	0.9		Zn (II)	19	50	0.9		Zn (II)	8	50	0.8	
Cr (VI)	10	210	0.99		Cr (VI)	25	70	0.09		Cr (VI)	5	70	0.04	
MPSD	81.02				MPSD	97.03				MPSD	112.58			
Extended- Langmuir model														
Adsorbate	K_{EL}		q_{max}		Adsorbate	K_{EL}	q_{max}			Adsorbate	K_{EL}		q_{max}	
Zn (II)	0.65		180		Zn (II)	0.99	75			Zn (II)	0.95		180	
Cr (VI)	0.992				Cr (VI)	0.8				Cr (VI)	0.95			
MPSD	80.94				MPSD	106.67				MPSD	77.43			
Extended-Freundlich model														
Adsorbate	x_i	y_i	z_i	K_F	Adsorbate	x_i	y_i	z_i	K_F	Adsorbate	x_i	y_i	z_i	K_F
Zn (II)	2.8	3	0.8	9	Zn (II)	1.3	8.5	0.1	9.2	Zn (II)	2	8	0.4	9.5
Cr (VI)	1	6	0.2	9	Cr (VI)	2	8.64	0.8	9.2	Cr (VI)	0.99	8.64	0.22	9.6
MPSD	263.95				MPSD	122.73				MPSD	99.95			
SRS model														
Adsorbate	a_{12}	a_{21}	K_F	n_i	Adsorbate	a_{12}	a_{21}	K_F	n_i	Adsorbate	a_{12}	a_{21}	K_F	n_i
Zn (II)	10.9	---	9	0.92	Zn (II)	9	--	9.2	0.81	Zn (II)	8.8	---	9.5	0.95
Cr (VI)	--	9.9	9	0.89	Cr (VI)	--	6	9.2	0.85	Cr (VI)	--	12.5	9.6	0.91
MPSD	205.94				MPSD	121.467				MPSD	105.61			
Non -Modified R-P model														
Adsorbate	K_R		β	a_R	Adsorbate	K_R	β	a_R		Adsorbate	K_R	β	a_R	
Zn (II)	0.99		0.08	0.8	Zn (II)	0.99	0.09	0.6		Zn (II)	0.89	0.09	0.8	
Cr (VI)	0.90		0.09	0.2	Cr (VI	0.99	0.09	0.3		Cr (VI)	0.9	0.09	0.1	
MPSD	113.74				MPSD	100.34				MPSD	118.71			
Modified R-P model														
Adsorbate	η				Adsorbate	η				Adsorbate	η			
Zn (II)	0.08				Zn (II)	0.09				Zn (II)	0.06			
Cr (VI)	0.07				Cr (VI)	0.09				Cr (VI)	0.75			
MPSD	174.76				MPSD	134.02				MPSD	74.47			

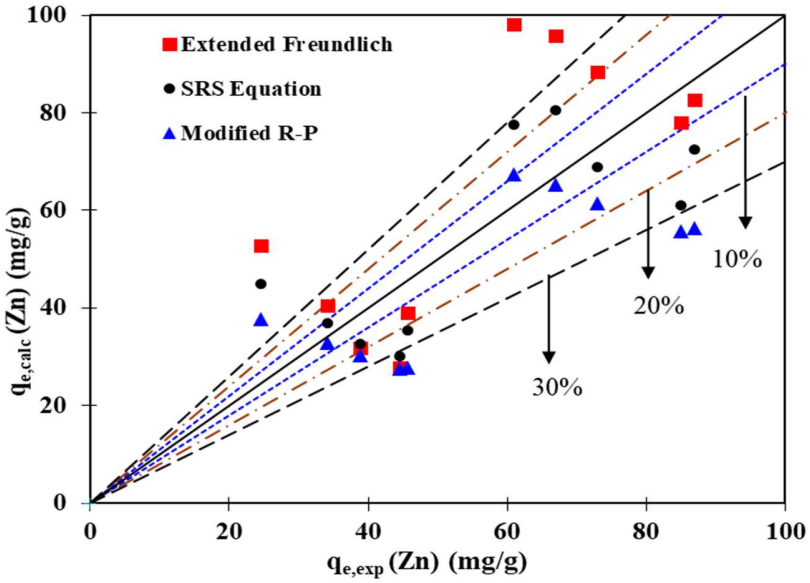

(a)

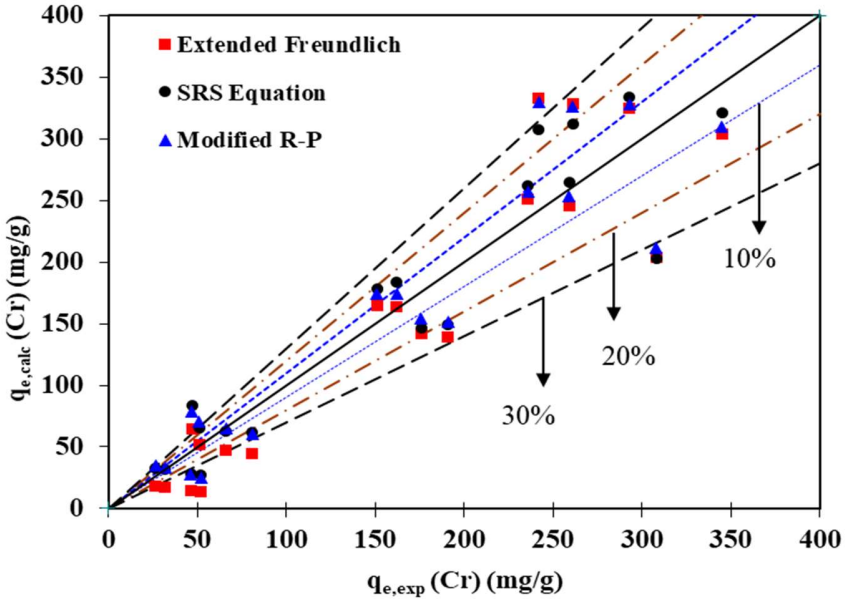

(b)

Fig. 5.9. Comparison of the q_e values (experimental and calculated) of (a) Zn (II) and (b) Cr (VI) in a binary mixture of Zn (II) and Cr (VI) ions at 288 K (pH_i =7, m_{opt} = 0.1 g/L, t = 2h).

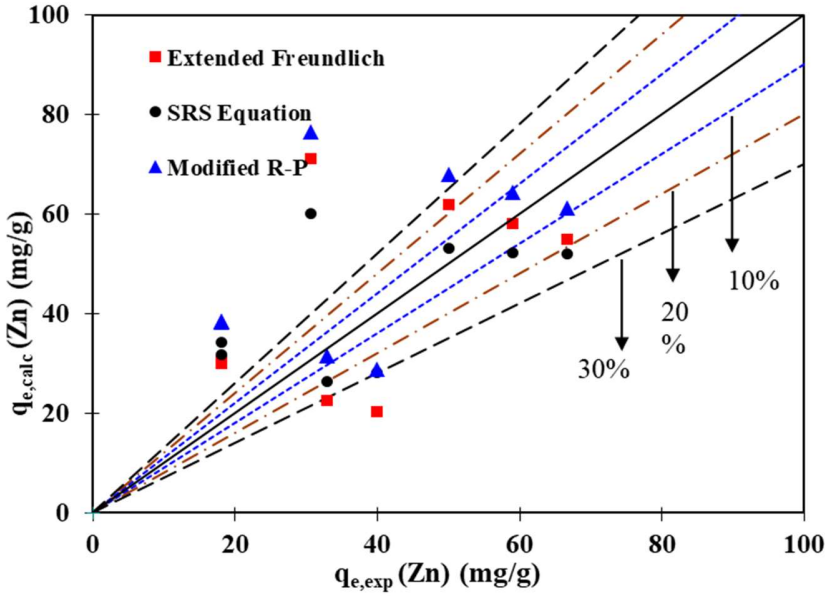

(a)

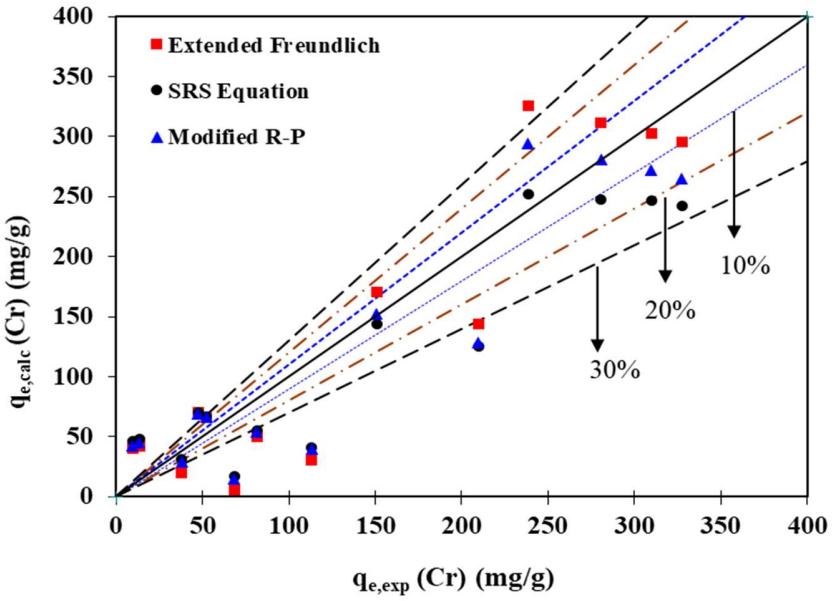

(b)

Fig. 5.10. Comparison of the *qe* values (experimental and calculated) of (a) Zn (II) and (b) Cr (VI) in a binary mixture of Zn (II) and Cr (VI) ions at 298 K (*pHi* =7, *mopt* = 0.1 g/L, *t* = 2h).

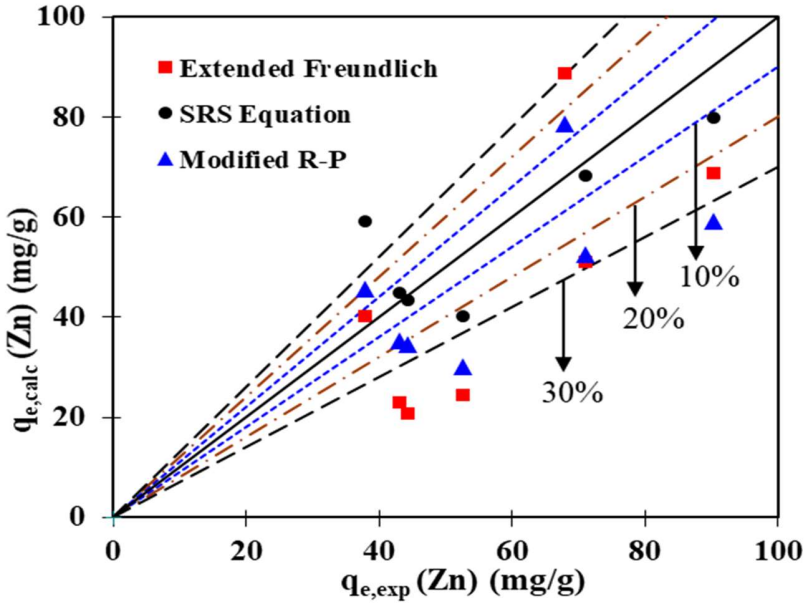

(a)

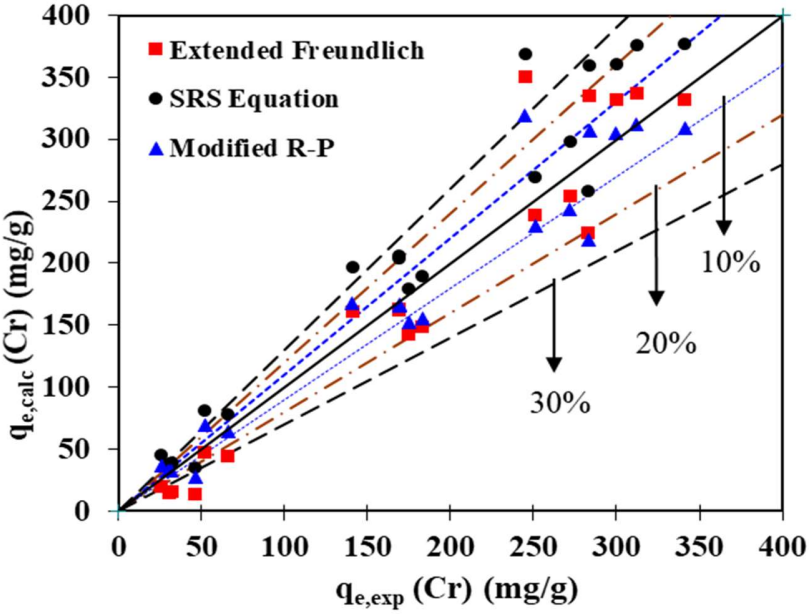

(b)

Fig 5.11. Comparison of the *qe* values (experimental and calculated) of (a) Zn (II) and (b) Cr (VI) in a binary mixture of Zn (II) and Cr (VI) ions at 308 K (*pHi* =7, *mopt* = 0.1 g/L, *t* = 2h).

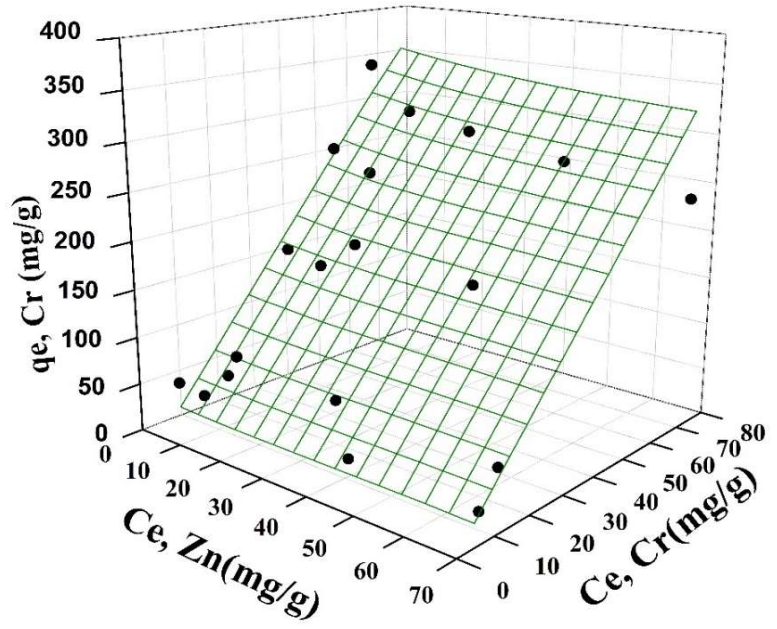

(a)

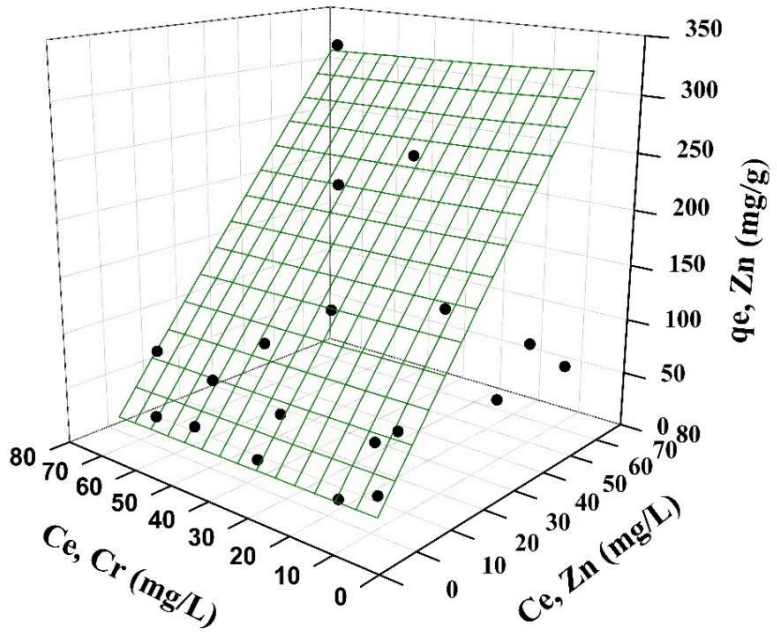

(b)

Fig. 5.12. 3-D Plot of binary adsorption isotherms of Zn (II) and Cr (VI) onto MCM- 41 at 288 K (modified R-P model) (a) Zn (II) uptake and (b) Cr (VI) uptake.

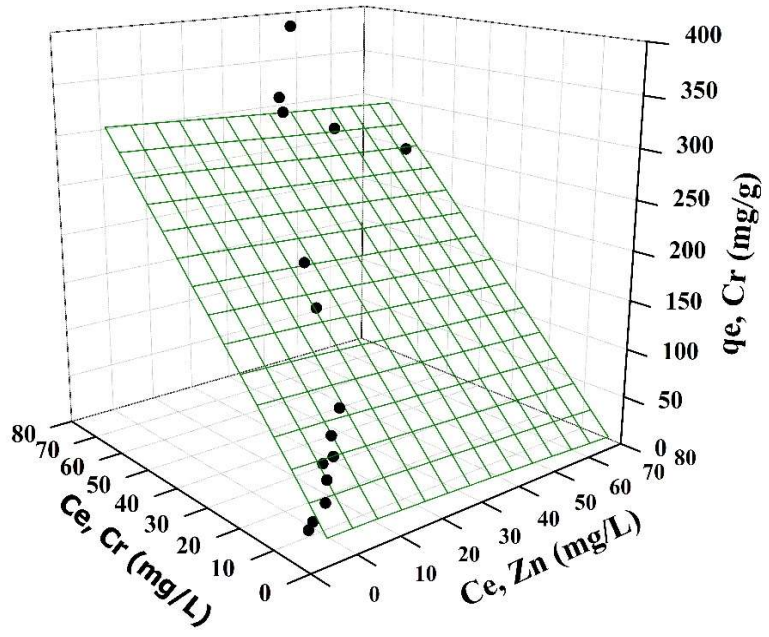

(a)

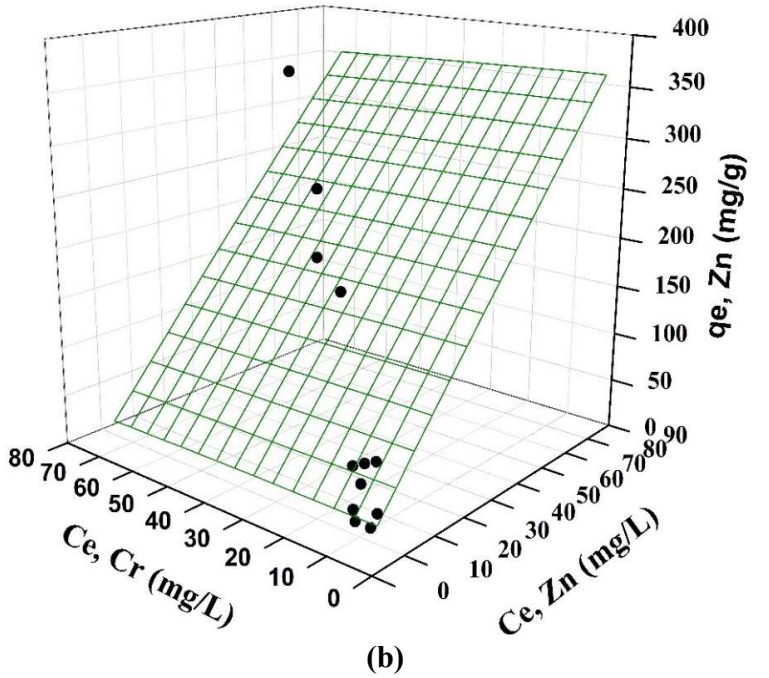

(b)

Fig. 5.13. 3-D Plot of binary adsorption isotherms of Zn (II) and Cr (VI) onto MCM- 41 at 298 K (modified R-P model) (a) Zn (II) uptake and (b) Cr (VI) uptake.

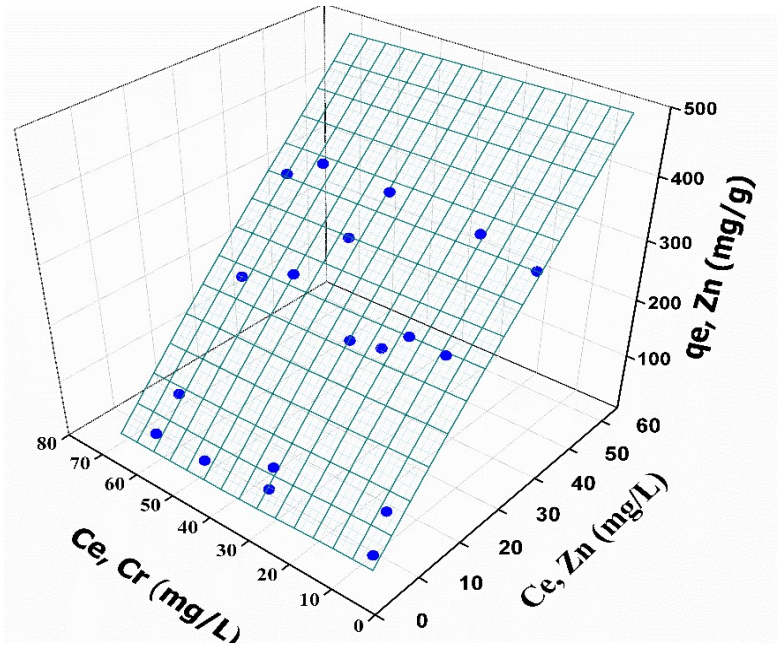

(a)

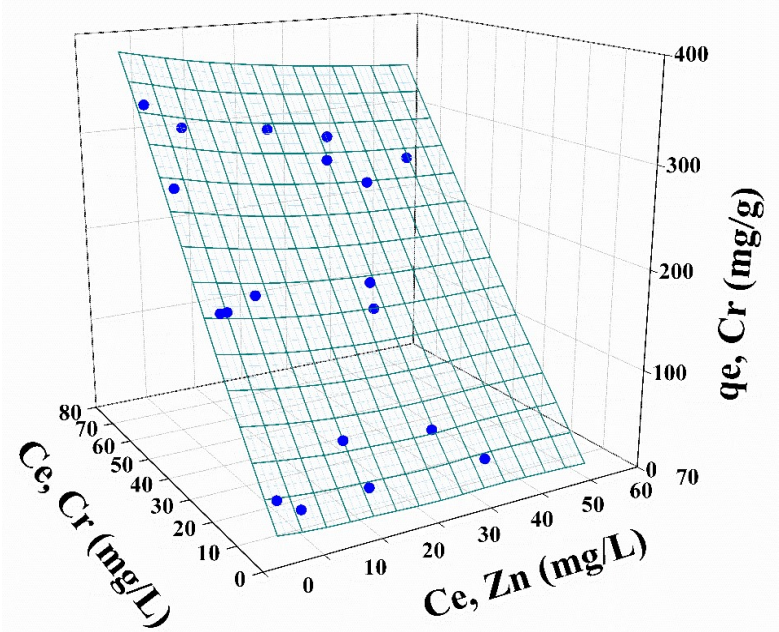

(b)

Fig. 5.14. 3-D Plot of binary adsorption isotherms of Zn (II) and Cr (VI) onto MCM- 41 at 308 K (modified R-P model) (a) Zn (II) uptake and (b) Cr (VI) uptake.

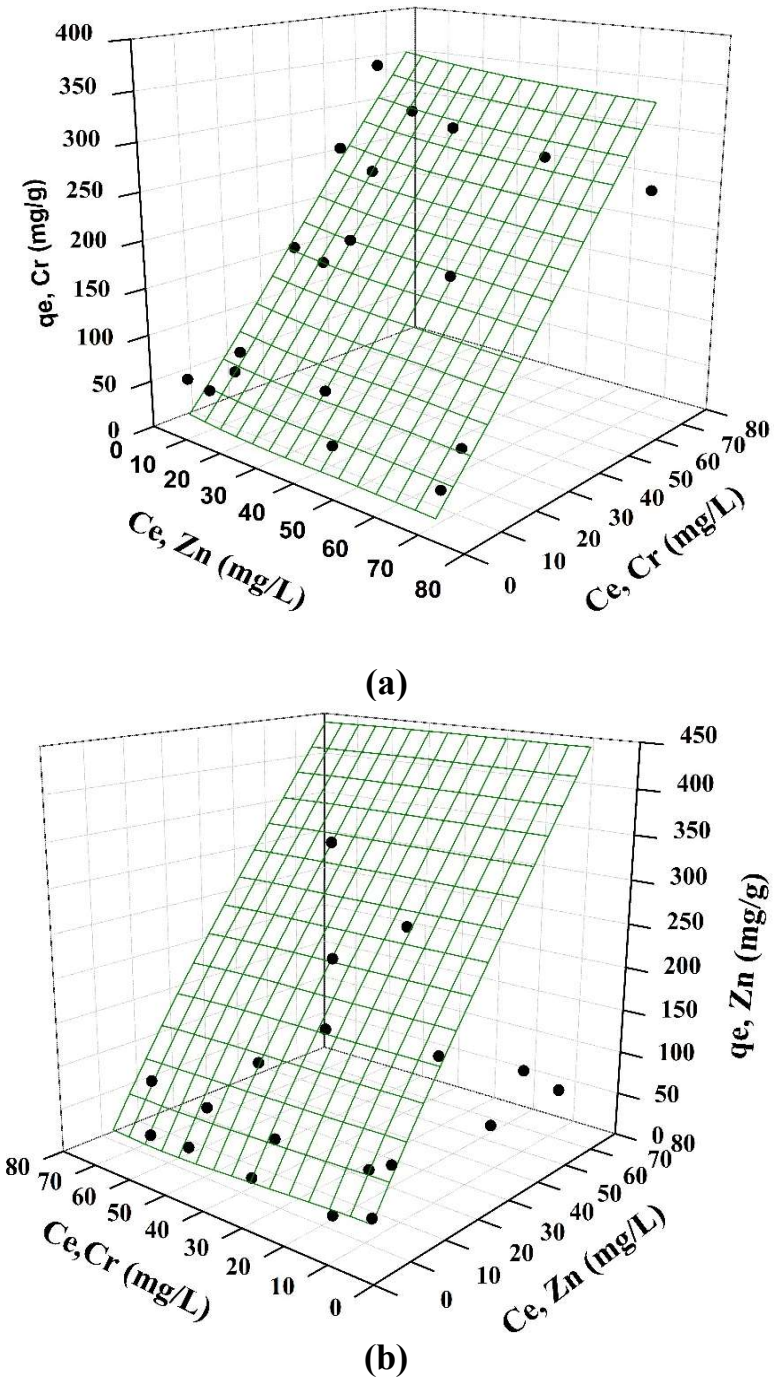

Fig. 5.15. 3-D Plot of binary adsorption isotherms of Zn (II) and Cr (VI) onto MCM- 41 at 288 K (Extended-Freundlich model) (a) Zn (II) uptake and (b) Cr (VI) uptake.

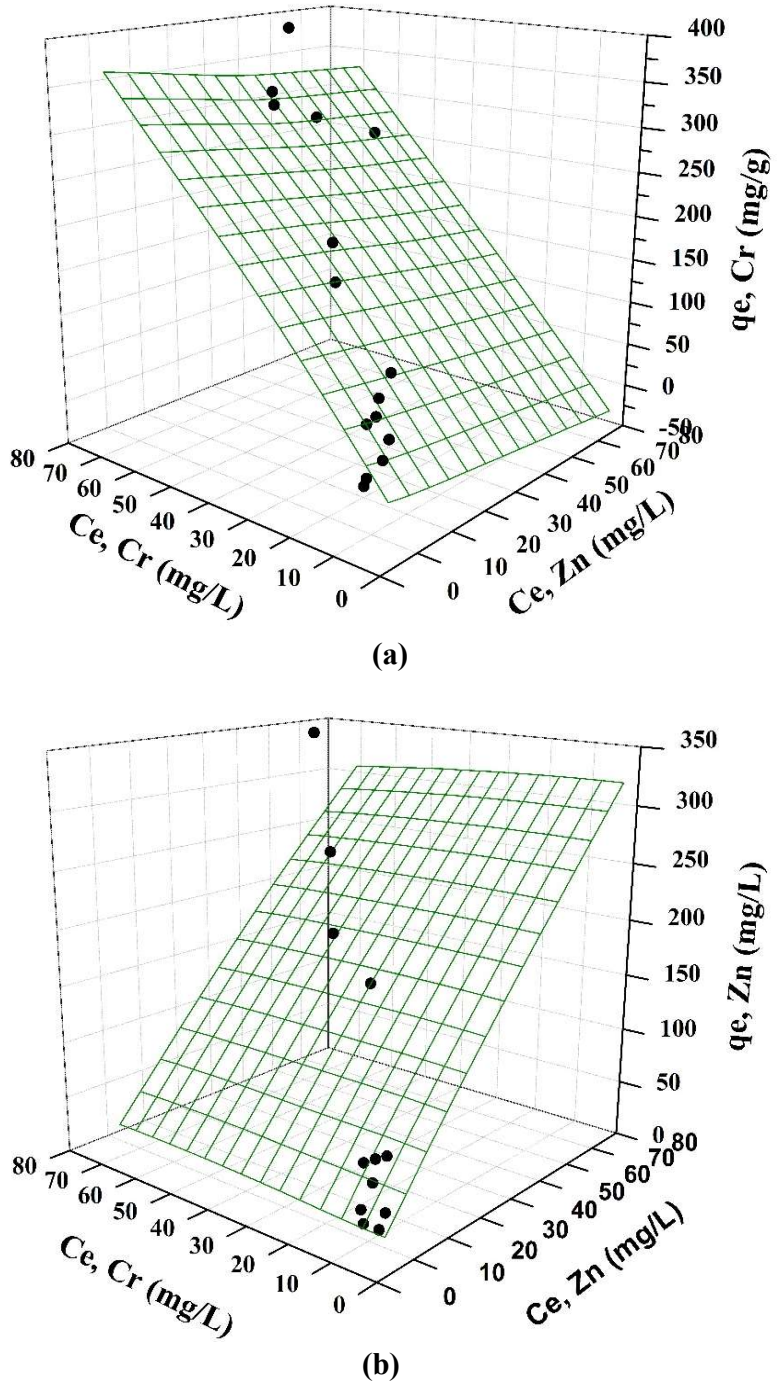

Fig 5.16. 3-D Plot of binary adsorption isotherms of Zn (II) and Cr (VI) onto MCM- 41 at 298 K (Extended-Freundlich model) (a) Zn (II) uptake and (b) Cr (VI) uptake.

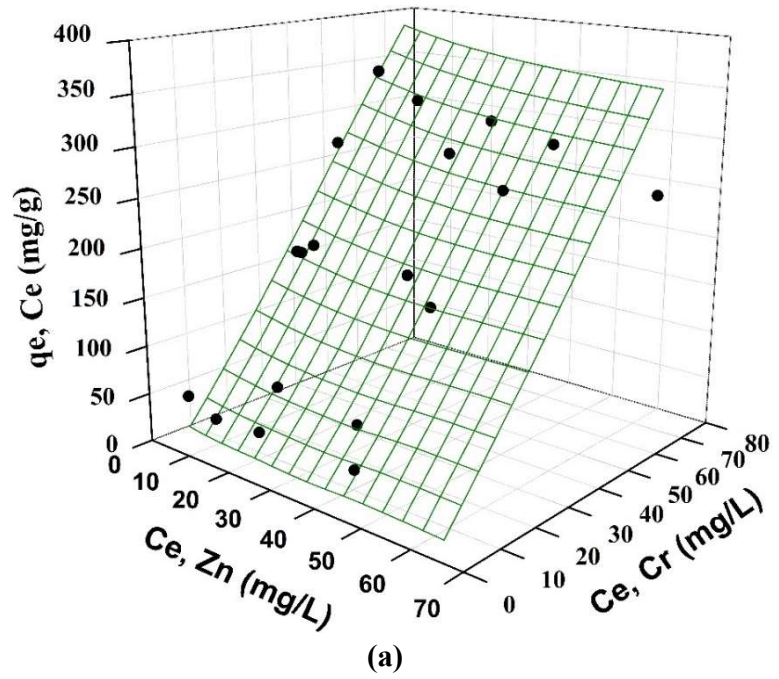

(a)

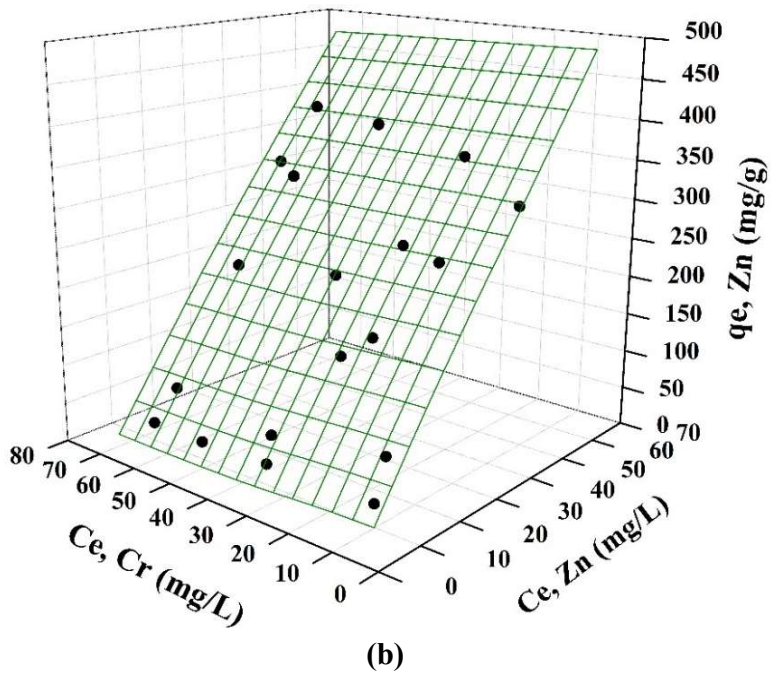

(b)

Fig 5.17. 3-D Plot of binary adsorption isotherms of Zn (II) and Cr (VI) onto MCM- 41 at 308 K (Extended-Freundlich model) (a) Zn (II) uptake and (b) Cr (VI) uptake.

Chapter - 6

CONCLUSIONS

6.0. GENERAL

On behalf of the outcomes obtained in the results and discussion section of all the three chapters i.e. Chapter 3,Chapter 4 and Chapter 5, following major conclusions were drawn:

6.1. SYNTHESIS OF MCM-41

MCM-41 was successfully synthesized, and well-defined pore structure of high surface area (502.77 m^2/g) with pore volume (0.85 cm^3/g) and pore diameter of 3.21 nm demonstrated it as an efficient adsorbent.

6.2. AROMATIC AMINES ADSORPTION

- Optimized conditions for efficient aromatic amines adsorption were found to be: $pH_i = 2$, $m = 0.2$ g/L and $t = 2$h.
- Highly acidic pH favoured the aromatic amines adsorption due to high electrostatic attraction between protonated 4-COT and 4-ABP and negatively charged MCM-41 surface. Increased pH of the aromatic amines aqueous solution, lowered the adsorption of 4-COT and 4-ABP due to the decrease in protonation and increase in negative charge density on MCM-41.
- pH study and FTIR analysis revealed high electrostatic attraction between aromatic amines (4-COT and 4-ABP) and MCM-41 responsible for adsorption. No chemical change of MCM-41 surface was observed.
- The adsorption capacity of MCM 41 were found increasing with increased concentration of 4-COT and 4-ABP and temperature, indicating the adsorption is substrate limiting and endothermic in nature.
- Adsorption of both the aromatic amines on MCM-41 followed pseudo-second order kinetics, and the values of K_f, h and q_e were found increasing with increasing concentration of 4-COT and 4-ABP.
- Intra-particle diffusion along with surface diffusion were found to be involved in adsorption rate controlling.

- Adsorption experimental equilibrium isothermal data well fitted the Freundlich and Temkin isotherm models for 4-COT adsorption. Whereas, 4-ABP experimental equilibrium data fits D-R isotherm model too along with Freundlich and Temkin isotherm models.
- Increasing value of A_T (Temkin isotherm parameter) and Q_{DR} (D-R isotherm parameter) along with temperature depicts the endothermic nature of adsorption.
- E (mean free energy) in D-R isotherm model revealed dominating physical adsorption role followed by chemisorption at eminent temperatures.
- Positive value of ΔS° suggested high randomness at the adsorbent/adsorbate contact point and high affinity between adsorbent and adsorbate.
- Negative ΔG° with increasing magnitude with increased temperature depicted the feasible and spontaneous adsorption of 4-COT and 4-ABP onto MCM-41.

6.3. HEAVY METALS ADSORPTION

- Optimized conditions for efficient Zn (II) adsorption were found to be: pH_i = 7, m = 0.1 g/L and t =2h, and for Cr (VI) adsorption the respective values were observed to be: 4, 0.1 g/L, 2h.
- With increase in the concentration of Zn (II) and Cr (VI) and temperature, q_e upsurges, showing adsorption process as adsorbate limiting.
- At any temperature, for persistent Cr (VI) concentration, q_e, $_{Zn\ (II)}$ upsurges with increase in C_0, $_{Zn\ (II)}$, whereas it declines uninterruptedly with increasing C_0, $_{Cr\ (VI).}$ Similar trend was detected for Cr (VI) adsorption with increasing concentration of Zn (II).
- The Zn (II) and Cr (IV) adsorption from their binary aqueous mixture were found antagonistic type.
- Freundlich constant K_F was observed increasing with increase in temperature from 9 to 9.5 for Zn (II) and 9 to 9.6 for Cr (VI). This rise in K_F with temperature reveals more uptake of heavy metals at higher temperature due to increased kinesis of the heavy metal ions which overcomes the activation energy barrier and boosts the intra-particle diffusion.

- The values of $n_{i,}$ (modified Langmuir coefficient), were found to be more than 1.0 at all the three temperatures (288, 298 and 308 K) indicating the unsuitability of the modified Langmuir isotherm model.
- The modified R-P isotherm model suits best to the equilibrium adsorption data obtained from binary adsorption for Zn(II) and Cr(VI) onto MCM-41 at 308 K with lowest MPSD value of 74.47, followed by extended-Freundlich isotherm model and SRS model.
- By comparing data (Table 6.1), it can be concluded that binary component adsorption for heavy metal Cr (VI) and Zn (II) ions removal onto MCM-41 is 392, 554 mg/g for Cr (VI) and Zn (II), respectively. The reported data in the present study is much higher than that of reported earlier except Tian et al. (2011)who reported adsorption capacity of 904 mg/g for single component adsorption of Cr (VI).

Table 6.1. Comparison of the adsorption capacity of functionalized and bared MCM-41 for Cr (VI) and Zn (II)

Adsorbent	Metal ions removed	Single/ Binary adsorption	Experimental conditions	Adsorption Capacity	Reference
Amino-functionalized MCM-41	Cr (VI)	Single	pH- 2 adsorbent dose -1 g/L contact time- 24 h temperature- 25°C	86.4 mg/g	Fellenz et al. (2017)
Aminopropyl-functionalized mesoporous silica	Cr(VI)	Single	pH- 2.2 adsorbent dose -1 g/L contact time- 24 h temperature- 25°C	87.1 mg/g	Fellenz et al. (2015)
Amino-functionalized MCM-41 and MCM-48	Cr(VI) , As(V)	Single	pH- 3.1 adsorbent dose -0.1 g/L contact time- 1.5 h temperature- 25°C	134.6 ± 2.2, 95.2 ± 3 mg/g for Cr(VI), As(V) respectively.	Benhamou et al. (2009)
MCM-41	Cr (VI)	Single	pH- 4 adsorbent dose -10 g/L temperature- 35°C contact time- 2 h	904 mg/g	Tian et al. (2011)
Magnetic MCM-41	Cr (VI)	Single	pH- 2–7	100 mg/g	Chen et al. (2011)
MCM-41/ Polymer nanocomposites	Cr (VI)	Single	pH 2–3	61.78-85.71%	Dinari et al. (2017)
EDTA- MCM-41	Cu(II), Zn(II), Ni(II)	Single	pH- 5.5 adsorbent dose -1 g/L contact time- 45 min temperature- 30°C	79.36, 74.07, 67.56 mg /g for Cu(II), Zn(II) and Ni(II) respectively.	Kumar et al. (2013)
MCM-41	Cr (VI), Zn (II)	Binary	pH- 7 adsorbent dose -0.1 g/L contact time- 120 min temperature- 25°C	392, 554 mg/g for Cr (VI) and Zn (II) respectively.	Present work

REFERENCES

Akceylan, E., Bahadir, M., & Yılmaz, M. (2009). Removal efficiency of a calix [4] arene-based polymer for water-soluble carcinogenic direct azo dyes and aromatic amines. *Journal of hazardous materials*, *162*(2-3), 960-966.

Aksoy, T., Erdemir, S., Yildiz, H.B., & Yilmaz,M. (2012). Novel water-soluble calix[4,6] arene appended magnetic nanoparticles for the removal of the carcinogenic aromatic amines. *Water Air Soil Pollution,* 223, 4129–4139.

Aksu, Z. & Kabasakal, E. (2004). Batch adsorption of 2, 4-dichlorophenoxy-acetic acid (2, 4-D) from aqueous solution by granular activated carbon. *Separation and Purification Technology*, *35*(3), 223-240.

Alam, T., Tarannum, H., & Kumar, M. R. (2000). Adsorption and oxidation of aromatic amines by metal hexacyanoferrates (II). *Talanta*, *51*(6), 1097-1105.

Algarra, M., Jiménez, M. V., Rodríguez-Castellón, E., Jiménez-López, A., & Jiménez-Jiménez, J. (2005). Heavy metals removal from electroplating wastewater by aminopropyl-Si MCM-41. *Chemosphere*, *59*(6), 779-786.

Ali, I. (2012). New generation adsorbents for water treatment. *Chemical Reviews*, *112*(10), 5073-5091.

Ali, I., & Gupta, V. K. (2006). Advances in water treatment by adsorption technology. *Nature Protocols*, *1*(6), 2661-2667.

ALOthman, Z. A. (2012). A review: fundamental aspects of silicate mesoporous materials. *Materials*, *5*(12), 2874-2902.

Amin, M. T., Alazba, A. A., & Manzoor, U. (2014). A review of removal of pollutants from water/wastewater using different types of nanomaterials. *Advances in Materials Science and Engineering*, vol. 2014, Article ID 825910, 1-24.

An, F., Feng, X., & Gao, B. (2009). Adsorption of aniline from aqueous solution using novel adsorbent PAM/SiO_2. *Chemical Engineering Journal*, *151*(1-3), 183-187.

Arslan, M., Sayin, S., & Yilmaz, M. (2013). Removal of carcinogenic azo dyes from water by new cyclodextrin-immobilized iron oxide magnetic nanoparticles. *Water, Air, & Soil Pollution, 224*(5), 1527- 1535.

Azimi, A., Azari, A., Rezakazemi, M., & Ansarpour, M. (2017). Removal of heavy metals from industrial wastewaters: a review. *ChemBioEng Reviews*, *4*(1), 37-59.

Azizi, P., Golshekan, M., Shariati, S., & Rahchamani, J. (2015). Solid phase extraction of Cu^{2+}, $Ni^{2+}$and Co^{2+} ions by a new magnetic nano-composite: excellent reactivity combined with facile extraction and determination. *Environmental Monitoring and Assessment*, *187*(4), 185.

Bafana, A., Devi, S. S., Krishnamurthi, K., & Chakrabarti, T. (2007). Kinetics of decolourisation and biotransformation of direct black 38 by C. hominis and P. stutzeri. *Applied microbiology and biotechnology*, *74*(5), 1145-1152.

Bafana, A., Krishnamurthi, K., Devi, S. S., & Chakrabarti, T. (2008). Biological decolourization of CI Direct Black 38 by E. gallinarum. *Journal of Hazardous Materials*, *157*(1), 187-193.

Bellot, J.C., Condoret J.S. (1993). Modelling of liquid chromatography equilibria. *Process Biochemistry,* 28, 365–376.

Benhamou, A., Basly, J. P., Baudu, M., Derriche, Z., & Hamacha, R. (2013). Amino-functionalized MCM-41 and MCM-48 for the removal of chromate and arsenate. *Journal of Colloid and Interface science*, *404*, 135-139.

Benhamou, A., Baudu, M., Derriche, Z., & Basly, J. P. (2009). Aqueous heavy metals removal on amine-functionalized Si-MCM-41 and Si-MCM-48. *Journal of Hazardous Materials*, *171*(1-3), 1001-1008.

Bhatnagar, A., & Minocha, A. K. (2006). Conventional and non-conventional adsorbents for removal of pollutants from water–A review. *Indian Journal of Chemical Technology*,13, 213-217.

Boczkaj, G., & Fernandes, A. (2017). Wastewater treatment by means of advanced oxidation processes at basic pH conditions: a review. *Chemical Engineering Journal*, *320*, 608-633.

Boyd, G. E., Adamson, A. W., & Myers Jr, L. S. (1947). The exchange adsorption of ions from aqueous solutions by organic zeolites. II. Kinetics1. *Journal of the American Chemical Society*, *69*(11), 2836-2848.

Cai, Q., Luo, Z. S., Pang, W. Q., Fan, Y. W., Chen, X. H., & Cui, F. Z. (2001). Dilute Solution Routes to Various Controllable Morphologies of MCM-41 Silica with a Basic Medium. *Chemistry of Materials*, 2001, 13, 258–263.

Casero, I., Sicilia, D., Rubio, S., & Pérez-Bendito, D. (1997). Chemical degradation of aromatic amines by Fenton's reagent. *Water Research*, *31*(8), 1985-1995.

Chan, A., Salsali, H., & McBean, E. (2013). Heavy metal removal (copper and zinc) in secondary effluent from wastewater treatment plants by microalgae. *ACS Sustainable Chemistry & Engineering*, *2*(2), 130-137.

Chen, W., Li, X., Pan, Z., Bao, Y., Ma, S., Li, L. (2015). Efficient adsorption of Norfloxacin by Fe-MCM-41 molecular sieves: Kinetic, isotherm and thermodynamic studies. *Chemical Engineering Journal, 281*, 397-403.

Dinker, M. K., & Kulkarni, P. S. (2015). Recent advances in silica-based materials for the removal of hexavalent chromium: a review. *Journal of Chemical & Engineering Data*, *60*(9), 2521-2540.

Directive 2002/61/EC of the European Parliament and of the Council.(2002). *Official Journal of the European Communities*, *243*, 15-18.

Du, E., Yu, S., Zuo, L., Zhang, J., Huang, X., & Wang, Y. (2011). Pb (II) sorption on molecular sieve analogues of MCM-41 synthesized from kaolinite and montmorillonite. *Applied Clay Science*, *51*(1-2), 94-101.

Dubinin, M.M., Radushkevich, L.V. (1947). The Equation of the Characteristic Curve of Activated Charcoal. *Proceedings of the USSR Academy of Sciences, Physical Chemical Section,* 55, 331–337.

Durán-Barrantes, M.M., Álvarez-Mateos, P., Jiménez-Rodriguez, A., Romero-Guzmán, F., & Fiestas-Ros de Ursinos J.A. (2009). Anaerobic Treatment of Swine Wastewater in Semicontinuous Clayey Support Reactors. *Chemical and biochemical engineering quarterly*, 23(3), 385-391.

Egodawatte, S., Datt, A., Burns, E. A., & Larsen, S. C. (2015). Chemical insight into the adsorption of chromium (III) on iron oxide/mesoporous silica nanocomposites. *Langmuir*, *31*(27), 7553-7562.

El-Safty, S. A., Ismael, M., Shahat, A., & Shenashen, M. A. (2013). Mesoporous hexagonal and cubic aluminosilica adsorbents for toxic nitroanilines from water. *Environmental Science and Pollution Research*, *20*(6), 3863-3876.

Erdemir, S., Bahadir, M., & Yilmaz, M. (2009). Extraction of carcinogenic aromatic amines from aqueous solution using calix [n] arene derivatives as carrier. *Journal of Hazardous Materials*, *168*(2-3), 1170-1176.

Fellenz, N., Martin, P., Marchetti, S., & Bengoa, F. (2015). Aminopropyl-modified mesoporous silica nanospheres for the adsorption of Cr (VI) from water. *Journal of Porous Materials*, *22*(3), 729-738.

Fellenz, N., Perez-Alonso, F. J., Martin, P. P., García-Fierro, J. L., Bengoa, J. F., Marchetti, S. G., & Rojas, S. (2017). Chromium (VI) removal from water by means of adsorption-reduction at the surface of amino-functionalized MCM-41 sorbents. *Microporous and Mesoporous Materials*, *239*, 138-146.

Fritz, W. (1974). Simultaneous Adsorption Equilibria of Organic Solute in Dilute Aqueous Solution on Activated Carbon. *Chemical Engineering Science*, *29*, 1279-1282.

Fu, F., & Wang, Q. (2011). Removal of heavy metal ions from wastewaters: a review. *Journal of Environmental Management*, *92*(3), 407-418.

Garrigós, M. C., Reche, F., Marın, M. L., & Jiménez, A. (2002). Determination of aromatic amines formed from azo colorants in toy products. *Journal of Chromatography A*, *976*(1-2), 309-317.

Ghiaci, M., Abbaspur, A., Kia, R., & Seyedeyn-Azad, F. (2004). Equilibrium isotherm studies for the sorption of benzene, toluene, and phenol onto organo-zeolites and as-synthesized MCM-41. *Separation and Purification Technology*, *40*(3), 217-229.

Gnanamani, A., Bhaskar, M., Ganga, R., Sekaran, G., & Sadulla, S. (2004). Chemical and enzymatic interactions of Direct Black 38 and Direct Brown 1 on release of carcinogenic amines. *Chemosphere*, *56*(9), 833-841.

Gómez, J. L., León, G., Hidalgo, A. M., Gómez, M., Murcia, M. D., & Griñán, G. (2009). Application of reverse osmosis to remove aniline from wastewater. *Desalination*, *245*(1-3), 687-693.

Gu, S. Y., Hsieh, C. T., Gandomi, Y. A., Yang, Z. F., Li, L., Fu, C. C., & Juang, R. S. (2019). Functionalization of activated carbons with magnetic Iron oxide nanoparticles for removal of copper ions from aqueous solution. *Journal of Molecular Liquids*, *277*, 499-505.

He, R., Wang, Z., Tan, L., Zhong, Y., Li, W., Xing, D. & Tang, Y. (2018). Design and fabrication of highly ordered ion imprinted SBA-15 and MCM-41 mesoporous organosilicas for efficient removal of Ni^{2+} from different properties of wastewaters. *Microporous and Mesoporous Materials*, *257*, 212-221.

Heidari, A., Younesi, H., & Mehraban, Z. (2009). Removal of Ni (II), Cd (II), and Pb (II) from a ternary aqueous solution by amino functionalized mesoporous and nano mesoporous silica. *Chemical Engineering Journal*, *153*(1-3), 70-79.

Ho, Y. S., McKay, G. (1999). Pseudo-second order model for sorption processes. *Process biochemistry, 34*(5), 451-465.

Hojati, S., & Landi, A. (2015). Kinetics and thermodynamics of zinc removal from a metal-plating wastewater by adsorption onto an Iranian sepiolite. *International Journal of Environmental Science and Technology*, *12*(1), 203-210.

https://www.explainthatstuff.com/waterpollution.html ; Water pollution: an introduction; (Assessed on March 24, 2019).

http://vilindia.com/waste-water/; Vishvaraj Infrastructure Ltd.; Wastewater reuse: A Civic Necessity and a business opportunity (Assessed on March 24, 2019)

Hua, M., Zhang, S., Pan, B., Zhang, W., Lv, L., & Zhang, Q. (2012). Heavy metal removal from water/wastewater by nanosized metal oxides: a review. *Journal of Hazardous Materials*, *211*, 317-331.

Husain, Q., & Jan, U. (2000). Detoxification of phenols and aromatic amines from polluted wastewater by using phenol oxidases. *Journal of Scientific and Industrial Research*, 59, 286-293.

Işik, M., & Teresa Sponza, D. (2003). Aromatic amine degradation in a UASB/CSTR sequential system treating Congo Red dye. *Journal of Environmental Science and Health, Part A*, *38*(10), 2301-2315.

Jayapal, M., Jagadeesan, H., Shanmugam, M., & Murugesan, S. (2018). Sequential anaerobic-aerobic treatment using plant microbe integrated system for degradation of azo dyes and their aromatic amines by-products. *Journal of Hazardous Materials*, *354*, 231-243.

Jianguo, C., Aimin, L., Hongyan, S., Zhenghao, F., Chao, L., & Quanxing, Z. (2005). Adsorption characteristics of aniline and 4-methylaniline onto bifunctional polymeric adsorbent modified by sulfonic groups. *Journal of Hazardous Materials*, 124 (B), 173–180.

Juang, L. C., Wang, C. C., Lee, C. K. (2006). Adsorption of basic dyes onto MCM-41. *Chemosphere, 64*(11), 1920-1928.

Jurado-Sanchez, B., Ballesteros, E., & Gallego, M. (2012). Occurrence of aromatic amines and N-nitrosamines in the different steps of a drinking water treatment plant. *Water Research*, *46*(14), 4543-4555.

Kakavandi, B., Jonidi, A., Rezaei, R., Nasseri, S., Ameri, A., & Esrafily, A. (2013). Synthesis and properties of Fe_3O_4-activated carbon magnetic nanoparticles for removal of aniline from aqueous solution: equilibrium, kinetic and thermodynamic studies. *Iranian Journal of Environmental Health Science & Engineering*, *10*(1), 10-19.

Kara, I., Yilmazer, D., Akar,S.T. (2017). Metakaolin based geopolymer as an effective adsorbent for adsorption of zinc (II) and nickel (II) ions from aqueous solutions. *Applied Clay Science*, 139, 54–63.

Kaur, S., Rani, S., Mahajan, R.K., Asif, M., Gupta, V.K. (2015). Synthesis and adsorption properties of mesoporous material for the removal of dye safranin: Kinetics, equilibrium, and thermodynamics. *Journal of industrial and Engineering Chemistry Research*, *22*, 19–27.

Khajeh, M., Laurent, S., & Dastafkan, K. (2013). Nanoadsorbents: classification, preparation, and applications (with emphasis on aqueous media). *Chemical reviews*, *113*(10), 7728-7768.

King, P., Anuradha, K., Lahari, S. B., Kumar, Y. P., & Prasad, V. S. R. K. (2008). Biosorption of zinc from aqueous solution using Azadirachta indica bark: equilibrium and kinetic studies. *Journal of Hazardous Materials*, *152*(1), 324-329.

Klibanov, A. M., & Morris, E. D. (1981). Horseradish peroxidase for the removal of carcinogenic aromatic amines from water. *Enzyme and Microbial Technology*, *3*(2), 119-122.

Koupaie, E. H., Moghaddam, M. A., & Hashemi, S. H. (2011). Post-treatment of anaerobically degraded azo dye Acid Red 18 using aerobic moving bed biofilm process: enhanced removal of aromatic amines. *Journal of Hazardous Materials*, *195*, 147-154.

Kumar, P., Prasad, B., Mishra, I.M., & Chand, S. (2008). Decolorization and COD Reduction of Dyeing Wastewater from a Cotton Textile Mill Using Thermolysis and Coagulation. *Journal of Hazardous Materials*, 153, 635-645.

Kumar, P., Prasad, B., Mishra, I.M., & Chand, S. (2008). Treatment of Composite Wastewater of a Cotton Textile Mill by Thermolysis and Coagulation. *Journal of Hazardous Materials*, 151, 770–779.

Kumar, P.S., Senthamarai, C., Durgadevi, A. (2014). Adsorption kinetics, mechanism, isotherm, and thermodynamic analysis of copper ions onto the surface modified agricultural waste. *Environmental Progress & Sustainable Energy*, *33*(1), 28-37.

Kumar, R., Barakat, M. A., Daza, Y. A., Woodcock, H. L., & Kuhn, J. N. (2013). EDTA functionalized silica for removal of Cu (II), Zn (II) and Ni (II) from aqueous solution. *Journal of Colloid and Interface Science*, *408*, 200-205.

Kumar, V., Majumdar, C., & Roy, P. (2008). Effects of endocrine disrupting chemicals from leather industry effluents on male reproductive system. *The Journal of Steroid biochemistry and molecular biology*, *111*(3-5), 208-216.

Kurniawan, T. A., Chan, G. Y., Lo, W. H., & Babel, S. (2006). Physico–chemical treatment techniques for wastewater laden with heavy metals. *Chemical Engineering Journal*, *118*(1-2), 83-98.

Kurniawan, T. A., Sillanpää, M. E., & Sillanpää, M. (2012). Nanoadsorbents for remediation of aquatic environment: local and practical solutions for global water pollution problems. *Critical Reviews in Environmental Science & Technology*, *42*(12), 1233-1295.

Kushwaha, J.P., Srivastava, V.C., Mall, I.D. (2010). Treatment of dairy wastewater by commercial activated carbon and bagasse fly ash Parametric, kinetic and equilibrium modelling, disposal studies. *Bioresource Technology, 101*, 3474–3483.

Kyzas, G. Z., & Matis, K. A. (2015). Nanoadsorbents for pollutants removal: a review. *Journal of Molecular Liquids*, *203*, 159-168.

Lagergren, S. (1989). About the theory of so-called adsorption of soluble substances. *Kungliga Svenska Vetenskaps akademiens. Handlingar*, *24* (4), 1-39.

Laha, S., & Luthy, R. G. (1990). Oxidation of aniline and other primary aromatic amines by manganese dioxide. *Environmental Science & Technology*, *24*(3), 363-373.

Li, B., Lei, Z., & Huang, Z. (2009). Surface-treated activated carbon for removal of aromatic compounds from water. *Chemical engineering & technology*, *32*(5), 763-770.

Li, G., Zhao, Z., Liu, J., & Jiang, G. (2011). Effective heavy metal removal from aqueous systems by thiol functionalized magnetic mesoporous silica. *Journal of Hazardous Materials*, *192*(1), 277-283.

Liang, Z., Shi, W., Zhao, Z., Sun, T., Cui, F. (2017). Enhanced removal and adsorption characters of aniline by the inorganically modified mesoporous silica nano-spheres. *Colloids Surfaces A: Physicochemical and Engineering Aspects, 513*, 250-258.

Lu, G.Q., & Zhau, X.S. (2004). Nanoporous materials: science and engineering. *World Scientific* (Vol.4).

Mangrulkar, P.A., Kamble , S.P., Meshram, J., Rayalu, S.S. (2008). Adsorption of phenol and o- Chlorophenol by mesoporous MCM-41. *Journal of Hazardous Materials,* 160, 414-421.

Manzetti, S. (2012). Ecotoxicity of polycyclic aromatic hydrocarbons, aromatic amines, and nitroarenes through molecular properties. *Environmental chemistry letters*, *10*(4), 349-361.

Marquardt, D. W. (1963). An algorithm for least-squares estimation of nonlinear parameters. *Journal of the society for Industrial and Applied Mathematics*, *11*(2), 431-441.

Megateli, S., Semsari, S., & Couderchet, M. (2009). Toxicity and removal of heavy metals (cadmium, copper, and zinc) by Lemna gibba. *Ecotoxicology and environmental safety*, *72*(6), 1774-1780.

Mehdinia, A., Akbari, M., Kayyal, T. B., & Azad, M. (2015). High-efficient mercury removal from environmental water samples using di-thio grafted on magnetic mesoporous silica nanoparticles. *Environmental Science and Pollution Research*, *22*(3), 2155-2165.

Meléndez-Ortiz, H.I., Mercado-Silva, A., García-Cerda, L.A., Castruita, G., Perera-Mercado, Y.A.(2013). Hydrothermal synthesis of mesoporous silica MCM-41 using commercial sodium silicate. *Journal of the Mexican Chemical Society* , *57*(2), 73-79.

Meziani, M.J., Zajac, J., Jones, D.J., Rozie`re, J., Partyka, S. (1997). Surface characterization of mesoporous silicoaluminates of the MCM-41 Type: Evaluation of polar surface sites using flow calorimetry, adsorption of a cationic surfactant as a function of pore size and aluminum content. *Langmuir*, *13*, 5409-5417.

Mirzajani, R., Pourreza, N., Zayadi, A., Malakooti, R., & Mahmoodi, H. (2016). Nanoporous calcined MCM-41 silica for adsorption and removal of Victoria blue dye from different natural water samples. *Desalination and Water Treatment*, *57*(13), 5903-5913.

Mishra, V. K., & Tripathi, B. D. (2009). Accumulation of chromium and zinc from aqueous solutions using water hyacinth (Eichhornia crassipes). *Journal of Hazardous Materials*, *164*(2-3), 1059-1063.

Monash, P., Pugazhenthi, G. (2010). Investigation of equilibrium and kinetic parameters of methylene blue adsorption onto MCM-41. *Korean Journal of Chemical Engineering*, *27*(4), 1184-1191.

NTP (National toxicology program) - Report on carcinogenic- Twelfth Edition (2011) US Department of health and human services, Public health service.

Nyssen, G. A., White, J. S., Bibring, P., & Wilson, D. J. (1990). Removal of trace levels of aromatic amines from aqueous solution by foam flotation. *Separation Science and Technology*, *25*(7-8), 809-824.

Oda, H., & Yokokawa, C. (1983). Adsorption of aromatic amines and o-substituted derivatives of phenol from organic solutions by activated carbons-effect of surface acidity. *Carbon*, *21*(5), 485-489.

Özcan, A., Öncü, E. M., & Özcan, A. S. (2006). Kinetics, isotherm and thermodynamic studies of adsorption of Acid Blue 193 from aqueous solutions onto natural sepiolite. *Colloids and Surfaces A: Physicochemical and Engineering Aspects*, *277*(1-3), 90-97.

Pacheco, M. J., Santos, V., Ciríaco, L., & Lopes, A. (2011). Electrochemical degradation of aromatic amines on BDD electrodes. *Journal of hazardous materials*, *186*(2-3), 1033-1041.

Parida, K., Mishra, K. G., & Dash, S. K. (2012). Adsorption of toxic metal ion Cr (VI) from aqueous state by TiO_2-MCM-41: Equilibrium and kinetic studies. *Journal of hazardous materials*, *241*, 395-403.

Popp, W., Schmieding, W., Speck, M., Vahrenholz, C., & Norpoth, K. (1992). Incidence of bladder cancer in a cohort of workers exposed to 4-chloro-o-toluidine while synthesising chlordimeform. *Occupational and Environmental Medicine*, *49*(8), 529-531.

Rameshraja, D., Srivastava, V. C., Kushwaha, J. P., & Mall, I. D. (2012). Quinoline adsorption onto granular activated carbon and bagasse fly ash. *Chemical Engineering Journal*, *181*, 343-351.

Rameshraja, D., Srivastava, V.C., Kushwaha, J.P., Mall, I.D. (2018). Competitive adsorption isotherm modelling of heterocyclic nitrogenous compounds, pyridine and quinoline, onto granular activated carbon and bagasse fly ash. *Chemical Papers.* 2018, 72(3), 617-621.

Rao, M. M., Rao, G. C., Seshaiah, K., Choudary, N. V., & Wang, M. C. (2008). Activated carbon from Ceiba pentandra hulls, an agricultural waste, as an adsorbent in the removal of lead and zinc from aqueous solutions. *Waste Management*, *28*(5), 849-858.

Rao, R. A., Ajmal, M., Ahmad, R., & Siddiqui, B. A. (2001). Adsorption behaviour of some aromatic amines on pyrolusite and activated carbon and recovery of β napthylamine from water sample. *Environmental monitoring and assessment*, *68*(3), 235-247.

Ravindranath, N., Ramesh, C., Ravinder Reddy, M., & Das, B. (2003). Selective Removal of N-Boc Protecting Group from Aromatic Amines Using Silica Gel-Supported Sodium Hydrogen Sulfate and HY-Zeolite as Heterogeneous Catalysts. *Advanced Synthesis & Catalysis*, *345*(11), 1207-1208.

Sahu, O., Mazumdar, B., & Chaudhari, P.K. (2019). Electrochemical treatment of sugar industry wastewater: process optimization by response surface methodology. *International Journal of Environmental Science and Technology*, 16, 1527–1540.

Salahshoor, Z., & Shahbazi, A. (2014). Review of the use of mesoporous silicas for removing dye from textile wastewater. *European Journal of Environmental Sciences*, *4*(2), 116–130.

Santos, D. O., Santos, M. D. L. N., Costa, J. A. S., de Jesus, R. A., Navickiene, S., Sussuchi, E. M., & de Mesquita, M. E. (2013). Investigating the potential of functionalized MCM-41 on adsorption of Remazol Red dye. *Environmental Science and Pollution Research*, *20*(7), 5028-5035.

Selvi, K., Pattabhi, S., & Kadirvelu, K. (2001). Removal of Cr (VI) from aqueous solution by adsorption onto activated carbon. *Bioresource technology*, *80*(1), 87-89.

Sharma, Y. C., Srivastava, V., Singh, V. K., Kaul, S. N., & Weng, C. H. (2009). Nano-adsorbents for the removal of metallic pollutants from water and wastewater. *Environmental Technology*, *30*(6), 583-609.

Sheindorf, C. H., Rebhun, M., & Sheintuch, M. (1981). A Freundlich-type multicomponent isotherm. *Journal of Colloid and Interface Science*, *79*(1), 136-142.

Singh, S., Kushwaha, J. P. (2014). Tannic acid adsorption/desorption study onto/from commercial activated carbon. *Desalination & Water Treateatment, 52*(16-18), 3301-3311

Srivastava, N. K., & Majumder, C. B. (2008). Novel biofiltration methods for the treatment of heavy metals from industrial wastewater. *Journal of Hazardous Materials*, *151*(1), 1-8.

Srivastava, V. C., Mall, I. D., & Mishra, I. M. (2007). Adsorption thermodynamics and isosteric heat of adsorption of toxic metal ions onto bagasse fly ash (BFA) and rice husk ash (RHA). *Chemical Engineering Journal*, *132*(1-3), 267-278.

Srivastava, V.C., Mall, I.D., Mishra, I.M. (2006). Equilibrium modelling of single and binary adsorption of cadmium and nickel onto bagasse fly ash. *Chemical Engineering Journal*, *117*, 79–91.

Tchounwou, P. B., Yedjou, C. G., Patlolla, A. K., & Sutton, D. J. (2012). Heavy metal toxicity and the environment. In *Molecular, Clinical and Environmental Toxicology* (pp. 133-164). Springer, Basel.

Temkin, M.J., Pyzhev V. (1940). Recent Modifications to Langmuir Isotherms. *Acta Physiochimica,* 12, 217-222.

Thomas, O., Burgess, C. (2007). U.V-Visible Spectrophotometry of water and wastewater, techniques and instrumentation in analytical chemistry. *27*. Elsevier, edition I.

Tian, L., Xie, G., Li, R. X., Yu, X. H., & Hou, Y. Q. (2011). Removal of Cr (VI) from aqueous solution using MCM-41. *Desalination and Water Treatment*, *36*(1-3), 334-343.

Villacañas, F., Pereira, M. F. R., Órfão, J. J., & Figueiredo, J. L. (2006). Adsorption of simple aromatic compounds on activated carbons. *Journal of Colloid and Interface Science*, *293*(1), 128-136.

Wada, S., Ichikawa, H., & Tastsumi, K. (1995). Removal of phenols and aromatic amines from wastewater by a combination treatment with tyrosinase and a coagulant. *Biotechnology and Bioengineering*, *45*(4), 304-309.

Wang, X., Guo, Y., Yang, L., Han, M., Zhao, J., & Cheng, X. (2012). Nanomaterials as sorbents to remove heavy metal ions in wastewater treatment. *Journal of Environmental and Analytical Toxicology*, *2*(7), 1000154.

Weber Jr., W.J., Morris, J.C. and Sanit, J. (1963). Kinetics of Adsorption on Carbon from Solution. *Journal of the Sanitary Engineering Division*, *American Society of Civil Engineers*, 89, 31-38.

Worch, E. (2012). Adsorption technology in water treatment: fundamentals, processes, and modeling. Walter de Gruyter.

Wu, F. C., Tseng, R. L., Juang, R. S. (2009). Initial behavior of intraparticle diffusion model used in the description of adsorption kinetics. *Chemical Engineering Journal, 153*(1-3), 1-8.

Wu, S., Li, F., Xu, R., Wei, S., & Li, G. (2010). Synthesis of thiol-functionalized MCM-41 mesoporous silicas and its application in Cu (II), Pb (II), Ag (I), and Cr (III) removal. *Journal of Nanoparticle Research*, *12*(6), 2111-2124.

Wu, X., Hui, K.N., Hui, K.S., Lee, S. K., Zhou, W., Chen, R., Hwang, D.H., Cho, Y. R., Son, Y.G.(2012). Adsorption of basic yellow 87 from aqueous solution onto two different mesoporous adsorbents. *Chemical Engineering Journal, 180***,** 91–98

Xu, J., Cao, Z., Zhang, Y., Yuan, Z., Lou, Z., Xu, X., & Wang, X. (2018). A review of functionalized carbon nanotubes and graphene for heavy metal adsorption from water: preparation, application, and mechanism. *Chemosphere*, *195*, 351-364.

Yang, X., Guan, Q., & Li, W. (2011). Effect of template in MCM-41 on the adsorption of aniline from aqueous solution. *Journal of Environmental Management*, *92*(11), 2939-2943.

Yilmaz, E., Memon, S., & Yilmaz, M. (2010). Removal of direct azo dyes and aromatic amines from aqueous solutions using two cyclodextrin-based polymers. *Journal of Hazardous Materials.* 174, 592–597.

Zavareh, S., & Beiramyan, P. (2015). Removal of Aromatic Amines from Water by Cu^{2+} impregnated Chitosan/alumina Bionanocomposite. *International Journal of Research in Chemical, Metallurgical and Civil Engineering,* 2(1), 63-66.

Zhao, D., Wan, Y., & Zhou, W. (2012). *Ordered mesoporous materials*. John Wiley & Sons.

Zhao, G., Huang, X., Tang, Z., Huang, Q., Niu, F., & Wang, X. (2018) (a). Polymer-based nanocomposites for heavy metal ions removal from aqueous solution: a review. *Polymer Chemistry*, *9*(26), 3562-3582.

Zhao, Y., Kang, D., Chen, Z., Zhan, J., & Wu, X. (2018) (b). Removal of Chromium Using Electrochemical Approaches: A. *International Journal of Electrochemical Science*, *13*, 1250-1259.

Zheng, S., Gao, L., Zhang, Q., Guo, J. (2000). Synthesis, characterization and photocatalytic properties of titania-modified mesoporous silicate MCM-41. *Journal of Materials Chemistry*, *10*, 723-727.

Zhu, Z., Yang, X., He, L. N., & Li, W. (2012). Adsorption of Hg^{2+} from aqueous solution on functionalized MCM-41. *Rsc Advances*, *2*(3), 1088-1095.

PUBLICATIONS FROM THESIS

Papers published/Accepted in SCI (International) Journals

1. Toor, S.K., Kushwaha, J.P., Sangal, V.K. (2019). Aromatic amines equilibrium sorptive interaction with synthesized silica based mesoporous MCM-41: Physicochemical evaluation and isotherm modelling, ***Journal of Environmental Science and Health Part A,*** 54(4), 286-294. **Impact factor: 1.536**

2. Toor, S.K., Kushwaha, J.P., Sangal, V.K. (2019). Single and Binary Adsorption of Zn (II) and Cr (VI) Heavy Metals onto Synthesized Silica -Based MCM-41, ***Chemistry Select,*** 4(9), 2576-2584. **Impact factor: 1.716**

3. Toor, S.K., Kushwaha, J.P., Sangal, V.K. (2019). Adsorptive interaction of 4-aminobiphenyl with mesoporous MCM-41, ***Physics and Chemistry of Liquids***, 57(6), 720-732. **Impact factor: 1.526**